

# A Novel Suction Cup for Vacuum-Assisted Delivery

**A comparative design study**

Pieter d'Hont





# A Novel Suction Cup for Vacuum-Assisted Delivery

A comparative design study

by

Pieter d'Hont

Daily Supervisor: Ir. Vera Kortman  
Ir. Kirsten Lussenburg  
Supervisors: Dr. Jovana Jovanova  
Dr.Ir. Aimée Sakes  
Faculty: Faculty of Mechanical Engineering (ME)  
Department: Department of Biomechanical Engineering  
Project Duration: November, 2023 - October, 2024  
Student number: 4720652



Copyright © P.G. d'Hont, 2024  
All rights reserved.

# Abstract

In many countries, Vacuum-Assisted Delivery (VAD) is the most common technique for instrumental vaginal delivery. Current VAD devices require the formation of a typical chignon on the infant's scalp to achieve the necessary traction forces. This chignon, a swelling on the infant's scalp, can lead to complications and, in severe cases, even death. This study addresses the question of how a new design for a VAD suction cup can reduce chignon formation while maintaining excellent adhesive performance. Three 3D-printed flexible suction cup designs with varying flexible lattice structures were designed to minimize chignon formation, and a bellow-shaped sealing lip was used to enhance the sealing performance. The performance of the novel designs are tested on an infant head surrogate and compared to a replica of the current commonly used Kiwi OmniCup®. Results indicated a significant reduction in scalp deformation, with the chignon volume ranging from 6.2% to 15.5% of that observed with the Kiwi replica. While the proposed suction cup designs show promise in reducing neonatal injuries by reducing the chignon formation, future work should focus on achieving a larger maximum traction force.

# Contents

<b>1</b>	<b>Introduction</b>	<b>1</b>
1.1	Current situation . . . . .	1
1.2	Problem definition . . . . .	2
1.3	Goal . . . . .	2
1.4	Approach . . . . .	2
<b>2</b>	<b>Background</b>	<b>3</b>
2.1	Instrumental vaginal delivery. . . . .	3
2.1.1	Forceps or VAD. . . . .	3
2.1.2	Evolution of VAD devices . . . . .	4
2.2	VAD procedures for successful Vacuum-Assisted Delivery . . . . .	6
2.3	Risk factors associated with VAD . . . . .	7
2.3.1	Maternal complications. . . . .	7
2.3.2	Neonatal complications . . . . .	7
2.4	Suction cup mechanics. . . . .	9
2.4.1	Vacuum- and contact area. . . . .	9
2.4.2	Free-body diagram of a standard rigid suction cup . . . . .	10
2.4.3	Sealing in regular and VAD suction cups . . . . .	11
2.4.4	Suction cup mechanics flexible suction cup. . . . .	12
2.5	Recommendations for Suction Cup Design . . . . .	12
<b>3</b>	<b>Ideation</b>	<b>14</b>
3.1	Design requirements . . . . .	14
3.2	Design components . . . . .	16
3.3	Decrease chignon formation . . . . .	16
3.3.1	Circular grid structure . . . . .	16
3.3.2	Flexible lattice structure . . . . .	17
3.3.3	Comparison flexible structure and grid structure . . . . .	20
3.4	Increase sealing . . . . .	20
3.4.1	Scalp-To-Cup sealing rim . . . . .	21
3.4.2	Cup-To-Scalp sealing rim . . . . .	21
3.4.3	Comparison of sealing concepts. . . . .	21
<b>4</b>	<b>Final Design</b>	<b>22</b>
4.1	Final design. . . . .	22
4.1.1	Bellow-shaped sealing lip . . . . .	22
4.1.2	Flexible lattice structure . . . . .	23
4.1.3	Vacuum inlet suction, cup thickness and grooves . . . . .	29
4.2	Prototype Development . . . . .	30
<b>5</b>	<b>Experimental validation</b>	<b>32</b>
5.1	Goal . . . . .	32
5.2	Experimental setup. . . . .	32
5.2.1	Infant surrogate design. . . . .	34
5.3	Experimental protocols. . . . .	35
5.3.1	Experiment 1: Maximum traction force and scalp displacement . . . . .	36
5.3.2	Experiment 2: Displacement without traction force . . . . .	36
5.3.3	Experiment 3: Pressure loss rate . . . . .	36
5.4	Experimental variables. . . . .	36
5.5	Data analysis . . . . .	37

5.6	Test results . . . . .	37
5.6.1	Experiment 1 results: Maximal traction force and displacement . . . . .	37
5.6.2	Experiment 2 results: Displacement without traction force . . . . .	38
5.6.3	Experiment 3 results: Pressure loss rate . . . . .	39
5.6.4	Detachment observations . . . . .	40
5.6.5	Evaluation of suction cup performance using the Force/Displacement ratio . . . . .	41
5.6.6	Force-displacement ratio plotted over time . . . . .	42
<b>6</b>	<b>Discussion</b>	<b>44</b>
6.1	Main findings . . . . .	44
6.1.1	Requirement check . . . . .	44
6.1.2	Maximal traction force . . . . .	44
6.1.3	Scalp deformation . . . . .	45
6.1.4	Pressure loss rate . . . . .	46
6.2	Experiment limitations . . . . .	47
6.3	Experiment recommendations . . . . .	47
6.4	Design recommendations . . . . .	48
<b>7</b>	<b>Conclusion</b>	<b>50</b>
	<b>References</b>	<b>54</b>
<b>A</b>	<b>Appendix</b>	<b>55</b>
A.1	Prerequisites and requirements before VAD is executed . . . . .	55
A.2	Other neonatal injuries . . . . .	55
A.3	Sealing features found in wildlife . . . . .	57
A.4	Technical datasheet Filaflex 60A . . . . .	59
A.5	Grid structure . . . . .	60
A.5.1	Comparison grid structures . . . . .	60
A.5.2	Circular grid configuration . . . . .	61
A.6	Stringing problem in 3D printing . . . . .	63
A.7	Sealing lip force . . . . .	63
A.8	Lattice forces . . . . .	64
A.9	Infant skull model . . . . .	65
A.10	Vacuum inlet diameter . . . . .	68
A.11	Simulation cup-scalp interface . . . . .	68
A.12	Dimensions final design . . . . .	69
A.13	Chignon formation compared to the Kiwi replica . . . . .	70
A.14	Conversion table from mmHg to kPa . . . . .	70

# Introduction

## 1.1. Current situation

Most childbirths occur naturally without the need for physical assistance. In a non-assisted delivery, a combination of the mother's expulsive efforts and the contractive force of the uterus results in a coordinated motive force to push the infant through the birth canal. The infant's head descends through the pelvis through stations of delivery (Figure 1.1) until its body is delivered. In most cases (85 – 95%) the delivery of the infant happens unassisted ([1]). However, in a smaller part of childbirths, complications may arise that hinder a smooth vaginal delivery or necessitate expedited delivery. Common contributing factors to such complications include the narrowing of the birth canal, fetal distress, intrapartum infections, maternal exhaustion, or irregularities in the infant's positioning or size ([2]).

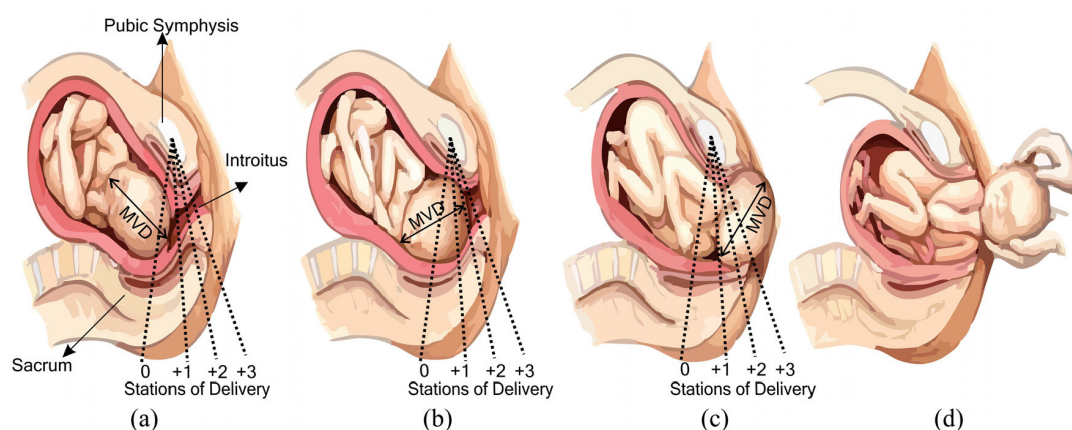


**Figure 1.1:** (a) Foetus aligns to the bony maternal pelvis in a cephalic presentation (head first). (b) The infant progresses through the stations of delivery, and vacuum-assisted delivery (VAD) can be performed starting from station 0. (c) The infant's scalp is visible at the introitus. (d) Delivery of the infant is completed when the body is delivered, either spontaneously or with the obstetrician holding the fetal head, sometimes to help with the delivery of the shoulders. [1]

In the case that a normal spontaneous vaginal delivery is not feasible or needs to be expedited, the obstetric team typically considers two main options: Instrumental Vaginal Delivery or a cesarean section (C-section) ([3]). However, due to the increased risk of maternal morbidity, C-sections are generally reserved as a last resort ([4]). They are applied to childbirth when instrumental delivery fails or is deemed unsafe or infeasible. Furthermore, C-sections result in increased maternal blood loss and the need for more extensive postnatal care ([1], [5]).

Currently, Vacuum-Assisted Delivery (VAD) is the predominant method for instrumental vaginal delivery in most countries. The widespread clinical adoption of VAD was facilitated by Malmstroem's proposed system in the 1950s, which aimed to apply to assist forces through a suction interface attached to the infant's head ([6]). In a typical VAD procedure, a suction cup is placed on the scalp, and negative pressure



is generated manually, allowing the obstetrician to aid delivery by pulling the VAD handle in coordination with the mother's contractions.

## 1.2. Problem definition

Since Malmstroem's original device, there has been limited innovation in VAD design or functionality. This lack of evolution should be viewed in light of growing clinical evidence suggesting the potential for enhancing VAD systems for improved safety and efficiency ([1]). Despite its widespread use in labor globally, there is a small risk of complications. The mechanical interaction between the VAD device and the scalp can potentially cause varying degrees of damage to the infant ([1]). For example, the characteristic chignon, a swelling on the infant's scalp formed in the VAD device, as depicted in Figure 1.2B, typically only remains visible for a short duration, often dissipating within hours to a day. However, in particular cases, studies show that the chignon formation results in complications like a Subgaleal Hemorrhage (SGH) (Figure 1.2C & 1.2D), intracranial hemorrhage, skull fractures, and even death ([7]).

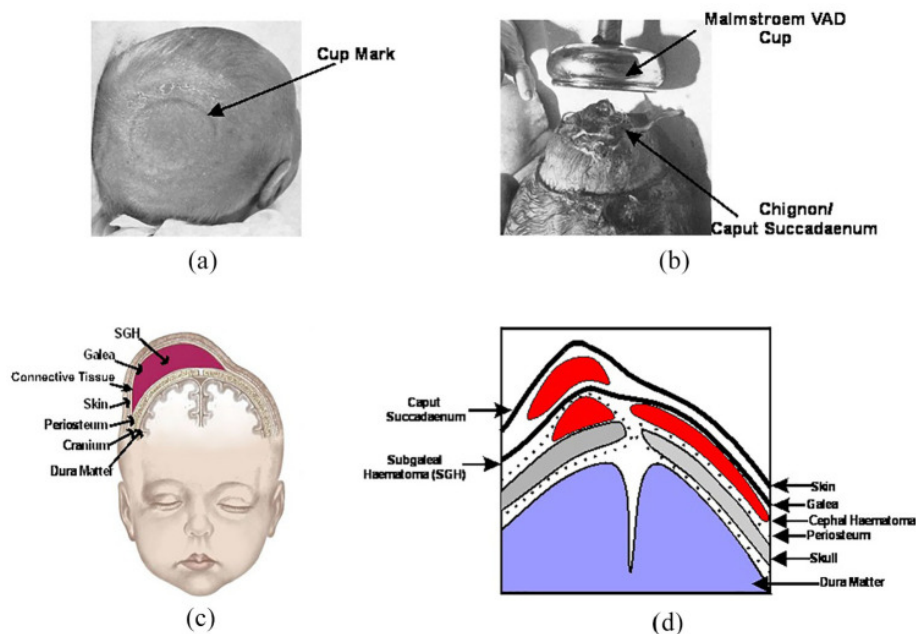


**Figure 1.2:** Trauma associated with VAD: (a) Dissipation of caput succedaneum after a few hours leading to a cup mark (b) Elevation of the scalp after VAD, (c) The head of the infant with an SGH, and (d) All trauma levels associated with VAD. [1]

## 1.3. Goal

The goal of this study is to develop a novel suction cup design aimed at reducing chignon formation while maintaining excellent adhesive performance.

## 1.4. Approach

This study is structured into seven sections. Section 2 provides background information to explain the functioning of current VAD devices and the mechanisms responsible for neonatal complications, concluding with recommendations for a novel design. In section 3 the design requirements are stated and various design concepts are compared. A final design is proposed and developed in Section 4. In Section 5 it is evaluated how the proposed design meets the specified requirements and its performance is tested experimentally and compared to a replica of the commonly used Kiwi OmniCup®. Finally, limitations and recommendations are discussed in Section 6, and the conclusions are presented in Section 7.

# 2

## Background

### 2.1. Instrumental vaginal delivery

Instrumental deliveries involve the use of obstetric instruments to assist in childbirth. The two primary types of instrumental deliveries are forceps delivery (Figure 2.1) and Vacuum-Assisted Delivery (VAD).

#### 2.1.1. Forceps or VAD

The choice of delivery methods and instruments varies between hospitals and regions, and even within hospitals, individual obstetricians may prefer different techniques ([8]). The decision to use either instrument is a nuanced evaluation by obstetricians, considering factors such as fetal position, size, labor progression, maternal effort, fetal head position, individual proficiency and skill, and the likelihood of successful delivery ([1], [4]). Both forceps and VAD aim to facilitate delivery by enhancing uterine contractions and maternal pushing efforts. They also help correct the position of the fetal head in cases of malposition, aiding its passage through the pelvis. Obstetric forceps can actively rotate the fetal head, while VAD assists in proper rotation. Neither forceps nor VAD should require excessive traction force, especially if the fetal head is not properly aligned. Although forceps can transmit more force, this should be reserved for acute, time-critical emergencies ([1]).

Forceps, which have been used since the 16th century, require extensive training and are linked to increased maternal morbidity and potentially severe injuries to the infant. Vacuum-assisted delivery (VAD) is often preferred over forceps because VAD is perceived as less traumatic despite its higher risk of Subgaleal Hemorrhage (SGH) due to the formation of a chignon ([1]).



**Figure 2.1:** Illustration of an obstetrician using forceps during an instrumental vaginal delivery to assist the infant's head through the birth canal. ([9])

### 2.1.2. Evolution of VAD devices

The initial purpose of instrumental deliveries was to extract fetuses from women at high risk of death due to prolonged or obstructed labor, prioritizing the mother's survival over potential fetal harm. With advancements in safer techniques for instrumental delivery, the focus has shifted to also ensuring fetal well-being. VAD, first documented in 1705 by Dr. James Yonge, did not gain widespread use until the 1950s when popularized by Swedish obstetrician Dr. Tage Malmström ([4]). Advancements in suction cup design have evolved from Malmström's metal cups to modern plastic cups, though their fundamental geometries and dimensions have remained largely unchanged (Figure 2.2) ([4]).

VAD devices can be categorized into rigid and soft cups. A summary of commercially available VAD devices is provided in Table 2.1. Rigid mushroom-shaped cups (M-cups) can generate more traction force than soft cups by creating both mechanical and vacuum links. However, soft cups are associated with fewer neonatal injuries despite a higher failure rate due to more frequent detachments (pop-offs) ([10]). A commonly used soft suction cup is the Silastic® (Figure 2.2 B), which initially showed promise but struggled with reaching the flexion point due to its high profile and had higher detachment rates ([11]).

Currently, the most widely utilized rigid plastic cup is the disposable Kiwi OmniCup® (Figure 2.2 C). It is renowned for its flexible stem and low-profile cup, which allows for placement over the fetal head flexion point if the infant is misaligned, thereby helping to correct malposition and facilitate the delivery process ([10], [12]).

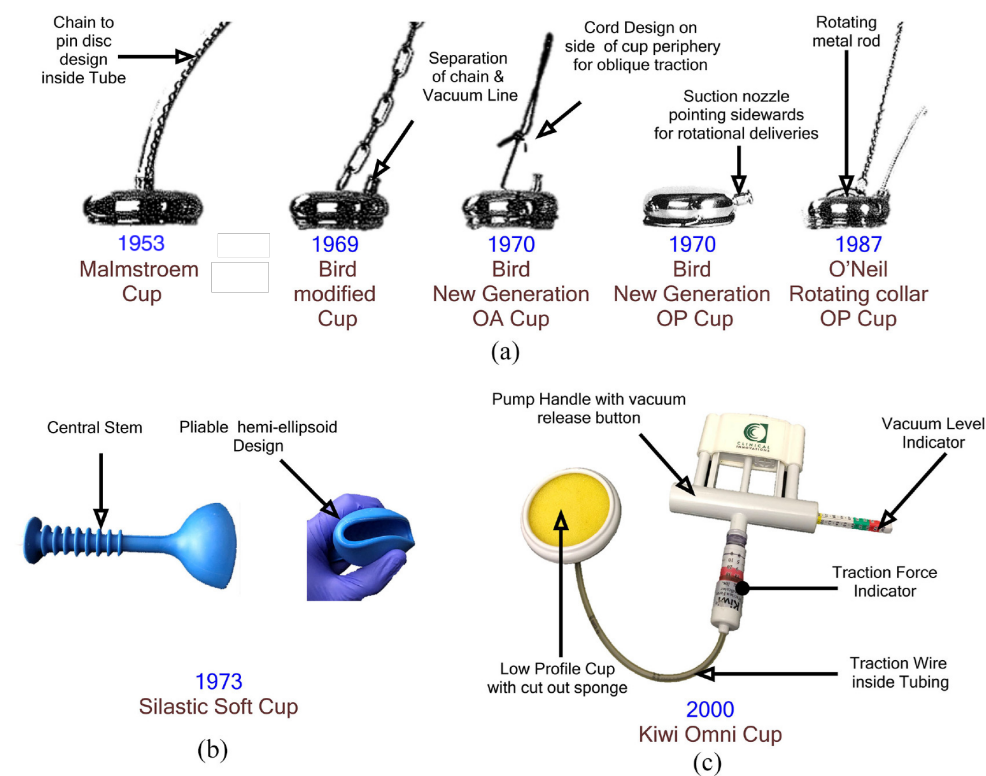


**Figure 2.2:** Evolution of modern VAD devices: (a) Metal cups, (b) the silastic soft cup, and (c) the single-use Kiwi OmniCup®. ([1])

**Table 2.1:** Types suction cup Devices for vacuum-assisted delivery ([4])

<b>Device</b>	<b>Size (Diameter)</b>	<b>Material</b>
<b>Soft Cups</b>		
Gentle Vac™ (OB Scientific)	60 mm	Soft rubber
Kiwi ProCup® (Clinical Innovations)	65 mm	Soft plastic
Silastic™	65 mm	Soft silicone
Mityvac MitySoft Bell® (Cooper-Surgical)	60 mm	Soft silicone
Secure Cup™ (Utah Medical)	63 mm	Rubber
Silc Cup	50–60 mm	Silicone rubber
Soft Touch™ (Utah Medical)	60 mm	Soft polyethylene
Tender Touch® (Utah Medical)	60 mm	Soft silicone
Vac-U-Nate™ (Utah Medical)	65 mm	Soft silicone
<b>Rigid Cups</b>		
Flex Cup™ (Utah Medical)	60 mm	Polyurethane
Kiwi OmniCup® (Clinical Innovations)	50 mm	Rigid plastic
Malmström (Dickinson Healthcare)	40–60 mm	Metal
Mityvac M-Style® (CooperSurgical)	50 mm	Rigid polyethylene
Bird posterior cup	40–60 mm	Metal

## 2.2. VAD procedures for successful Vacuum-Assisted Delivery

When childbirth proceeds as expected, the infant undergoes several typical movements until delivery, as depicted in Figure 2.3.

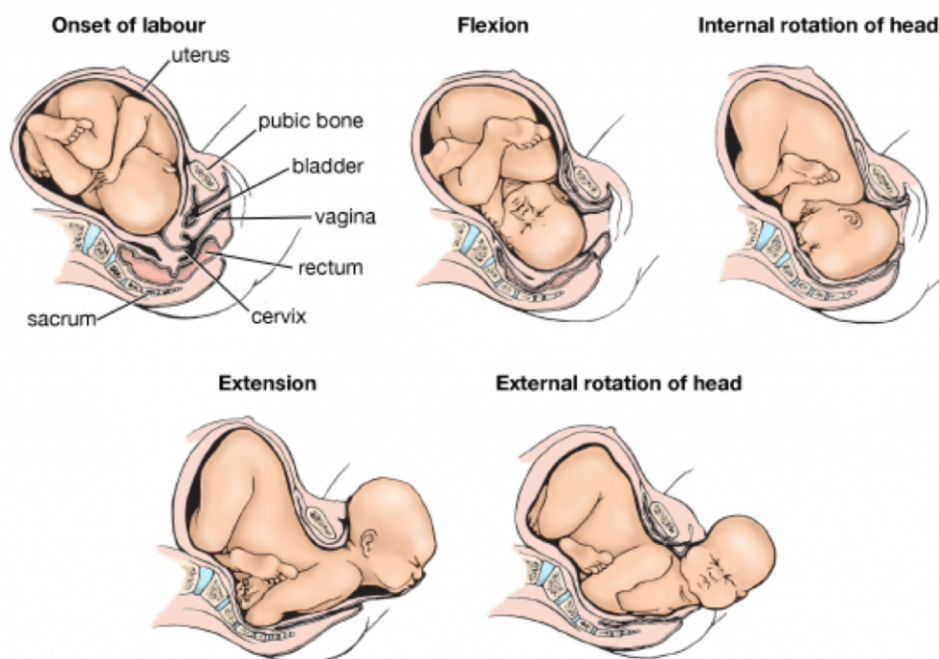


**Figure 2.3:** The force generated by uterine contractions and pushing movements propels the baby's buttocks, transmitting pressure along the spine to guide the head through the pelvis. This pressure causes the head to flex, with the back of the head leading until the chin touches the breastbone. As the head descends further, it encounters resistance from the bony pelvis and pelvic floor, causing it to rotate internally, aligning its longest diameter with the pelvic outlet for smoother passage. Despite resistance from the mother's pelvis, the softer lower birth canal allows the head to advance, gradually extending as it emerges. Once born, the twisted neck untwists, turning the head backward. ([13])

VAD can be considered to assist when the infant poorly progresses during labor, starting from the zeroth station of delivery (Figure 1.1). Other indications for VAD include maternal exhaustion, asynclitism (malposition of the fetal head), and fetal distress ([14]). Important requirements for assisted vaginal delivery include ensuring full dilation of the cervix, determining the position and station of the fetal head, and providing sufficient analgesia ([1]). Other requirements and prerequisites before performing VAD are summarized in Appendix A.1. Once these are met, the VAD procedure may be started. The obstetrician should locate the flexion point, situated 3 cm anterior to the posterior fontanelle along the midline of the sagittal suture (Figure 2.4A). The suction cup must be placed on this point to ensure the shortest perimeter of the infant's head passes through the birth canal. The VAD device is then carefully maneuvered to this point, and a vacuum is applied to secure attachment to the scalp. This vacuum creates a differential pressure with the atmosphere, causing the scalp to expand and fill the suction cup, forming a caput succedaneum or 'chignon' (Figure 2.5) ([1]).

A traction force can be applied during each maternal contraction to help the infant move through the birth canal or correct fetal head malposition (Figure 2.4B). Once the infant reaches the third station, the cup may be detached (Figure 2.4A).

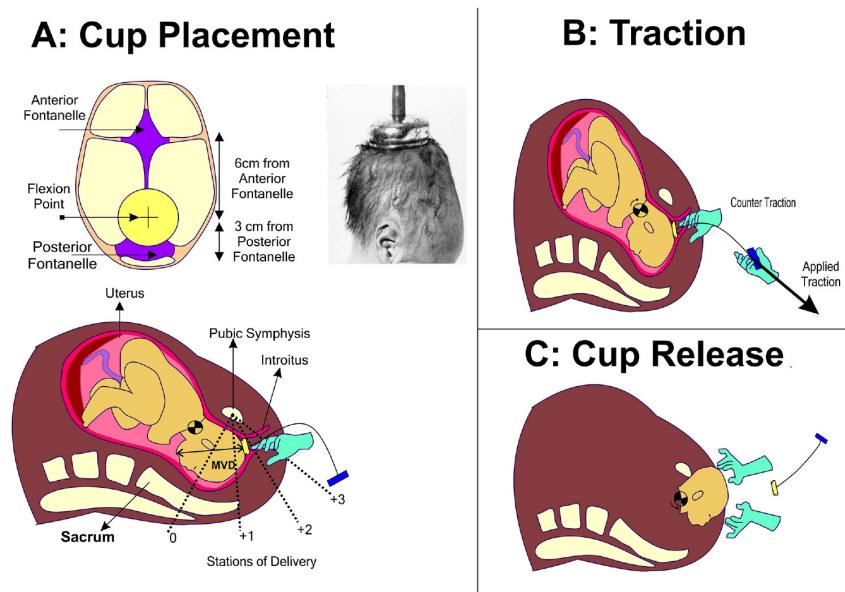


**Figure 2.4:** Process steps during VAD: (a) A suction cup is applied to create a chignon by pumping air out of the suction cup after placement on the flexion point. (b) A traction force is applied with counter-traction used to decrease the chance of detachment. (c) The VAD device is released to proceed with the delivery of the head. ([1])

## 2.3. Risk factors associated with VAD

VAD prevents injuries from birth asphyxia and complications associated with prolonged second-stage labor, making it a potentially life-saving intervention. Furthermore, VAD plays a crucial role in maintaining the cesarean rate at an acceptable level ([15]). However, there are still certain risks associated with VAD for both the mother and infant.

### 2.3.1. Maternal complications

Complications such as perineal pain at delivery, pain in the immediate postpartum period, perineal lacerations, hematomas, blood loss and anemia, urinary retention, and long-term issues with urinary and fecal incontinence can arise from VAD ([4]). A review of over 50,000 vaginal deliveries at the University of Miami shows that the incidence of third and fourth-degree maternal perineal lacerations, the most severe obstetric anal sphincter injuries (OASIS) during childbirth, is higher in vacuum-assisted (10%) and forceps deliveries (20%) compared with spontaneous vaginal deliveries (2%) ([16]). OASIS have the most significant negative impact on women's health among the various types of visible birth tears ([17])

### 2.3.2. Neonatal complications

Neonatal complications range from minor to significant injuries. The most significant injury is a Subgaleal Hemorrhage (SGH), other injuries are discussed in Appendix A.2.

The characteristic chignon, a swelling on the infant's scalp formed in the VAD device, typically remains visible for a short duration, often dissipating within hours to a day. In severe cases, a large chignon and excessive forces inside the scalp can rupture blood vessels which increases the likelihood of developing an SGH ([18]). An SGH is an accumulation of blood inside the scalp between the tough, fibrous connective tissue (galea aponeurotica) and the membrane tissue (periosteum) that covers the surface of a newborn's skull (Figure 2.5). Eliachar et al. calculated that this hemispheric space, filled to just 1 cm in thickness, could accommodate as much as 260 mL of blood, an amount exceeding the entire blood volume of some newborns ([19]). This blood loss can result in hypovolemic shock or even death ([20]). The mortality rate associated with an SGH is around 14 percent ([15]). The occurrence rate of an SGH is approximately 0.04% in non-assisted deliveries and 0.59% in vacuum-assisted deliveries, making it 14.75 times more common in vacuum-assisted deliveries [19]. Factors contributing to an SGH include maternal nulliparity, placement of the VAD cup over the sagittal suture near the infant's anterior fontanel, and failed vacuum extraction attempts ([21]).

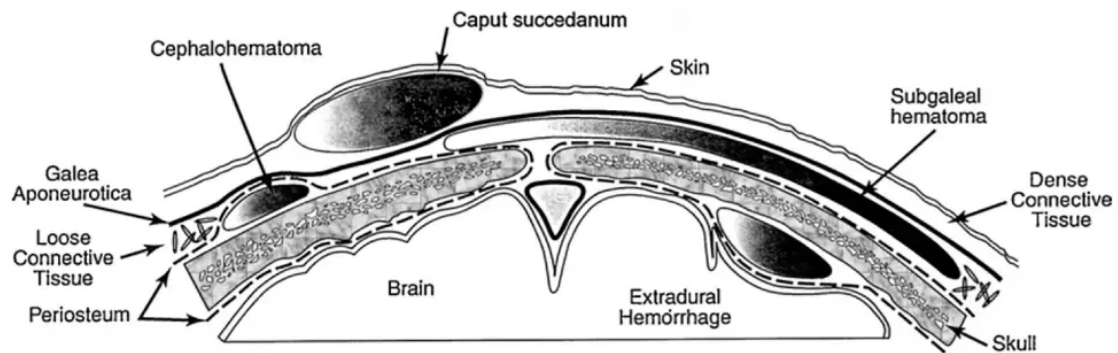


**Figure 2.5:** Schematic representation of the layers of the scalp, skull and Brain showing the different types of hematomas ([15])

Similar to the limited evidence explaining the evolution of VAD devices, there is also a scarcity of literature regarding how suction cups interact with an infant's scalp. According to Malmström, the vacuum-induced chignon in a rigid mushroom-shaped suction cup behaves like "a semi-firm scalp knob," providing grip to the cup even in the absence of vacuum, similar to "interlocking pieces in a jigsaw puzzle" (Figure 2.6). It takes around two minutes after vacuum application for the chignon to fill with enough fluid to form an interlocking ([4]).

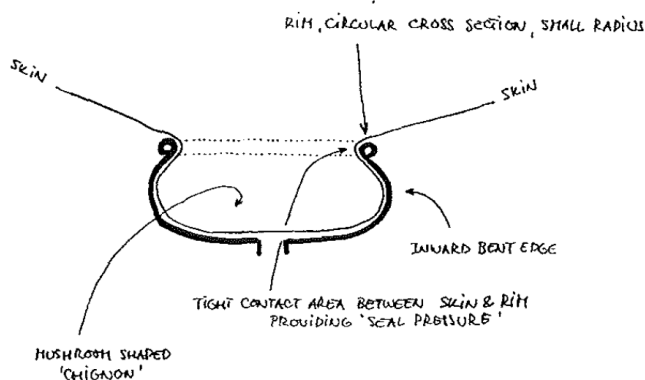


**Figure 2.6:** Alignment of the fetal scalp skin in a rigid mushroom-shaped cup ([22]).



**Figure 2.7:** An example of a commonly used soft VAD device, the Silc Cup (Medela Inc.) ([23])

By creating a mechanical as well as vacuum link, the rigid mushroom cup is able to generate more traction force than the soft cup ([24]). This mechanical link is achieved by the development of a chignon. However, in soft suction cups, the adhesiveness is reduced after the development of the chignon ([4]). This reduction occurs because the chignon tends to get 'sucked' against the inner cavity, decreasing the effective vacuum area where the suction force is applied. To minimize this issue, current soft cup designs feature a high cup profile, which limits the ability to reach the flexion point in cases of infant malposition. Some designs attempt to enlarge the effective vacuum area by incorporating grooves and ridges, but research indicates that these grooves often fail to distribute the negative pressure effectively ([22]). Therefore, when using a soft suction cup, like the Silc Cup (Figure 2.7), it is suggested to minimize chignon formation by applying vacuum only with traction ([25]).

## 2.4. Suction cup mechanics

From a mechanical point of view, the suction cup should distribute the traction force to the infant. The traction force is distributed through the flexible scalp and skin to the skull and eventually the whole body. It is assumed that the traction force is increased slowly, therefore a static situation is assumed. In this section, the suction cup is considered rigid. The mechanics of a soft suction cup are discussed in Section 2.4.4.

### 2.4.1. Vacuum- and contact area

The vacuum area ( $A$ ) and contact area ( $C$ ) of the suction cup are illustrated in Figure 2.8. The vacuum area ( $A$ ) refers to the inner cross-section of the suction cup where negative pressure is applied to the scalp. The effective vacuum area ( $A_{eff}$ ), however, is the portion of this vacuum area that effectively contributes to the suction force. For instance, if the scalp is drawn against the inner wall of the suction cup due to chignon formation, that portion of the area ceases to contribute to the suction force. The contact area ( $C$ ) represents the portion of the suction cup that comes into contact with the scalp during suction ([12]).

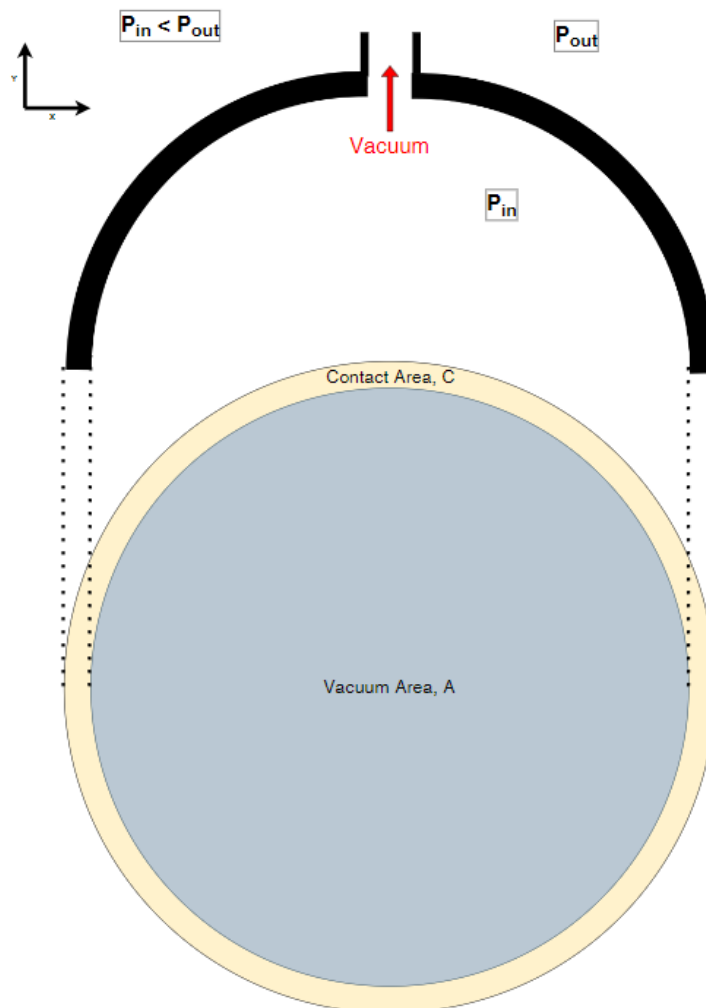


**Figure 2.8:** Schematic diagram of the vacuum area ( $A$ ) and the contact area ( $C$ ) on the cup-scalp contact surface



### 2.4.2. Free-body diagram of a standard rigid suction cup

The free-body diagram (FBD) of the suction cup and scalp during suction is shown in Figure 2.9. It illustrates the contact forces assuming no leakage occurs.

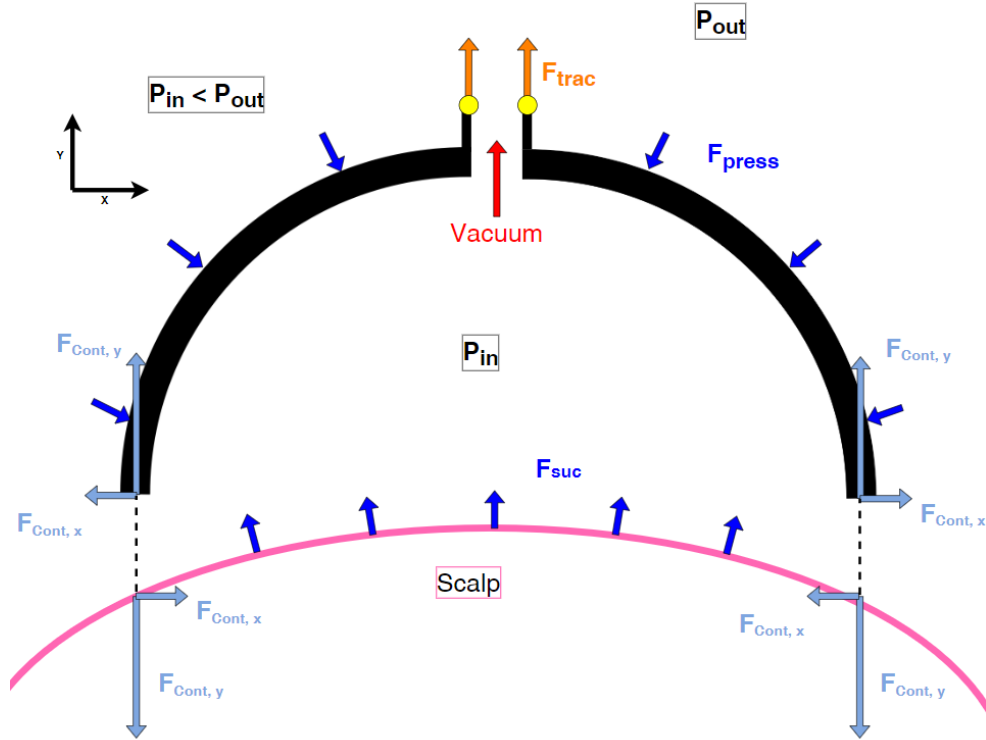


**Figure 2.9:** Free-body diagram, showing the forces acting on the suction cup and scalp. The diagram is split at the contact point to show the contact forces.

The vacuum is generated, as in the case of the Kiwi OmniCup®, using a manual handpump. Once the partial vacuum is applied, a pressure difference ( $\Delta P$ ) arises between the pressure inside the suction cup ( $P_{in}$ ) and the pressure outside the suction cup ( $P_{out}$ ) (Equation 2.1).

$$\Delta P = |P_{out} - P_{in}| \quad (2.1)$$

$F_{press}$  is the resultant force from the pressure difference, acting normally to the surface of the suction cup. For a rigid and symmetrical suction cup, the  $X$  components of  $F_{press}$  cancel out. The sum of all  $F_{press}$  vectors in the  $Y$  direction,  $F_{press,y}$ , is calculated by multiplying the pressure difference ( $\Delta P$ ) with the vacuum area  $A$  (Equation 2.2).

$$F_{press,y} = \Delta P \cdot A \quad (2.2)$$

The formation of a chignon is a direct result of the suction force ( $F_{suc}$ ) acting on the scalp. The sum of all resultant suction forces in the  $Y$  direction ( $F_{suc,y}$ ) is equal to  $F_{press,y}$ , only acting in opposite direction:

$$F_{suc,y} = F_{press,y} = \Delta P \cdot A \quad (2.3)$$

In the free-body diagram depicted in Figure 2.9, the traction force  $F_{trac}$  is drawn in a positive  $Y$  direction, which results in an equal force distribution over the whole contact area ( $C$ ). The contact force, distributed over the contact area ( $C$ ), acts in  $X$  and  $Y$  directions on the suction cup and scalp.

The static force equilibrium in  $y$ -direction is represented as:

$$F_{trac} + F_{cont,y} - F_{press,y} = 0 \quad (2.4)$$

Assuming static equilibrium, the  $Y$  component of the contact force,  $F_{cont,y}$ , is:

$$F_{cont,y} = \Delta P \cdot A - F_{trac} \quad (2.5)$$

To prevent detachment, the contact force ( $F_{cont,y}$ ) must remain positive:

$$F_{cont,y} = \Delta P \cdot A - F_{trac} > 0 \quad (2.6)$$

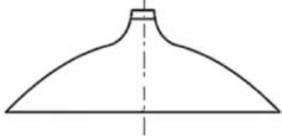
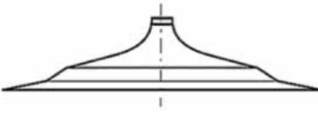
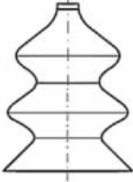
Therefore, detachment occurs when  $F_{trac}$  exceeds  $\Delta P \cdot A$ . The following relation should be satisfied to ensure attachment:

$$F_{trac} < \Delta P \cdot A \quad \text{for} \quad F_{cont,y} > 0 \quad (2.7)$$

### 2.4.3. Sealing in regular and VAD suction cups

The generation of differential pressure ( $\Delta P$ ) would not be possible without the excellent sealing of the sucker cavity from the environment ([12]).

In industrial applications, different types of suction cups are commonly used and are summarized in Figure 2.10. The primary criterion for choosing the most suitable vacuum cup is the shape of the load to be grasped: flat vacuum cups without cleats are used to grip flat and rigid loads (for vertical handling); flat vacuum cups with cleats are used to handle sheet-like loads (increases resistance to lateral forces); suction cups with bellows compensates of differences in height to hold irregular loads ([12], [26]).

Type	Flat without cleat	Flat with cleat	With bellow
Shape			
Surface	Flat	Flat	Irregular

**Figure 2.10:** Regular industrial suction cup types and associated shapes and load surfaces ([12]).

From a mechanical perspective, industrial standards and criteria can be applied to the obstetric field. For example, since the fetal head is irregular, industrial guidelines suggest using a suction cup with bellows (as illustrated in Figure 2.10) rather than a flat, rigid cup. Although this approach does not consider tissue damage or skull deformation, it raises questions about the current design of the obstetric cup ([12]).

Human skin is not entirely smooth. In adult skin, irregularities are found in the form of microchannels with dimensions of  $200\mu m$  in width and  $300\mu m$  in height ([27]). Besides channels inside the skin, some infants are born with little or no hair and others are born with a full head of hair. Neonatal hair differs from adult hair. The thickness of normal adult hair is generally  $80 - 110\mu m$ , and neonate's hair is approximately  $25\mu m$ , which is more than threefold thinner ([28]). Both the channels and the hair may result in leakage channels between the cup-scalp interface when the sealing is not optimal.

To ensure attachment during VAD,  $\Delta P * A$  should be larger than the traction force ( $F_{trac}$ ) (Equation 2.7). In current Vacuum-Assisted Delivery (VAD) devices, achieving this involves elevating the negative

pressure ( $\Delta P$ ). As this force intensifies, the suction cup presses against the scalp, closing the leakage channels and enhancing sealing at the contact area ( $C$ ).

Moreover, for mushroom-shaped cups, the chignon that is formed results in the scalp being 'sucked' against the suction cup's inner wall, providing 'seal pressure' (Figure 2.6) which further increases the sealing capabilities [22]). However, chignon formation correlates with greater damage to the infant's scalp (Section 2.3).

#### 2.4.4. Suction cup mechanics flexible suction cup

Soft VAD suction cups have a lower success rate in delivery compared to rigid cups. However, soft cups are easier to use and associated with reduced neonatal trauma ([29], [30]).

The primary difference between a soft suction cup and a rigid cup lies in their behavior under the application of a traction force. A rigid suction cup does not deform, while a soft cup does. As schematically depicted in Figure 2.11, the deformation of the soft suction cup may result in an inward slip of the rim, reducing the vacuum area ( $A$ ) ([31]). The deformation also causes changes in volume, which in turn alter the internal pressure and directly impact the suction force (Equation 2.3).

In current flexible VAD designs, such as the Silc Cup (Medela Inc.) (Figure 2.7) and the Silastic™ (Figure 2.2B), a spherical shape is designed to prevent excessive deformation. This spherical shape provides stability both during suction and when a traction force is applied. However, it limits the ability to reach the flexion point during infant malposition ([4]).

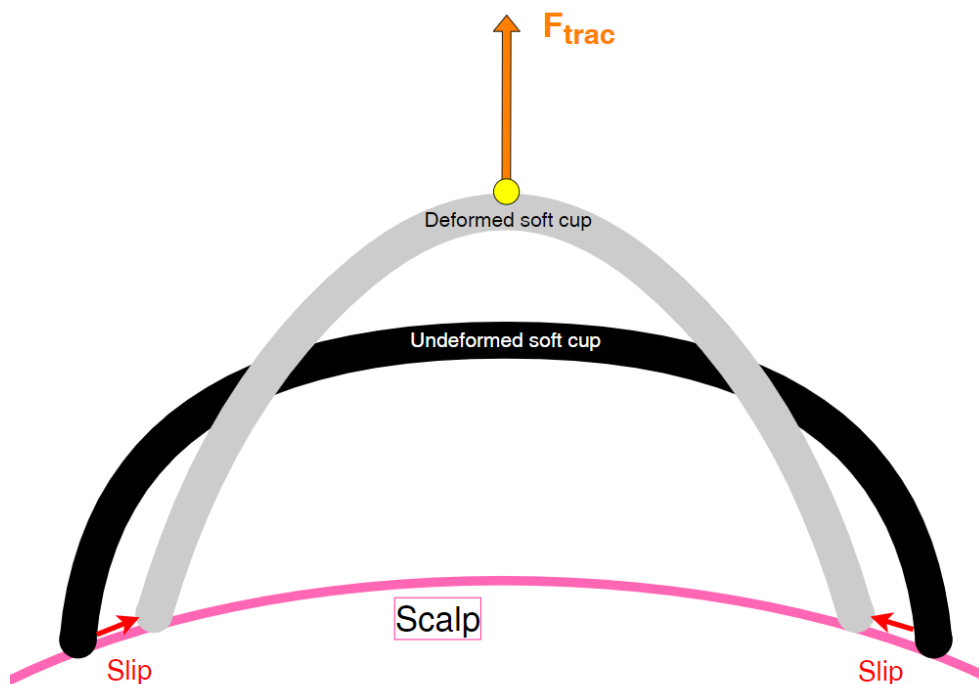


**Figure 2.11:** Schematic overview of the deformation of a flexible suction cup after the application of a traction force.

## 2.5. Recommendations for Suction Cup Design

Many injuries that occur during instrumented vaginal delivery are attributed to the excessive forces exerted on both the infant and mother due to the confined space in the birth canal. However, these injuries cannot be entirely prevented by enhancing the suction cup design, as instrumental delivery will always involve the application of an external traction force on the infant, which increases the risk of trauma. However, the risk of injuries related to the suction force, which result in chignon formation inside the suction cup, could be reduced.

Both currently used rigid mushroom-shaped and soft suction cups result in chignon formation. For rigid mushroom-shaped cups, like the Kiwi OmniCup®, the chignon is important for achieving a high

traction force due to the interlocking mechanism. Chignon formation in current soft suction cup designs is undesirable because it decreases the effective vacuum area ( $A_{eff}$ ) (Section 2.3.2). To reduce the risk of neonatal injuries, the chignon formation should be minimized in a new VAD suction cup design.

Maintaining attachment to a surface with asperities is challenging due to the numerous leakage 'channels' on irregular surfaces ([32]). Mushroom-shaped suction cups, like the Kiwi OmniCup® (Section 2.3.2) rely on chignon formation to create a tight seal. Since the proposed design aims to minimize chignon formation, an alternative sealing solution will need to be implemented. A flexible suction cup lip is proposed which can form a seal with the scalp. The flexible lip compensates for height differences by conforming around irregularities, effectively closing the leakage 'channels'. A schematic representation is depicted in Figure 2.12.

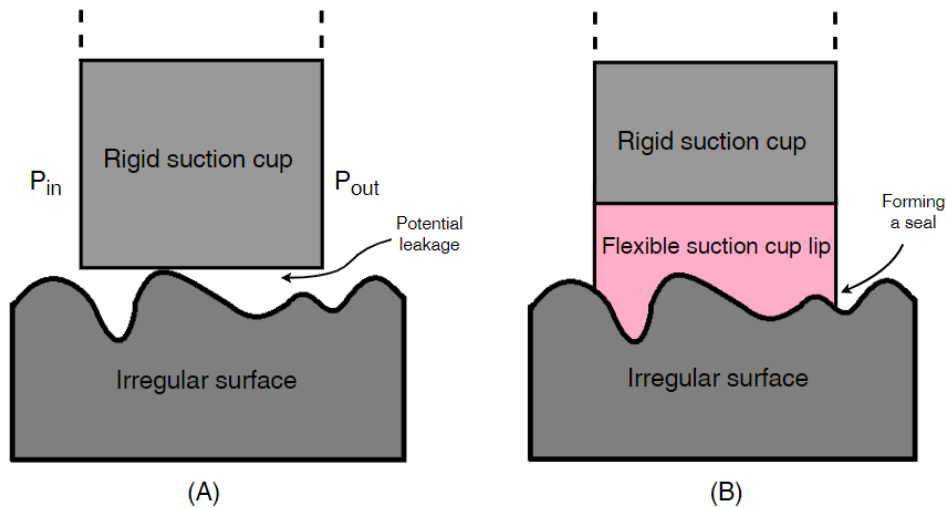


**Figure 2.12:** Figure showing the risk of leakage when adhering to an irregular surface. (A) A rigid suction cup has difficulties forming a seal with an irregular surface. (B) A soft suction cup lip forms around irregular surfaces and prevents leakage by creating a seal.

Suction cups found in nature share a common architecture: a rigid muscular part connected to the skeleton, preventing deformation, and a soft tissue part isolating an inner cavity to ensure good sealing ([12]) (Appendix A.3). The proposed suction cup needs to strike a delicate balance: the body must be rigid enough to prevent deformation to maintain its seal, while also being flexible enough for effortless insertion. Additionally, the rim should be highly flexible to form around scalp irregularities, providing a tight seal. A schematic representation of the proposed suction cup is depicted in Figure 2.13.

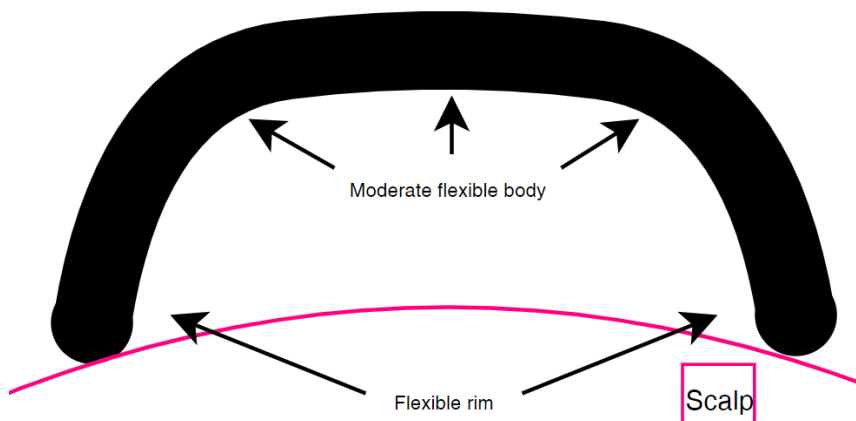


**Figure 2.13:** Schematic overview of the two main components of the suction cup

### 3.1. Design requirements

To design a novel VAD suction cup that decreases chignon formation while showing sufficient attachment performance the following requirements and wishes should be fulfilled.

#### R1, 3D printable

*It should be feasible to manufacture the design with an Fused Deposition Modeling (FDM) 3D printer. 3D printing makes it possible to manufacture complex geometries quickly and cost-effectively. The minimum thickness required to ensure airtightness in this design is 1.2 mm. Additionally, a minimum overhang angle of 40° is necessary to guarantee the design's suitability for 3D printing.*

#### R2, flexible material

*The proposed design should be made from a single, flexible material. Utilizing a single material is advantageous as it enables the entire design to be 3D-printed as a single piece. TPU with a shore hardness of 60A (Filaflex, Recreus) has been chosen (Appendix A.4), being the most flexible material for an FDM 3D printer commercially available. The design can be modeled to be flexible in specific areas while being more rigid in others.*

#### R3, adhesive performance

In an observational study of 119 vacuum-assisted vaginal deliveries using the Kiwi OmniCup®, nearly all deliveries were successfully achieved with a peak traction force of 135 N ([33]). Given that the Kiwi OmniCup® is the most widely used VAD device, the proposed design should demonstrate comparable performance. Therefore, *the proposed design should reach a peak traction force of 135 N without detachment.*

#### R4, sustaining pressure difference

In current rigid VAD suction cup designs, a negative pressure of 80 kPa (600 mmHg) is commonly reached and is therefore considered safe to be sustained in the proposed suction cup design ([34]). During VAD, if pressure leakage occurs, the obstetrician must pump to maintain a constant differential pressure ( $\Delta P$ ). Minimizing leakage is essential to reduce the amount of pumping required. Therefore, *the pressure difference ( $\Delta P$ ) of 80 kPa should remain constant for 90 seconds (the average duration of a contraction ([35])).*

#### R5, decrease chignon formation

The risk of blood vessel rupture, and consequently subgaleal hemorrhage (SGH), arises from increased pressure in the scalp tissue, which increases as more scalp is drawn into the suction cup (chignon formation) ([18], [36]). Therefore, the volume of the chignon within the suction cup during suction is considered a key indicator of the risk of scalp trauma. To mitigate the risk of scalp trauma, *the chignon volume inside the suction cup should be reduced to 10% of the chignon volume induced by the Kiwi OmniCup®.* Consequently, the potential displacement of the scalp inside the suction cup must be limited to a maximum of 1.36 mm, as this would correspond to a chignon formation of 10.0% relative to the Kiwi OmniCup® (Section A.13).

**R6, dimensions**

To ensure the proposed design is suitable for challenging fetal positions, it should maintain a low profile with a maximum height of 20 mm from the scalp, like the Kiwi OmniCup®. Commercially available VAD soft suction cups, such as the Silc Cup (Figure 2.7) have a larger outer diameter (65 mm) compared to rigid cups. Due to its flexibility it makes insertion easier and therefore a larger diameter is justified. A larger inner diameter results in an increased theoretical maximum traction force (Equation 2.7). However, due to their height (approximately 50 mm-60 mm, depends on the design), current soft cup designs are typically used only for assisting when the head is properly aligned and the flexion point is reachable. Therefore, a flexible low-profile, large-diameter design is proposed to combine the advantages of both rigid and soft cups. The outer dimensions of the proposed design should be lower than current VAD designs. *The outer dimensions of the suction cup are 20 mm in height from the scalp and 65 mm diameter.* Compared to the Kiwi OmniCup®, the inner diameter of the proposed design is increased from 50 mm to 55 mm, thereby increasing the vacuum area from 1963 mm<sup>2</sup> to 2376 mm<sup>2</sup>, while still leaving space for a 5 mm sealing lip.

**R7, environmental conditions**

*The suction cup should work in different environmental conditions.* Lubricant and bristles of a brush is used to mimic the maternal fluids and infant hair.

**R8, non-toxic materials**

*The suction cup should be made out of non-toxic materials.*

**R9, pneumatically actuated**

*The actuation of the suction cup should be pneumatic.* As all VAD suction cup designs are pneumatically actuated, the suction cup can be implemented easily and compared to current suction cup designs.

**W1, smooth surfaces**

To decrease the chance of maternal and neonatal complications, *no sharp edges should be designed.*

## 3.2. Design components

The design of the suction cup is divided into two components: decreasing chignon formation and increasing sealing. Decreasing chignon formation is essential to minimize trauma to the infant's scalp, ensuring a safer and more comfortable delivery. Increasing sealing is important to maintain a stable pressure difference ( $\Delta P$ ), which is necessary to maintain attachment (Equation 2.7). After evaluating the potential of these design components, a final conceptual design is proposed. The proposed suction cup will be tested against a 3D-printed replica of the Kiwi OmniCup®, referred to as the "Kiwi replica" from here on.

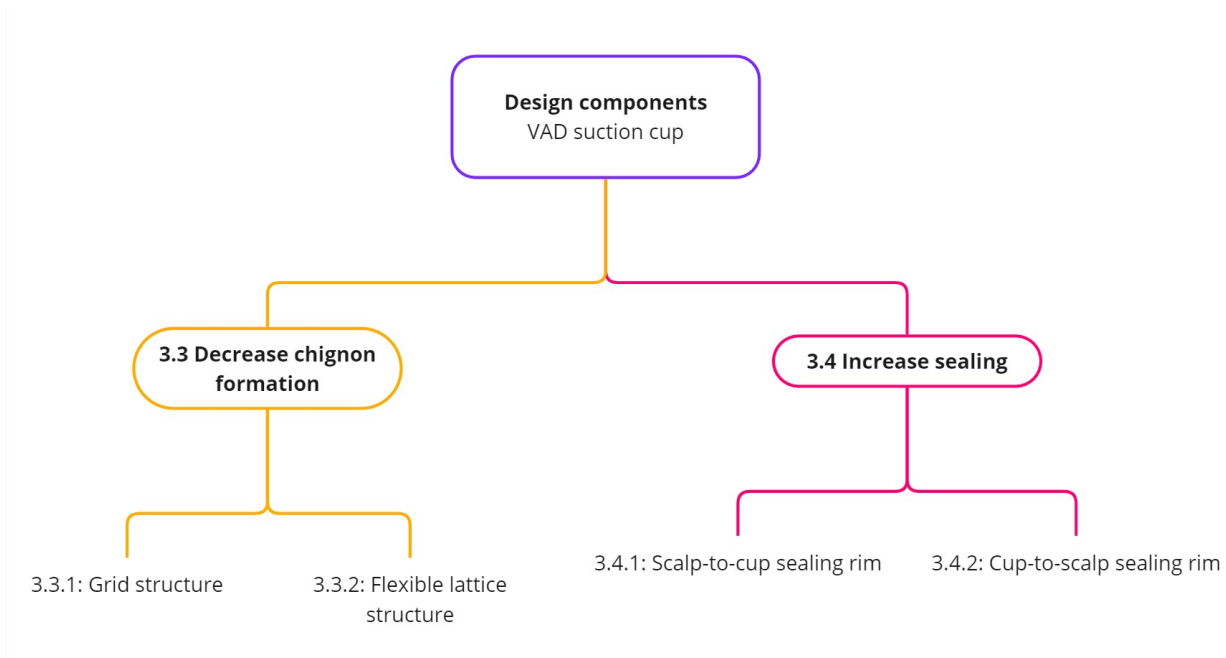


**Figure 3.1:** The design components that are considered before determining the final conceptual design.

## 3.3. Decrease chignon formation

In Section 2.4.2, it is explained that the suction force ( $F_{suc}$ ) is the direct cause of the formation of a chignon. This chignon increases the risk of neonatal injuries. Furthermore, in Section 2.4.1, it is discussed that the formation of the chignon reduces the effective vacuum area ( $A_{eff}$ ) and, consequently, the maximum achievable traction force when the chignon reaches the inner wall of the suction cup. To address this, two concepts are proposed, both of which provide a counterforce to minimize chignon formation while maintaining a large effective vacuum area ( $A_{eff}$ ). The first concept involves dividing the vacuum area into smaller sections using a circular grid structure which is discussed in Section 3.3.1. This approach leads to the formation of multiple smaller chignons rather than a single large chignon by providing a constant counterforce through the grid structure. The second concept is discussed in Section 3.3.2, where a flexible lattice structure that behaves like a spring is implemented that counteracts chignon formation while maintaining a constant effective vacuum area ( $A_{eff}$ ). This lattice structure behaves as a spring and provides a variable counterforce depending on the lattice deformation.

### 3.3.1. Circular grid structure

As discussed in Section 2.4.2, a large vacuum area results in a larger suction force ( $F_{suc}$ ), which directly leads to chignon formation. Tham et al. ([37]) concluded that a larger suction cup diameter is correlated to increased stresses within the skin (Figure A.26), leading to a higher risk of injuries. To minimize peak stresses inside the scalp, the vacuum area is distributed into smaller areas by incorporating rigid structures. The space between the structures is the effective vacuum area ( $A_{eff}$ ) where a suction force will be exerted on the scalp. To ensure the attainment of substantial traction forces, the effective vacuum area ( $A_{eff}$ ) must be at least equivalent to that of the commonly utilized Kiwi OmniCup®, which is  $1963 \text{ mm}^2$ .

In selecting the optimal grid structure, a trade-off must be considered between minimizing chignon

formation through the inclusion of a grid structure and maximizing suction force by increasing the effective vacuum area. A concentric circular grid structure was selected for this purpose, as shown in Figure 3.2. The circular grid consists of concentric rings designed to limit chignon formation. Chignon formation leads to a uniformly distributed force on the rings. Unlike a straight wall, the curvature of the rings allows forces to be distributed along a continuous, closed loop, which reduces the likelihood of buckling compared to a linear wall ([38]). The number and thickness of the rings can be adjusted to further optimize performance. A detailed comparison of different configurations is presented in Appendix A.5.2, where variations in ring number and thickness are evaluated. This comparison considers the effective vacuum area ( $A_{eff}$ ) and the spacing between rings. The key findings from this comparison include:

- A configuration of four concentric rings, each with a thickness of 1 mm, provides a larger effective vacuum area ( $A_{eff}$ ) of 2069 mm<sup>2</sup> compared to the Kiwi OmniCup®, while leaving space for a 5 mm sealing solution. Thinner rings are not considered because they would be prone to structural failure when manufactured using a 3D printer.
- This design decreases chignon formation, as the distance between the rings is only 5.11 mm. Tham et al. ([37]) concluded that small diameters of suction cups resulted in decreased chignon formation (Appendix A.11).
- The stability of rings with a thickness of 1 mm needs to be validated experimentally. Ring buckling could lead to the collapse of the suction cup, reducing the effective vacuum area ( $A_{eff}$ ).

During suction, the chignon will form inside the cavities. The rings must be of sufficient height to prevent the scalp from reaching the 'cavity ceiling,' as this would reduce the effective vacuum area ( $A_{eff}$ ) where a suction force could be exerted. However, a lower height is advantageous as it directly influences the outer dimensions of the suction cup, making it easier to insert. The optimal height of the rings should be determined experimentally since it is unknown how the scalp will deform inside the rings and if the scalp reaches the 'cavity ceiling' at a pressure difference of  $80kPa$ .

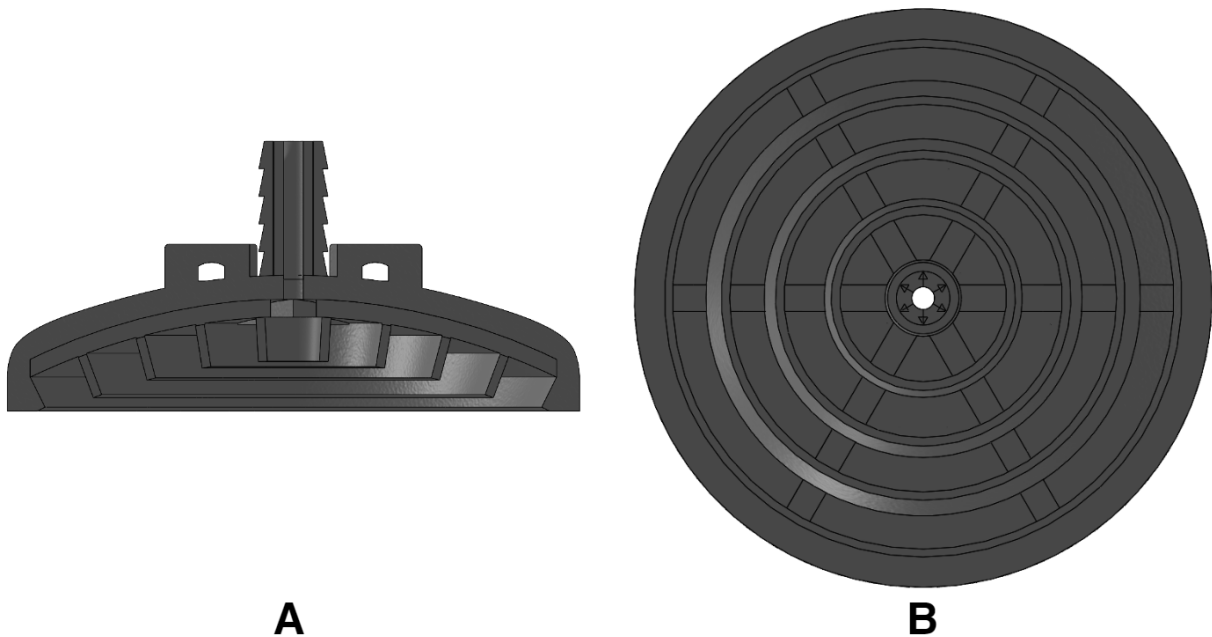


**Figure 3.2:** A section view of the suction cup with a circular grid consisting of four rings which divides the vacuum area into smaller sections showing the side view (A) and bottom view (B). The sealing solution is not shown.

### 3.3.2. Flexible lattice structure

To reduce chignon formation, a flexible lattice structure is added. This structure prevents the scalp from being drawn into the suction cup by providing a counterforce ( $F_{latt}$ ). The lattice structure behaves like a spring which means that the counterforce increases with scalp deformation. The free-body diagram in Section 2.4.2 has been updated to include this structure as a linear spring (Figure 3.3). The revised static force equilibrium for the rigid suction cup is represented as follows:



$$F_{trac} + F_{cont,y} + F_{latt} - F_{press,y} = 0 \quad (3.1)$$

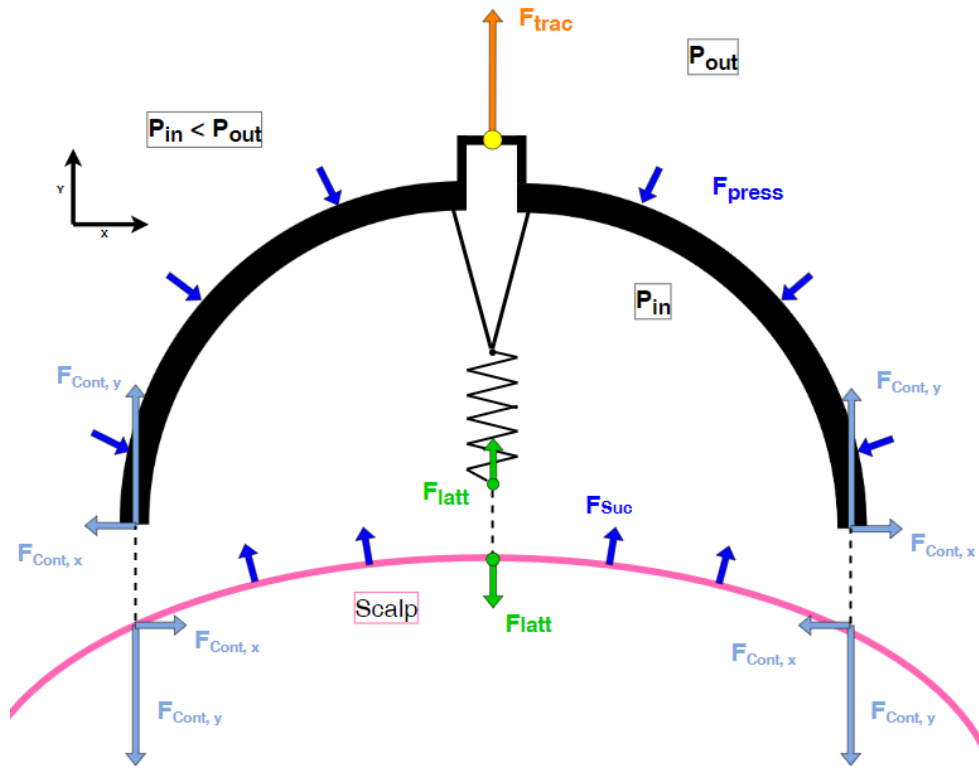


**Figure 3.3:** Free-body diagram of the suction cup with an added internal suction, showing the forces acting on the suction cup and scalp. The free-body diagram is split where the suction cup makes contact with the scalp to show the contact forces.

The contact force in this situation is calculated by combining Equation 2.2 and Equation 3.1, resulting in:

$$F_{cont,y} = \Delta P * A - F_{trac} - F_{latt} \quad (3.2)$$

To ensure attachment, the contact force should be positive, and Equation 3.2 can be rewritten as:

$$F_{trac} < \Delta P * A - F_{latt} \quad \text{for } F_{cont,y} > 0 \quad (3.3)$$

The added flexible structure provides a counterforce that reduces chignon formation, resulting in a decrease in the maximal traction force when the vacuum area ( $A$ ) and pressure difference ( $\Delta P$ ) are kept constant (Equation 3.3). However, the increased vacuum area, compared to the Kiwi replica, compensates for this reduction, resulting in a similar maximal traction force. Figure 3.4 illustrates the flexible lattice structure acting as a spring, along with its force distribution of the lattice force ( $F_{latt}$ ).

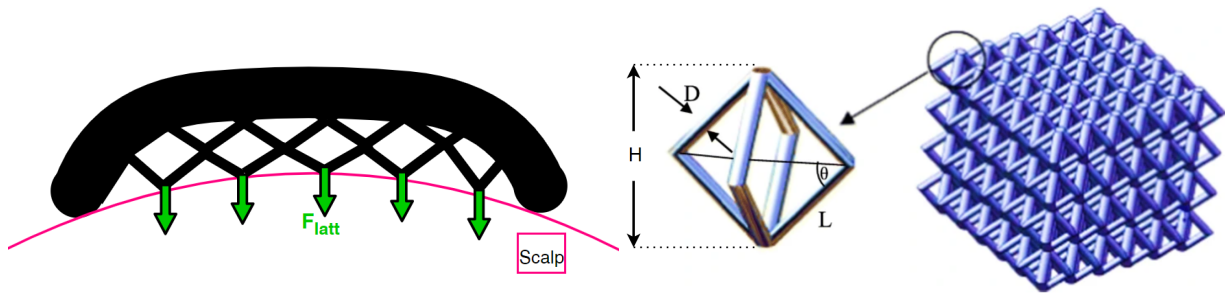


**Figure 3.4:** Schematic representation of the force ( $F_{latt}$ ) that the structure exerts on the scalp

**Figure 3.5:** The BCC lattice structure (right), consisting of unit cells (left) showing the unit cell height ( $H$ ), strut diameter ( $D$ ), strut length ( $L$ ) and strut orientation angle ( $\theta$ ) ([39])

Lattice structures have unit cells constructed from a network of struts connected at nodes forming a truss-like structure ([40]). The most commonly studied strut-based cell topologies are body-centered cubic (BCC) and face-centered cubic (FCC), as well as their variations like BCC with z-struts (BCCZ) and FCC with z-struts (FCCZ), which are named after their analogous crystalline structures. Additionally, other strut-based topologies, such as cubic, octet-truss, and diamond also exist (Figure 3.6) ([41]).

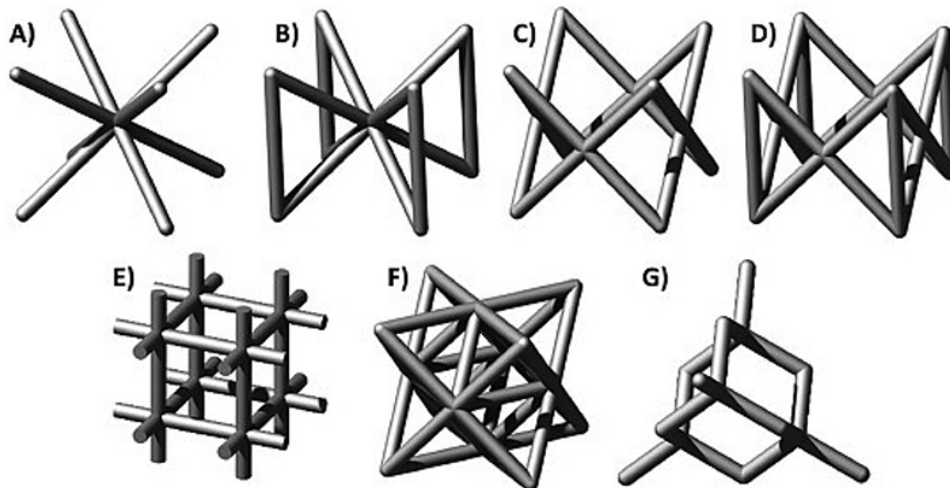


**Figure 3.6:** Different lattice structures: BCC (A), BCCZ (B), FCC (C), FCCZ (D), cubic (E), Octet-truss (F), and diamond (G) ([41]).

Many lattice configurations could be used in this analysis. However, the chosen cubic lattice structure for this study is the BCC lattice and is illustrated in Figure 3.5. The unit cell configuration of the BCC lattice in Figure 3.5 differs from that in Figure 3.6A, however when replicating both unit cells the whole structure becomes similar. The BCC lattice is chosen due to the following reasons:

- **Manufacturability:** The lattice is relatively simple to design in SolidWorks and to manufacture using FDM 3D printing techniques. Its consistent strut orientation of  $45^\circ$  reduces the likelihood of defects during the printing process.
- **Uniform stress distribution:** The BCC lattice structure has a relative isotropic stress distribution ([42]). By spreading the force evenly through the lattice, the structure minimizes the occurrence of high-pressure points that can cause localized scalp deformation. For uniform force distribution, the orientation angle ( $\theta$ ) is maintained at  $45^\circ$ .

The properties of the cubic lattice can be tuned by varying the design parameters, which are the strut diameter ( $D$ ), unit cell height ( $H$ ), and the strut orientation angle ( $\theta$ ). This tunability allows for the

customization of mechanical properties to meet specific requirements, such as varying degrees of flexibility, stiffness, and strength. It is found that the unit cell height and strut diameter is the most significant design parameter ([39]). Each unit cell comprises four nodally connected struts, which can be modeled as a combination of four parallel linear springs. Consequently, the entire lattice structure can be approximated as a linear spring using Hooke's Law, which makes calculations relative easy ([40]). This is experimentally validated by roughly measuring the displacement and corresponding lattice force, which showed linear behaviour (Appendix A.8).

### 3.3.3. Comparison flexible structure and grid structure

A schematic overview of the chignon formation for the circular grid structure and the flexible lattice structure is depicted in Figure 3.7. A flexible lattice structure has the highest potential and is recommended for incorporation into the final design. A disadvantage of grid structures is the risk of buckling. The advantages of the flexible lattice over the circular grid structure are as follows:

- **Distributed Counterforce:** The flexible lattice can be designed to distribute the counterforce as desired, thereby minimizing peak high-pressure points and local chignon formation.
- **Continuous Counterforce:** The lattice structure ensures that a counterforce is always present, which immediately limits chignon formation after the application of the VAD device, even at low pressure differences.
- **Targeted Counterforce:** The lattice structure can be designed to exert a larger counterforce at the center, where scalp deformation will be the greatest ([37]).
- **Time-Delaying factor:** Over time the suction force result in a growing chignon, which increases vascular pressure that cause rupture of blood vessels. The flexible nature of the lattice structure introduces a delay in chignon formation. With the lattice structure, the chignon is not necessary for mechanical interlocking, allowing for the immediate application of traction force. This delay provides sufficient time for the scalp to gradually deform, creating a smoother transition for the tissue. As a result, pressure increases more slowly, reducing the risk of vessel rupture ([43]).

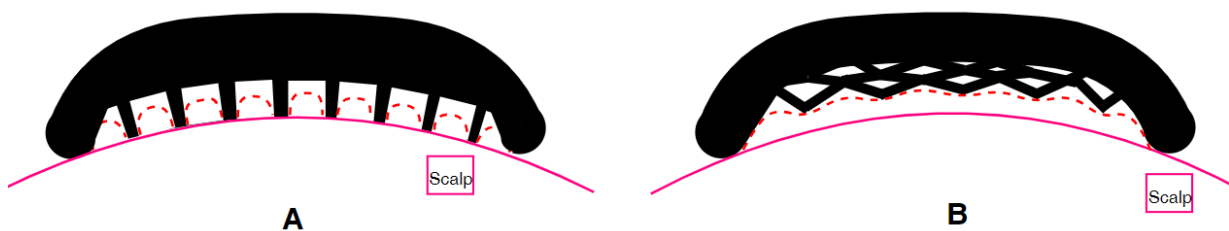


**Figure 3.7:** Schematic representation of the formation of the chignon (red dotted line) inside (A) the circular grid cavities and (B) below the flexible structure. The chignon formation is dependent on the pressure difference and stiffness of the lattice structure.

## 3.4. Increase sealing

As discussed in Section 2.4.3, excellent sealing of the suction cup cavity from the environment is necessary to maintain the pressure difference. The static force equilibrium analysis in Section 3.3.2 concludes that the added structure results in a lower contact force at the rim (Equation 3.2). This can be explained by the fact that, in addition to providing a counterforce to the scalp, the lattice structure also exerts a force that pushes the suction cup away from the scalp, thereby decreasing the contact force at the rim. However, a large contact force at the rim is desired to close leakage channels. Moreover, as discussed in Section 2.3.2, chignon formation results in 'seal pressure,' which enhances the sealing capabilities. Since the chignon formation is reduced and the contact force is distributed over an internal structure, an alternative sealing solution should be proposed.

Two sealing concepts are considered. In Section 3.4.1, a scalp-to-cup solution is proposed, where a chignon forms at the rim, utilizing the deformation of the scalp to create 'seal pressure'. The second concept, discussed in Section 3.4.2, is a cup-to-scalp solution where a flexible sealing lip acts as a spring to increase the contact force at the rim, effectively closing leakage channels.

### 3.4.1. Scalp-To-Cup sealing rim

In current Vacuum-Assisted Delivery (VAD) designs, sealing is achieved by forming a chignon. This chignon is sucked against the inner wall of the suction cup, inducing a sealing effect. In the proposed concept, a ring-shaped cavity is integrated at the rim to facilitate chignon formation locally, thereby enhancing the sealing effect (Figure 3.8A). The ring-shaped cavity must fit within the 5 mm ring. Consequently, experimental testing is required to determine whether this size is sufficient to achieve an effective sealing pressure between the scalp and cup ([22]).

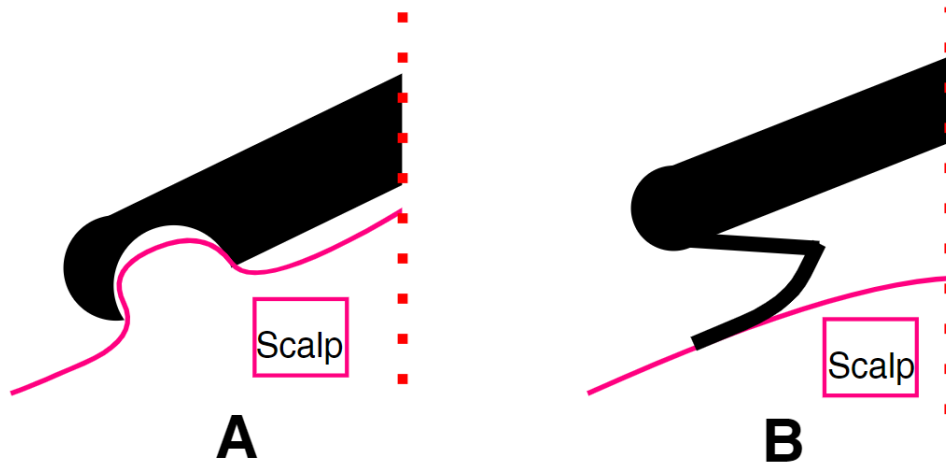


**Figure 3.8:** Schematic representation of both sealing concepts. The concept where the scalp is sealed to a cup inside (A) and the concept where the cup is sealed to scalp (B).

### 3.4.2. Cup-To-Scalp sealing rim

Drawing inspiration from industrial applications, a bellow-shaped flexible sealing rim is proposed for gripping spherical, uneven objects, such as an infant's head (Section 2.4.3). The bellows shape gives the suction cup more flexibility in height and makes it better at conforming to uneven surfaces, ensuring a tight seal ([26]). A flexible, bellow-shaped suction cup lip can enhance the seal with the scalp (Figure 3.8B). The flexibility of the lip allows it to conform around irregularities and compensate for height differences by adapting to the scalp's contours, effectively closing the leakage channels, as depicted in Figure 2.12. The bellows should have a minimal overhang angle of  $40^\circ$ , due to 3D printing limitations.

### 3.4.3. Comparison of sealing concepts

The cup-to-scalp concept is preferred over the scalp-to-cup approach. A significant drawback of the scalp-to-cup concept is the necessity of chignon formation to achieve sealing, which should be minimized. While the rigid sealing cavity may encounter difficulties, the spring-like behavior of the bellow-shaped sealing rim is expected to adapt to surface irregularities and height differences, effectively closing the leakage channels. A bellow-shaped sealing lip provides flexibility primarily in height differences, allowing it to conform to irregular surfaces without compromising the vacuum area, which makes it an interesting solution for VAD ([26]).

## Final Design

### 4.1. Final design

The final design integrates a lattice structure and a flexible sealing lip, both of which provide a counterforce to the scalp. The lattice structure is designed to distribute the counterforce, minimizing peak-pressure points and limiting chignon formation. The flexible sealing lip, exhibiting a spring-like behavior, adapts to surface irregularities and height differences, effectively closing leakage channels by providing a 'seal pressure'. The final design and its components are depicted in Figure 4.1.

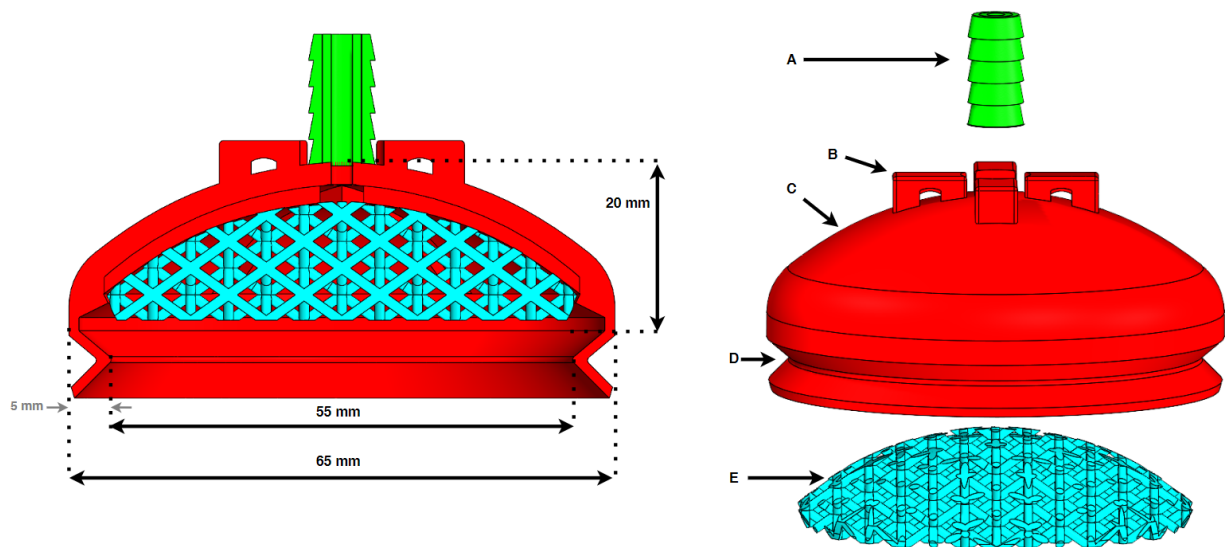


**Figure 4.1:** Cross-section (Left) and exploded view (Right) of the final design, consisting of a vacuum inlet connector (A, green), traction cable connector (B), suction cup main body (C, red), bellow-shaped sealing lip (D) and lattice structure (E, cyan).

#### 4.1.1. Bellow-shaped sealing lip

To enhance sealing performance, a sealing rim of 5 mm is proposed. A sealing rim of 5 mm is sufficient to design a bellow-shaped sealing lip that is large enough to adapt to the surface irregularities found in the infant skull model (Appendix A.9). Different sealing lip thicknesses were printed, which was a trade-off between flexibility and air-tightness, and a 1.2 mm sealing lip was chosen because smaller thicknesses resulted in air leakages due to 3D printing limitations (Appendix A.6). These air leakages were observed because maintaining a constant vacuum was very difficult. The bellow-shaped sealing lip is designed to compress as the suction force increases. Due to the material's stiffness, it acts like a spring during suction, thereby conforming to surface irregularities. The angle of the bellow should be at least  $40^\circ$  to ensure it is 3D printable. The flexible lip requires a force to form a seal. This sealing force cannot be neglected as it counteracts the suction force ( $F_{suc}$ ). The force was estimated with a kitchen scale. The suction cup was

pushed slowly on the infant surrogate while pumping. The lowest force at which a pressure difference could be created by providing a seal was 9.27 N (Appendix A.7).

#### 4.1.2. Flexible lattice structure

To determine the maximum theoretical traction force of the suction cup, Equation 2.7 is used. Using the inner diameter of 55 mm of the proposed design and maintaining a pressure difference of  $80kPa$  results in a theoretical maximum traction force of 190 N. This represents an increase of  $33N$  larger compared to the theoretical maximum traction force of the Kiwi Omnicup of  $157N$ . The combined lattice force ( $F_{latt}$ ) and the sealing force needed to conform to the scalp both result in increased probability of detachment (Equation 3.3). Therefore, those forces should not exceed 33.0 N. The proposed sealing lip functions as a spring, exerting an outward force that pushes the cup away from the scalp. The force required to establish a seal, as measured in Section 4.1.1 is 9.27 N, leaving approximately 23.7 N available for the lattice structure (Figure 3.3). From this point on, the sum of the sealing force and lattice force will be referred to as the structure force ( $F_{struc}$ ). If this limit of 33 N is exceeded, the maximum achievable traction force will be reduced, thus affecting the performance of the suction cup.

To determine the force and strain, various lattice cubical structures with  $3 \times 3 \times 3$  unit cells were experimentally tested. These lattice structures are labeled and depicted in Figure 4.2, with their corresponding parameters detailed in Table 4.1. The two parameters varied include the strut diameter and unit cell height (Figure 3.5). Specifically, cubicals A, B, C, D, and E differ in unit cell height while maintaining a constant strut diameter, whereas cubicals F, B, G, and H vary in strut diameter while keeping the unit cell height constant. The test setup and force-displacement plots for these measurements are provided in Appendix A.8. To measure the maximum forces of the different lattice structures, each was manually compressed until it no longer exhibited linear behavior, reaching what is referred to as the 'fully compressed' state (Figure 4.3, right). The fully compressed state plays an important role in the design, as it determines the maximum chignon formation inside the suction cup. The change in length to reach the fully compressed state and the corresponding force are presented in Table 4.2. Although theoretically, the lattice could be compressed further, further compression beyond the 'fully compressed' state is undesirable. At this point, the lattice behaves more like a rigid structure rather than a linear elastic spring. As a result, the structure force ( $F_{struc}$ ) will increase rapidly in response to the suction force ([40]). Additionally, if the structure becomes rigid, the effective vacuum area ( $A_{eff}$ ) will decrease, being limited by the area between the struts. A reduction of the vacuum area leads to a decrease of the maximum achievable traction force (Equation 3.3).

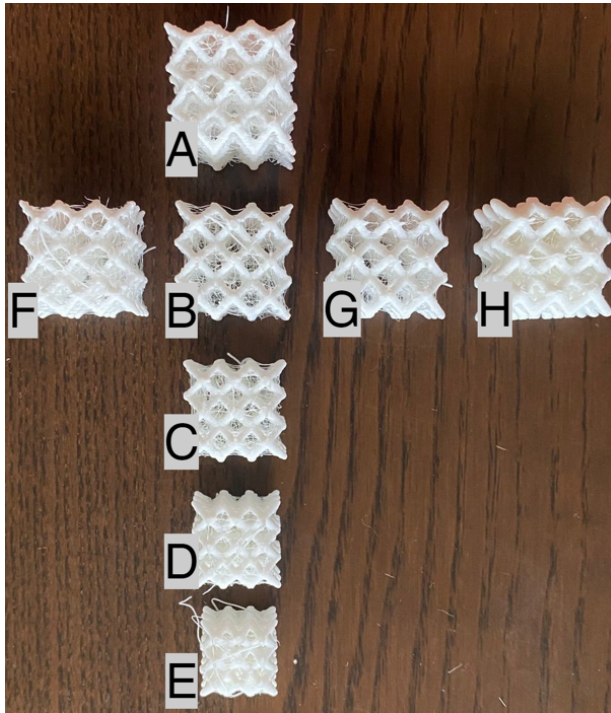


**Figure 4.2:** Different lattice structures all consisting of  $3 \times 3 \times 3$  unit cells with varying unit cell height (A-B-C-D-E) and varying strut diameter (F-B-G-H).

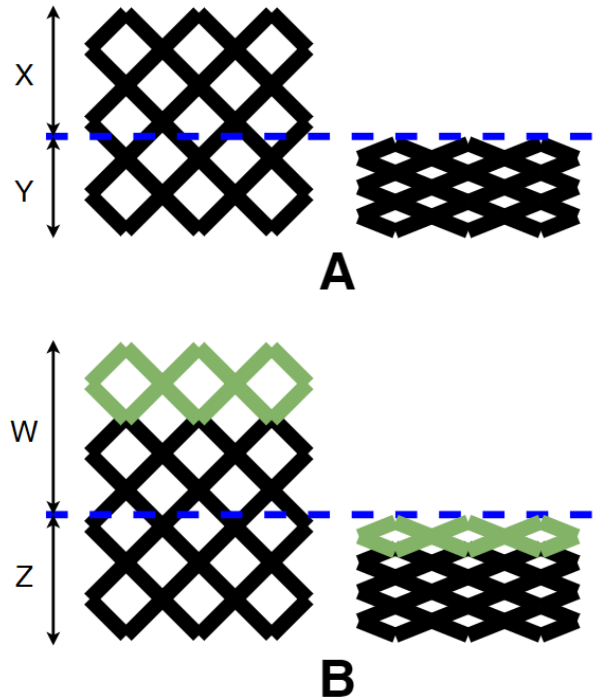


**Figure 4.3:** Lattice structures (left) with its 'fully compressed' state (right). When the unit cell height and strut diameter are kept constant, added unit cells in height (green cells) result in similar maximal strain ( $\epsilon$ ).

$$\epsilon_{LatticeA} = \epsilon_{LatticeB}: \frac{X}{X+Y} = \frac{W}{W+Z}$$

**Table 4.1:** Comparison of different lattice parameters

Lattice	Strut Diameter (D) (mm)	Unit Cell Height (H) (mm)
A	1.2	$\cos(45^\circ) \times 10 \approx 7.07$
B	1.2	$\cos(45^\circ) \times 9 \approx 6.36$
C	1.2	$\cos(45^\circ) \times 8 \approx 5.66$
D	1.2	$\cos(45^\circ) \times 7 \approx 4.95$
E	1.2	$\cos(45^\circ) \times 6 \approx 4.24$
F	1.0	$\cos(45^\circ) \times 9 \approx 6.36$
G	1.4	$\cos(45^\circ) \times 9 \approx 6.36$
H	1.6	$\cos(45^\circ) \times 9 \approx 6.36$

The lattice is assumed to behave as a linear elastic structure according to Hooke's Law ([40]). Hooke's Law, represented in Equation 4.1, states that the force  $F$  exerted by a spring is proportional to its change in length  $\Delta L$ , where  $k$  is the spring constant. Strain ( $\epsilon$ ) is the ratio of the change in length to the original length, as shown in Equation 4.2. Strain is a relative measure of deformation, and as long as the material properties remain unchanged, increasing the original length  $L_0$  does not affect the maximum strain ([40]).

$$F = k\Delta L \tag{4.1}$$

$$\epsilon = \Delta L/L_0 \tag{4.2}$$

Similarly, in lattice structures, the maximum linear strain ( $\epsilon$ ) remains constant even when additional unit cells or portions of unit cells are incorporated in the height or width, as illustrated in Figure 4.3. If the lattice structures do not have the same fully compressed state, the space required for each lattice (i.e., the shape of the suction cup) and the potential for chignon formation will vary, making comparison problematic. To facilitate a valid comparison of maximum lattice forces, the lattices are designed such that they all achieve the same fully compressed state. For this purpose, a minimum lattice height of 6 mm (fully compressed state) was selected for all tested lattices (Figure 4.2). With the difference in lattice height ( $L_0$ ) substituted with the maximum height ( $L_0$ ) minus the minimal height ( $L_{min}$ ), Equation 4.2 can be rewritten to:

$$L_0 = \frac{L_{min}}{1 - \epsilon} \quad (4.3)$$

Based on the measured maximum strain values shown in Table 4.2 (Maximum Elastic Strain), and assuming a fully compressed height of 6 mm, the maximum height of most lattice structures will remain below 15 mm (Table 4.2, Max Lattice Height). This provides sufficient space to accommodate a suction cup with a maximum thickness of 5 mm which meets the design requirements.

**Table 4.2:** Comparison of different lattice parameters and their performance. The change in length to reach the fully compressed state and the corresponding force and strain are presented. The test setup and force-displacement plots for these measurements can be found in Appendix A.8. For comparison purposes, the minimal lattice height is set to 6 mm. The new maximum lattice height is calculated, and the associated total force, when the lattice is distributed over the entire vacuum area with the same height, is shown in the last column.

Lattice	Measurement (Appendix A.8)				Calculation (Fully Compressed State ( $L_{min}$ ) = 6mm)		
	Force (N)	$\Delta L$ (mm)	Maximum Elastic Strain $\epsilon$ (%)	Fully Compressed State (mm)	# of Unit-cells (Height)	Max. Lattice Height ( $L_0$ ) (mm)	Tot. Lattice Force ( $F_{latt}$ ) (N)
A	7.4	12	57	9.2	1.9	13.8	25.4
B	8.0	11	58	8.1	2.2	14.2	38.8
C	10.0	10	59	7.0	2.6	14.6	70.5
D	15.5	9	61	5.8	3.1	15.3	173.9
E	21.6	5	39	7.7	2.3	9.9	247.7
F	5.5	15	79	4.1	4.4	28.0	52.4
B	8.0	11	58	8.1	2.2	14.2	38.8
G	12.6	9	47	10.1	1.8	11.6	48.6
H	28.4	8	42	11.1	1.6	10.3	100.2

The total lattice force distribution ( $F_{latt}$ ) at the fully compressed state (maximum desired lattice deformation) is illustrated in Figure 4.4A, assuming uniform lattice deformation and height across the entire vacuum area. Using Hooke's Law, the corresponding calculated lattice force ( $F_{latt}$ ) for the respective lattice structures are depicted in the final column of Table 4.2. However, in current VAD suction cups, the scalp deformation is greatest at the center of the suction cup ([37]). Therefore the lattice force should be highest at the center of the proposed design. As depicted in Figure 4.4B, the lattice structure is designed with a gradually decreasing height towards the rim of the suction cup, ensuring that both the lattice deformation and the corresponding counterforce decrease towards the rim. As the total height decreases, the minimal height also decreases, maintaining the same elastic strain.



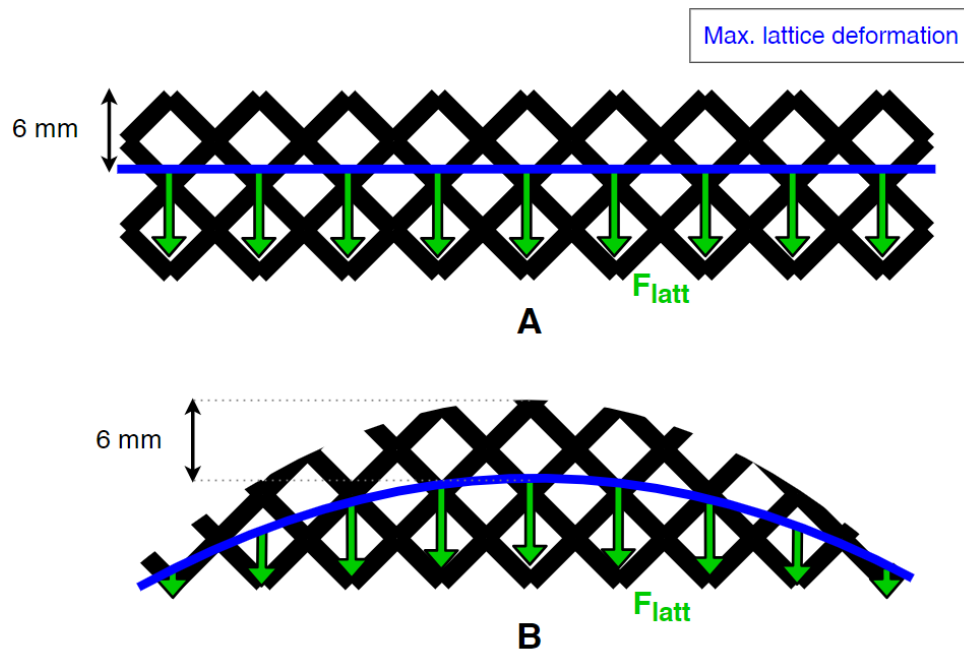


**Figure 4.4:** The blue line represents the maximum lattice deformation (Fully deformed state), set at a height of 6 mm. (A) Initially, the lattice forces ( $F_{latt}$ ) for all tested lattices are calculated based on an equal distribution of the lattices across the vacuum area, as shown in the final column (Total Force) of Table 4.2. (B) Subsequently, the lattice structure is designed with a decreasing height towards the rim of the suction cup to ensure that the total lattice force ( $F_{latt}$ ), decrease toward the rim, while maintaining uniform maximum strain throughout the entire lattice structure.

To prevent the lattice structure from reaching a fully compressed state, the 'fully compressed' position (represented by the blue line in Figure 4.5) is set 2 mm above the scalp (Appendix A.9). This configuration allows for scalp deformation of up to 2 mm, resulting in a theoretical maximal chignon formation of 14.7% compared to that produced by the Kiwi replica (Appendix A.13). However, given the unknown mechanical properties of the skin, experimental validation is required to assess whether the lattice structure generates sufficient counterforce to further reduce chignon formation to 10.0% relative to the Kiwi Replica. Should full compression occur, a stiffer lattice structure may be required. An alternative solution is to adjust the position of the blue line in Figure 4.5 (indicating the fully compressed state) further away from the scalp. This can be done by moving the whole lattice away from the scalp, although this would increase chignon formation and necessitate a larger suction cup.

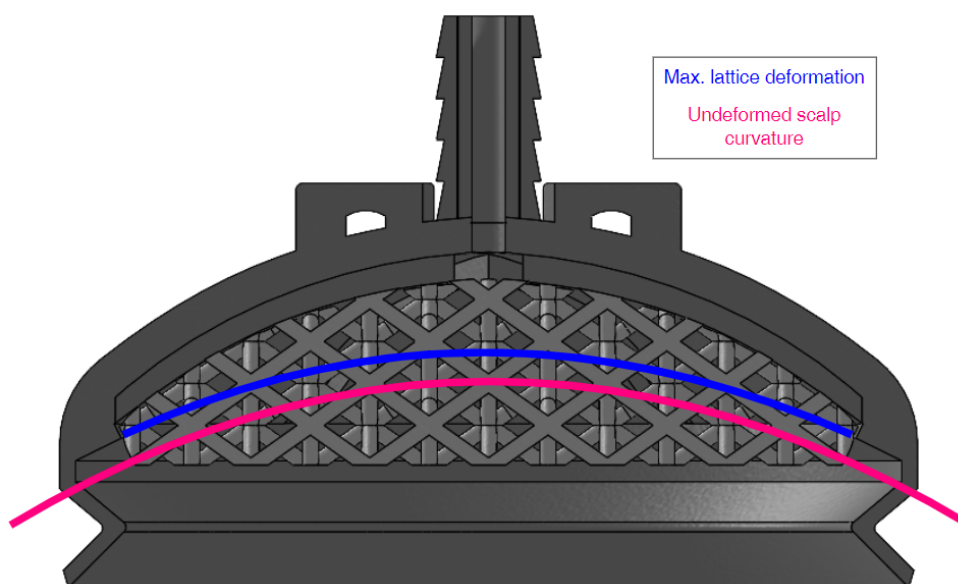


**Figure 4.5:** The pink line represents the average curvature of the infant's scalp at the flexion point (Appendix A.9). The blue line represents the maximal desired lattice deformation in the final suction cup design and is situated 2 mm from the undeformed scalp. The strain is similar for the three proposed lattice structures and therefore the maximal desired lattice deformation (the blue line) is the same in all proposed designs.

Three models with varying lattice structure parameters and corresponding total structural forces ( $F_{struc}$ ) are proposed to examine the relationship between lattice forces and scalp deformation, and to determine whether the lattice structure can exert sufficient force prior to reaching the 'fully compressed' state. For comparative purposes, it is essential that the lattices exhibit consistent maximum strain, as the external dimensions of the lattice structures remain constant across the models. Therefore, the proposed lattice structures, denoted as lattices A, B, and C, demonstrate similar maximum strains (approximately 58%, as shown in Table 4.3), while maintaining total forces close to the target structural force,  $F_{struc}$ .

Three models with varying lattice structure parameters and varying total structural forces ( $F_{struc}$ ) are proposed to examine the relationship between lattice forces and scalp deformation and how this influences the maximum achievable traction forces. For comparative analysis, it is advantageous for the lattices to exhibit uniform maximum strain. With similar strain, the outer dimensions of the lattice structures will be consistent across all models, allowing the suction cup dimensions to remain the same for each configuration. Therefore, the proposed lattice structures are lattices A, B, and C. These lattices have similar maximum strain ( $\approx 58\%$ , Table 4.2), while maintaining total forces relative close to the target structural force ( $F_{struc}$ ) of 33 N. Keeping the bottom part of the lattice horizontal, the 58% strain value is used to calculate the total lattice height at every point based on the skull's curvature (blue line in Figure 4.5) in SolidWorks. This results in a maximum lattice force that decreases towards the rim. The total lattice force for the three models was calculated separately by dividing the lattice into sections, as illustrated in Figure 4.6. After measuring the maximum lattice deformation until the lattice reaches the 'fully compressed' state, the lattice force and pressure for each section can be calculated independently. The total structure forces ( $F_{struc}$ ) for the three models are presented in Table 4.3, showing a variation of approximately 10 N between the models.

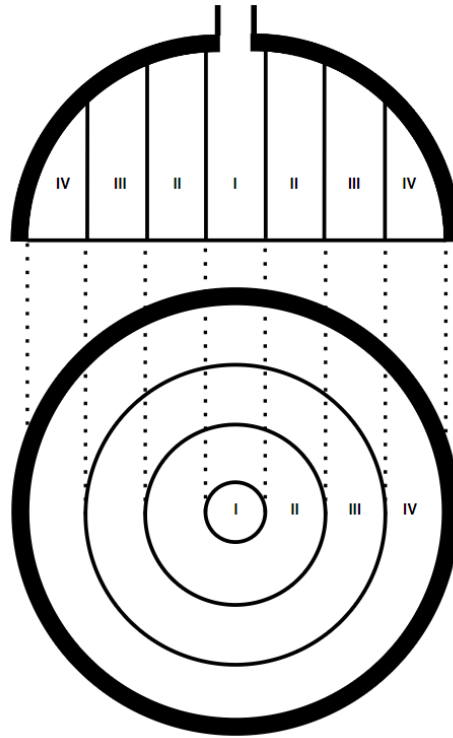


**Figure 4.6:** The sections of the lattice structure

**Table 4.3:** Lattice force variation for the three proposed model iterations, showing the pressure and force exerted by the lattice structures for every section when the lattice is 'fully compressed'. The last column depicts the total structure force ( $F_{struc}$ ) of the lattice structure and the sealing lip force, which should theoretically be less than 33 N.

Model Iterations	Section I		Section II		Section III		Section IV		Sealing Lip Force (N)	Tot. lattice Force (N)	Total Force ( $F_{struc}$ ) (N)
	Pressure (Pa)	Force (N)	Pressure (Pa)	Force (N)	Pressure (Pa)	Force (N)	Pressure (Pa)	Force (N)			
<b>Model 1 (Lattice C)</b>	28815	1.4	25864	10.0	18180	14.1	6881	8.0	9.3	33.5	<b>42.8</b>
<b>Model 2 (Lattice B)</b>	16334	0.8	14974	5.8	11727	9.1	6314	7.4	9.3	23.1	<b>32.3</b>
<b>Model 3 (Lattice A)</b>	10925	0.5	10016	3.9	7191	5.6	2780	3.2	9.3	13.2	<b>22.5</b>

A variation of 10 N in the structure forces leads to a corresponding change in the theoretical achievable traction force ( $F_{trac}$ ). An increase in structure force is expected to reduce the maximum traction force (Equation 3.3). However, whether the fully deformed state and maximum structure forces are achieved depends on the mechanical properties of the skin and will be evaluated experimentally. A bottom and side view of the three proposed designs with varying lattice structures is shown in Figure 4.7. It is observed that all models possess similar overall dimensions; however, the unit cell dimensions vary, from small unit cells in model 1 (which exhibits a large structural force) to large unit cells in model 3 (which exhibits a smaller structural force). Smaller structural forces are theoretically associated with an increased risk of chignon formation; however, they may also allow for the achievement of higher traction forces (Equation 3.3).

**Table 4.4:** Theoretical traction forces for the different models are compared to the Kiwi replica. These forces were calculated by subtracting the structure forces in the fully compressed state from the theoretical traction force without the lattice structure and sealing lip (Equation 3.3).

	Kiwi replica	Model 1	Model 2	Model 3
Theoretical traction force (No structure) (N) (Equation 2.7)	157.1	190.1	190.1	190.1
Structure force ( $F_{struc}$ ) (N) (Table 4.3)	0.0	42.8	32.3	22.5
Theoretical traction force (With structure) (N) (Equation 3.3)	157.1	147.3	157.8	167.6

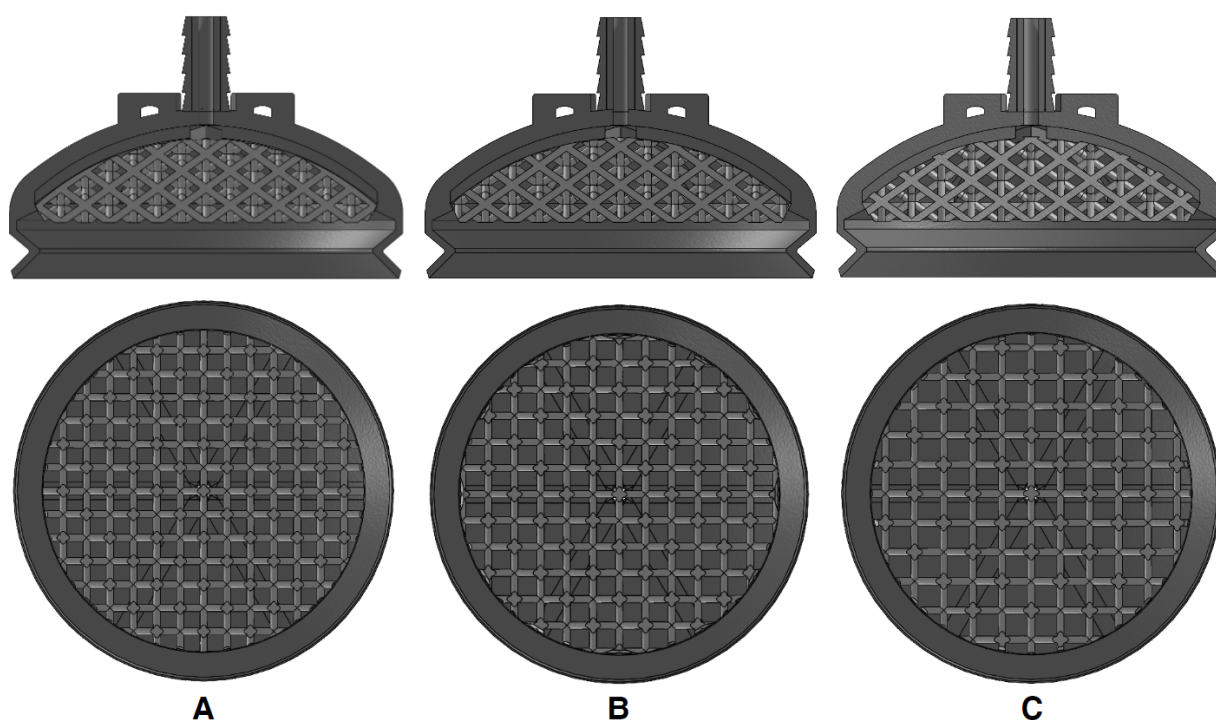


**Figure 4.7:** The final proposed designs showing the side- and bottom view for model 1 (A), model 2 (B) and model 3 (C).

#### 4.1.3. Vacuum inlet suction, cup thickness and grooves

In the current Kiwi OmniCup® design, the vacuum inlet is positioned on the side (Figure 2.2). In this study, the vacuum inlet and traction cable connectors are placed on top of the suction cup to facilitate testing in the direction normal to the vacuum area, which is the primary focus of this study. The addition of the vacuum inlet and traction cable connectors increases the overall height of the suction cup, which is deemed suitable for evaluation during the testing phase. Future studies could integrate the traction cable within the suction tube, allowing for the evaluation of maximum traction force when applying a force at an angle. The vacuum inlet diameter is varied to determine the optimal diameter at which no leakage occurs. The methodology for this testing is detailed in Appendix A.10.

The outer dimensions of the lattice structure are determined based on the scalp curvature and the required lattice dimensions. The highest part of the lattice structure is at the center, measuring 14.15 mm. Requirement R6 specifies that the outer dimensions of the suction cup should be 20 mm from the scalp. Consequently, the wall thickness for all three models is chosen to be 4.7 mm, which makes the total height of the cup 20 mm when the sealing lip is fully compressed (Figure 4.1).

It is expected that the lattice structure will ensure the negative pressure difference is evenly distributed over the entire vacuum area due to the spaces between the struts. However, to increase the chance that the negative pressure is distributed over the whole vacuum area grooves are incorporated into the final design (Figure 4.7)

## 4.2. Prototype Development

A schematic representation of an FDM printer is shown in Figure 4.8. To build an object, hot thermoplastic filament is melted and extruded through a heated nozzle in multiple layers [44]. Various parameters affects print quality like nozzle diameter, temperature, print speed, print pattern, and layer height can be adjusted to enhance the print quality.

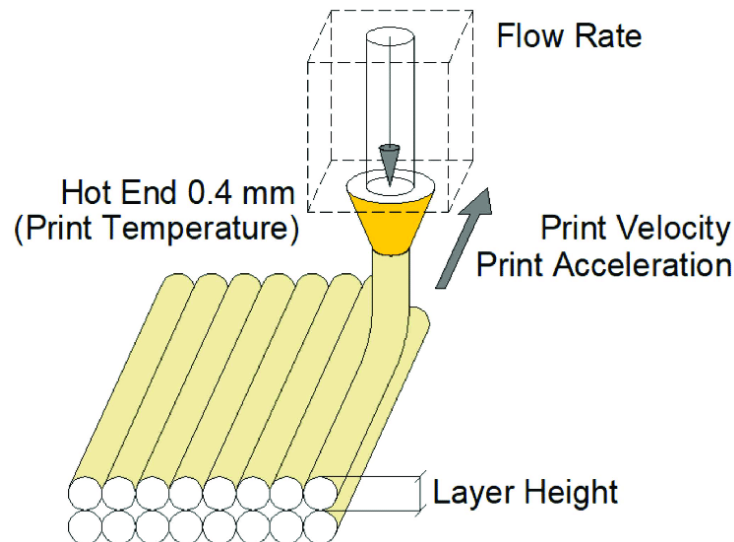


**Figure 4.8:** Schematic representation of a Fused Deposition Modeling (FDM) 3D printer ([45])

Printing with TPU introduces additional challenges due to its flexibility. Stringing, where filament unintentionally leaks between different parts of the print, can result in a web-like appearance and cause under-extrusion in other areas. Extrusion is also more difficult because the extruder may slip while extruding TPU. Therefore, the material flow ratio is increased. The print speed is reduced to prevent under-extrusion, a condition where the nozzle moves too quickly for the filament to extrude properly. This reduction in speed is further applied to the walls, the parts of the design that come into contact with the environment, to ensure an airtight seal. These and other printer settings to make the suction cup airtight and printable are depicted below:

- **Layer Height:** 0.20 mm
- **Line Width:** 0.42 mm
- **Wall Line Count:** 6.00
- **Infill Density:** 100.00%
- **Printing Temperature:** 245.00 °C
- **Build Plate Temperature:** 50.00 °C
- **Print speed:** 22 mm/s
- **Inner Wall Speed:** 11.00 mm/s
- **Outer Wall Speed:** 11.00 mm/s
- **Material Flow Ratio:** 175.00%

The final prototypes are depicted in Figures 4.9 and 4.10.



**Figure 4.9:** Side view of all 3D-printed models, with model 1, model 2, and model 3 shown from left to right.



**Figure 4.10:** Bottom view of all 3D-printed models, with model 1, model 2, and model 3 shown from left to right.

# 5

## Experimental validation

### 5.1. Goal

The main goal of this research is to develop a novel suction cup design aimed at reducing chignon formation while maintaining sufficient adhesive performance. The experimental goal is to investigate the performance of the three model iterations of the final VAD design in comparison to a standard Kiwi replica. This performance was evaluated in two aspects: 1) the maximum traction force achieved by the suction cups. And 2) the displacement of the scalp inside the suction cup, which is a measurement of chignon formation. In this manner, the influence of the lattice stiffness on these performance aspects will also be evaluated. Additionally, the performance of the suction cups will be evaluated under two environmental conditions: in a dry environment and with lubricant applied to the silicone scalp.

### 5.2. Experimental setup

An overview of the experimental setup is shown in Figure 5.1. The suction cups are connected to the load cell (LSB-200, Pimzos, The Netherlands), via traction cables and attached to the infant surrogate model. Suction is induced by creating negative pressure using a manual vacuum pump (14-Piece Vacuum Pump Set, HBM Machines, The Netherlands) (Figure 5.2). A linear stage (SSM 24Q, MOONS', CHINA) operates at an upward velocity of 0.5 mm/s. The traction force is measured by a load cell positioned between the linear stage and the suction cup, with the load cell connected to the suction cup via four steel chains. The displacement of the scalp is measured by a displacement sensor (optoNCDT 1420-50LL, Micro-epsilon, Germany) located inside the infant surrogate model (Figure 5.1). The sensor measures the height of the scalp through a hole inside the skull model located at the flexion point. All parts are mounted on a breadboard (MB1560/M, THORLABS, USA)

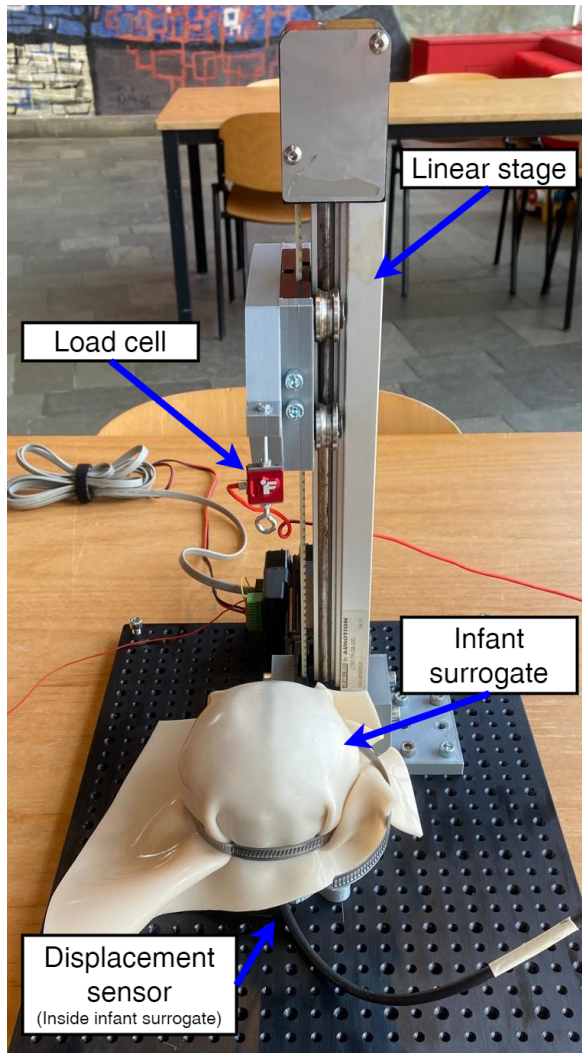


Figure 5.1: Overview of test setup

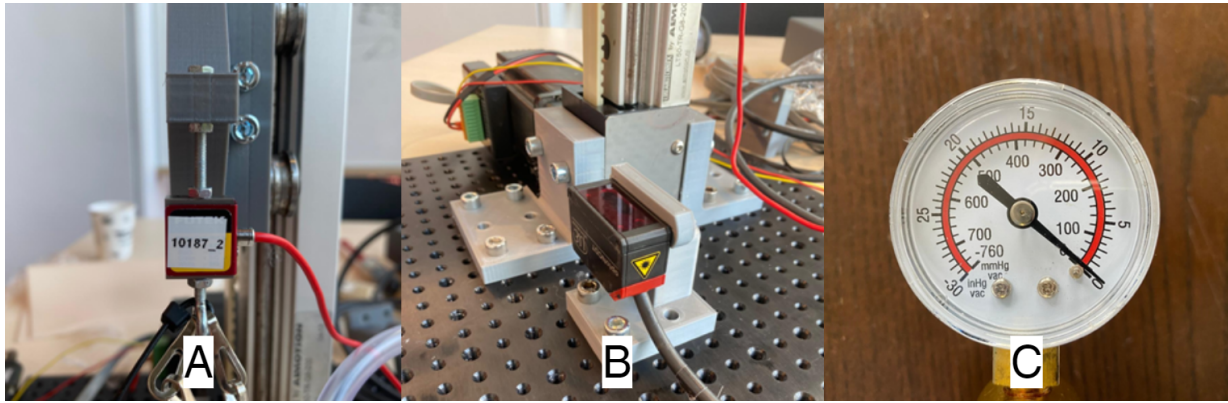


Figure 5.2: The vacuum pump that is used in this study

The measurement instruments used in this study are depicted in Figure 5.3 and are as follows:

- **Load Cell, LSB-200 (Pimzos).** The load cell is positioned between the linear stage and suction cup, calibrated to measure traction forces up to 250 N with high precision ( $\pm 0.1\%$ ) (Figure 5.3A).
- **Displacement Sensor, optoNCDT 1420-50LL (Micro-epsilon).** The displacement sensor, located inside the infant surrogate, has a measurement range of 50 mm and an accuracy of  $\pm 40\mu\text{m}$ . A 3D-printed holder mounts the sensor on the breadboard (Figure 5.3B).
- **Vacuum Gauge, 14-Piece Vacuum Pump Set (HBM Machines).** The pressure difference ( $\Delta P$ ) is controlled using a manual vacuum pump, with the pressure difference measured using an analog gauge (Figure 5.3C).





**Figure 5.3:** The measurement instruments utilized in this study are as follows: (A) a load cell for tracking traction forces, (B) a displacement sensor for measuring scalp displacement, and (C) an analog pressure gauge for monitoring pressure levels.

The manufactured models shown in Figures 4.9 and 4.10 will be tested. The final designs will be compared to the Kiwi replica, which will be made out of a rigid plastic (Polylactic Acid (PLA)). The dimensions of the Kiwi replica is depicted in Figure 5.4 and the 3D-printed model is shown in Figure 5.5.

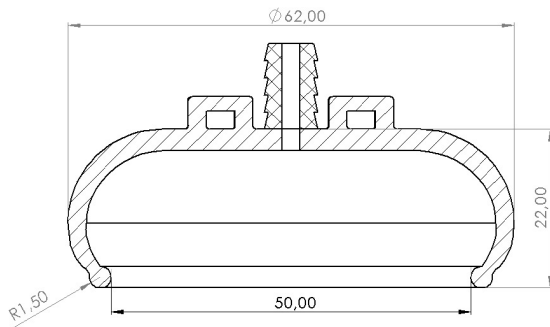


**Figure 5.4:** Section view of the Kiwi replica, showing the dimensions



**Figure 5.5:** 3D-printed Kiwi replica (bottom view)

### 5.2.1. Infant surrogate design

To compare the proposed design to the Kiwi replica, a 3D model of an infant's skull is used in this analysis (Appendix A.9). The model, scaled to represent an average-sized newborn ([46]), is depicted in Figure 5.6A. The model is positioned so that the flexion point faces upwards for suction cup application. Additionally, mounting holes are incorporated to secure the surrogate on the breadboard, and a hole is designed at the center to allow the laser from the displacement sensor to pass through the skull and measure scalp displacement. The infant head surrogate is 3D-printed with PLA. To mimic underlying scalp tissue, a sponge is placed between the scalp and skull, as shown in Figure 5.6B. Finally, a silicone synthetic tattoo practice skin (Synthetic Practice Vel A3, Reelskin, UK) is stretched over the model to mimic the scalp (Figure 5.6C).

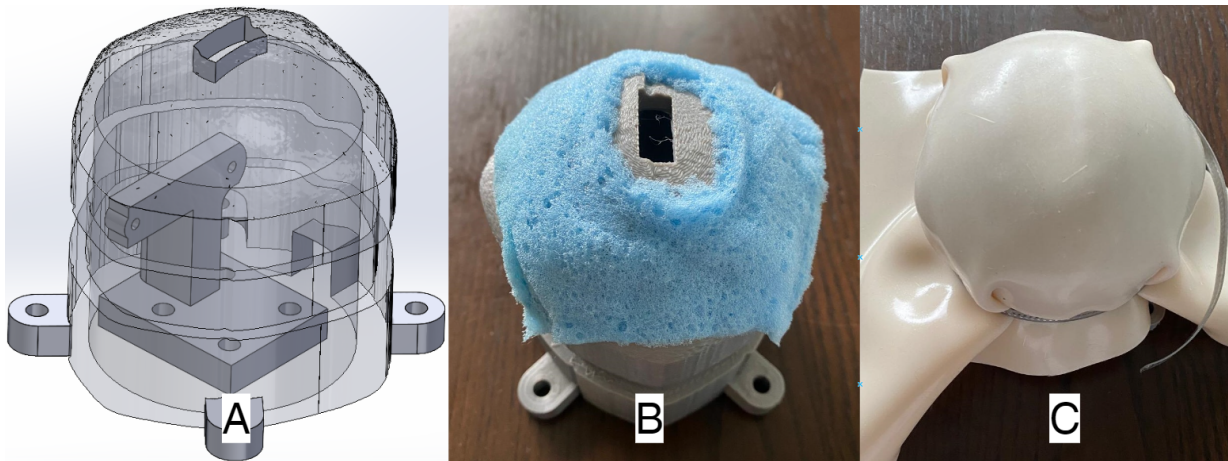


**Figure 5.6:** Development of the infant surrogate. Infant surrogate 3D model ([47]), depicting the hole for the displacement sensor at the flexion point and showing the holder for the sensor inside the model (A), infant surrogate with sponge to mimic underlying scalp tissue (B) and the final infant surrogate model with a silicon scalp (C).

### 5.3. Experimental protocols

Two different environmental conditions are tested during the experiments. The first condition is dry silicone, as depicted in Figure 5.7A. The second condition involves a silicone-based lubricant (MI Glijmiddel, Etos), shown in Figure 5.7B. A silicone-based lubricant is chosen as it tends to evaporate more slowly than water-based lubricants. The lubricant is deposited and evenly distributed with a paintbrush between each measurement to ensure a consistent amount of lubricant. Before starting the experiments, both the load cell and the displacement sensor were calibrated to ensure accurate measurements:

- The load cell was calibrated by measuring the force when the traction cables were not under tension, accounting for the weight of the traction cables and connection rings.
- The displacement sensor was calibrated by measuring the distance of the scalp when no suction cup was attached.

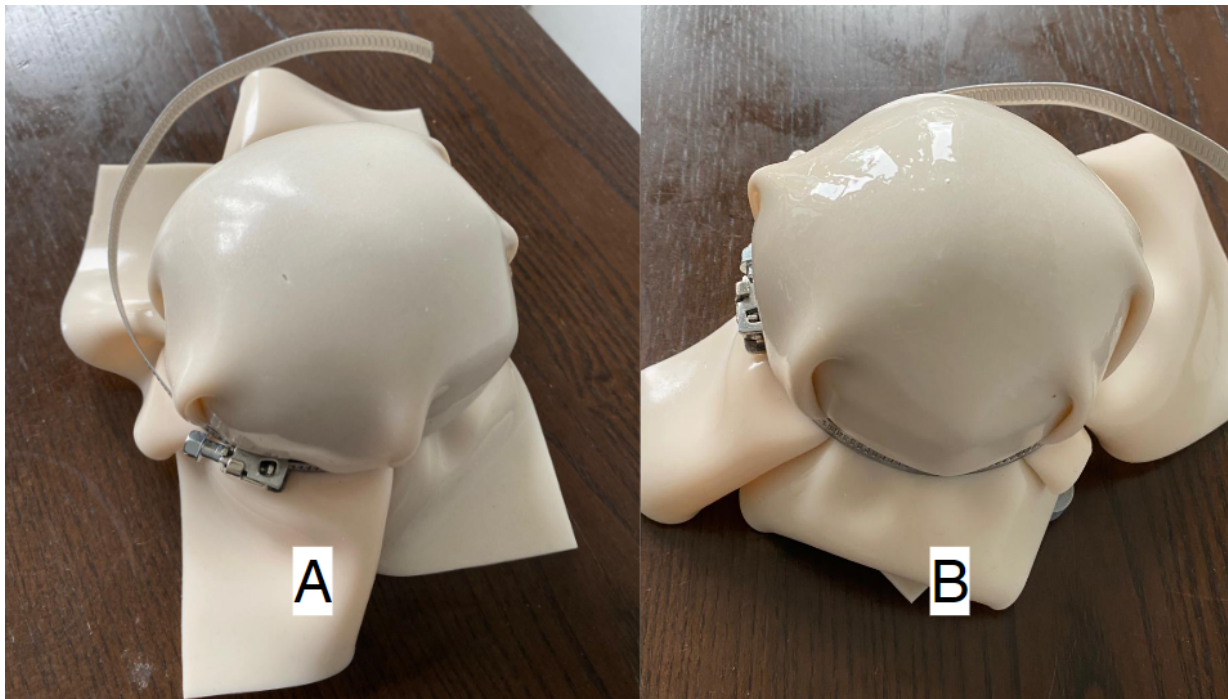


**Figure 5.7:** The three different environments tested: dry silicone surface (A), silicone-based lubricant surface (B).

### 5.3.1. Experiment 1: Maximum traction force and scalp displacement

In this experiment, the performance of the proposed designs was compared to that of the Kiwi replica. While the traction force is increased by pulling with a prescribed movement, the traction force and displacement were measured simultaneously until detachment occurs.

The procedure for the experiment is as follows:

1. Position the suction cup on the flexion point of the infant surrogate.
2. Establish a pressure difference of 80 kPa (equivalent to 600 mmHg). The pressure gauge displays the pressure difference in mmHg, and a conversion table from mmHg to kPa is provided in Appendix A.14.
3. Monitor the pressure difference during testing, which may decrease due to leakage. Perform an extra pump when the pressure gauge measures 560 mmHg. One pump increases the pressure difference back to 640 mmHg, maintaining the pressure difference between 560 and 640 mmHg until detachment occurs.
4. Once the suction cup is attached to the infant surrogate, move the linear stage upwards at a velocity of 0.5 mm/s. This movement is controlled with Q-programmer and increases the traction force and displacement until detachment occurs.
5. Repeat the experiment five times for each model in both dry and lubricant environment.

### 5.3.2. Experiment 2: Displacement without traction force

In this experiment the displacement of scalp is measured without applying a traction force to determine chignon formation. After positioning the suction cup on the flexion point, the pressure is increased from 0 to 600 mmHg in increments of 100 mmHg. At each increment, the displacement of the scalp is recorded. This experiment is repeated three times for every model in a dry environment.

### 5.3.3. Experiment 3: Pressure loss rate

This experiment aims to assess the sealing capabilities of the suction cup designs by measuring the pressure loss rate. The results from this experiment will provide insights into the sealing efficiency of each suction cup design compared to the Kiwi replica. A lower rate of pressure loss indicates a more effective seal, which reduces the frequency of manual pumping needed and decreases the risk of suction cup detachment. Similar to Experiment 2, the suction cups are not connected to the load cell. The procedure is as follows:

1. Position the suction cup on the flexion point.
2. Apply a pressure difference of 600 mmHg.
3. Record the time taken for the pressure to decrease by 100 mmHg using a stopwatch. Continue this process until detachment occurs.
4. If the duration exceeds 300 seconds, record it as 300+.
5. Repeat the experiment three times for each suction cup model.
6. Perform the experiment under both dry and lubricant conditions to compare the sealing performance.

## 5.4. Experimental variables

The **independent variables** are:

- **Model Variations:** Different suction cup models with varying lattice forces are tested. This variable allows for the comparison of performance characteristics across different designs, aiming to identify the optimal configuration for reducing chignon formation while maintaining adhesive performance.
- **Environmental Conditions:** The experiments are conducted under two different conditions—dry and with a silicone-based lubricant.
- **Pressure Difference:** The negative pressure applied by the suction cup is manipulated in Experiments 1 and 2. In Experiment 1, a constant pressure difference is maintained between 560 and 640 mmHg. In Experiment 2, the pressure is increased in increments of 100 mmHg from 0 to 600 mmHg.

The **dependent variables** are:

- Traction Force: Measured using the calibrated load cell, this variable quantifies the force applied to the suction cup before detachment occurs.
- Displacement: Recorded by the displacement sensor, this variable measures the displacement of the scalp within the suction cup.
- Pressure Loss Rate: In Experiment 3, the rate at which the pressure decreases due to leakage is recorded using a stopwatch. This variable assesses the sealing capabilities of the suction cup designs by measuring the time taken for the pressure to drop by 100 mmHg until detachment occurs. Therefore, the pressure difference acts as a dependent variable in this experiment.

## 5.5. Data analysis

The data collected from the load cell and displacement sensor are processed using LabVIEW 2018, Excel, and Python. Initially, the datasets are acquired and recorded in LabVIEW 2018. These datasets are then processed in Excel or Python for data visualization. Python is used to plot the datasets over time, providing a visualization of the sensor output. Additionally, Python scripts extract the maximum values from both the load cell and displacement sensor datasets. These maximum values are used to create boxplots in Excel, which help to understand the data distribution and variability. For the ratio between the maximum force and maximum displacement and for the visualization of the pressure loss rate, Python is used to generate boxplots. The displacement data without applied traction force is plotted in Excel to interpret how the displacement varies for different pressure differences.

## 5.6. Test results

### 5.6.1. Experiment 1 results: Maximal traction force and displacement

The experiments demonstrate that the Kiwi replica achieves the highest traction forces and displacement in both dry and lubricated environments. The three proposed models exhibit significantly lower maximum traction forces in both conditions, as illustrated in Figures 5.8 and 5.9. Additionally, all models show a slight reduction in maximum traction forces in the lubricated environment compared to the dry environment.

Figures 5.10 and 5.11 present the maximum displacement for the dry and lubricated environments, respectively. The Kiwi replica exhibits the largest maximum displacement, while the displacements for the three proposed models are significantly lower in both environments. The mean theoretical and measured values are summarized in Table 5.1.

**Table 5.1:** Comparison of theoretical (Theo.) and measured (Meas.) values for traction force ( $F_{trac}$ ) and displacement across different models.

	Kiwi replica		Model 1		Model 2		Model 3	
	Theo.	Meas.	Theo.	Meas.	Theo.	Meas.	Theo.	Meas.
Mean max. $F_{trac}$ (Dry) (N)	157.1	94.1	147.2	42.7	157.7	46.0	167.5	50.5
Mean max. $F_{trac}$ (Lube) (N)	157.1	84.9	147.2	39.4	157.7	45.1	167.5	47.6
Mean max. disp. (Dry) (mm)	x	39.8	x	8.4	x	11.6	x	14.4
Mean max. disp. (Lube) (mm)	x	37.4	x	7.6	x	11.4	x	13.1

Model 1, characterized by the highest structural force ( $F_{struc}$ ), achieves the lowest maximum traction force and displacement. As the structural force decreases in Models 2 and 3, both the maximum traction force and displacement increase.

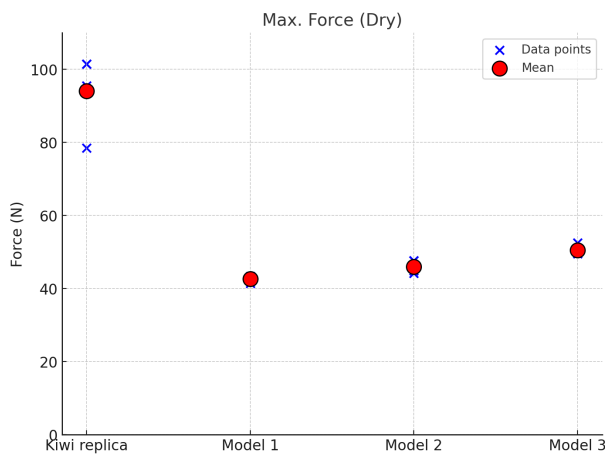


**Figure 5.8:** The maximum traction force achieved by the three models and the Kiwi replica under dry conditions.

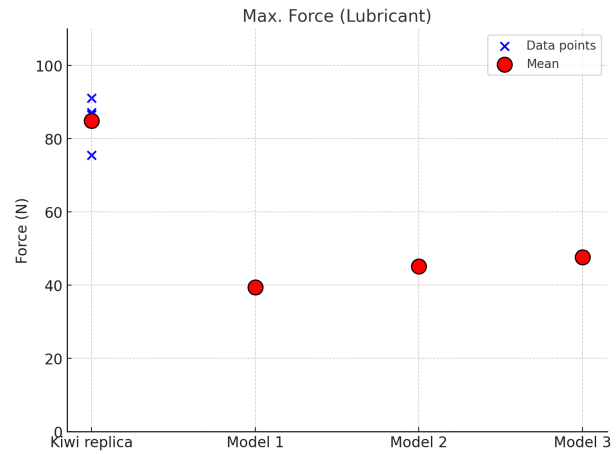


**Figure 5.9:** The maximum traction force achieved by the three models and the Kiwi replica under lubricated conditions.

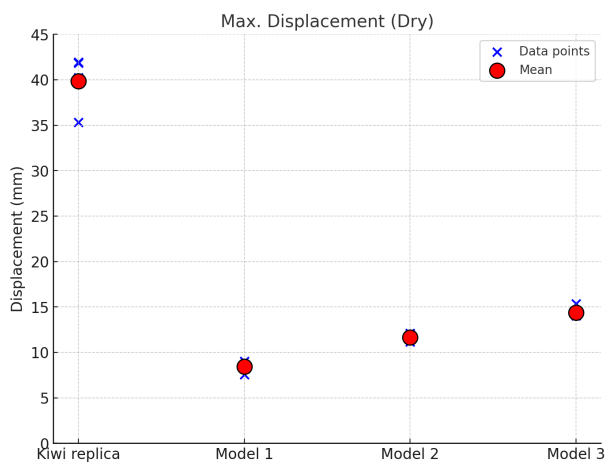


**Figure 5.10:** The maximum displacement of the silicon scalp within the three models and the Kiwi replica under dry conditions when a traction force is applied.

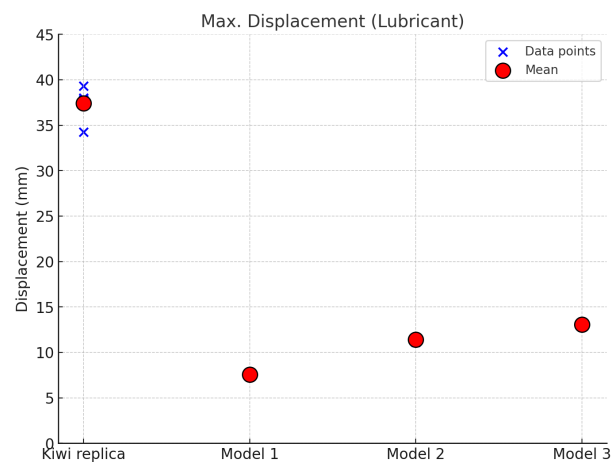


**Figure 5.11:** The maximum displacement of the silicon scalp within the three models and the Kiwi replica under lubricated conditions when a traction force is applied.

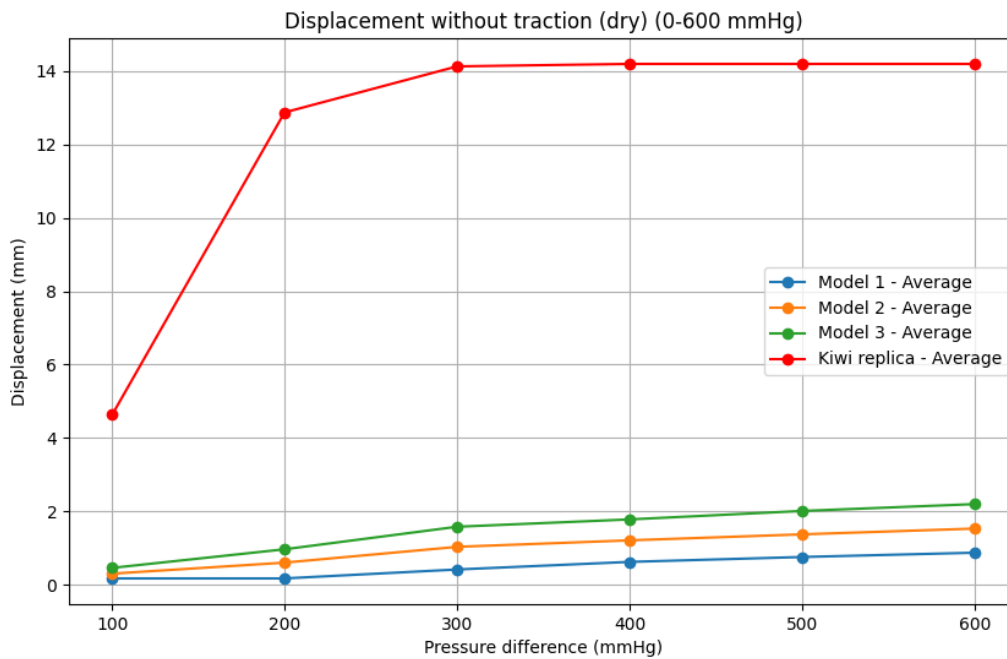
### 5.6.2. Experiment 2 results: Displacement without traction force

Figure 5.12 presents the average displacement of the scalp under varying levels of negative pressure without applying any traction force. The graph compares the performance of the three proposed models with the Kiwi replica.

The Kiwi replica exhibited the highest displacement values, showing already large displacements at low pressure differences. The deformation in the Kiwi replica reaches a maximum of 14.19 mm, indicating that the silicone scalp is fully drawn against the ceiling of the suction cup cavity. Model 1, Model 2, and Model 3 showed substantially lower displacement at maximal pressure difference compared to the Kiwi replica. With a mean maximum displacement of 0.88 mm, 1.54 mm and 2.20 mm respectively (Table 5.2). All three models demonstrated a relatively consistent increase in displacement with increasing pressure difference. Model 3 is the only proposed model where the scalp is deformed more than 2 mm, this indicates the the lattice structure is 'fully compressed' (Figure 4.5).

**Table 5.2:** Comparison of the displacement between the Kiwi replica and the proposed models at a pressure difference of  $600\text{mmHg}$  when no traction force is applied.

	Kiwi replica	Model 1	Model 2	Model 3
Mean max. displacement (mm)	14.19	0.88	1.54	2.20
Percentage compared to the Kiwi replica	100.0%	6.2%	10.8%	15.5%



**Figure 5.12:** The displacement of the silicon scalp within the three models and the Kiwi replica under dry conditions for incrementally increased pressure differences ( $\Delta P$ ).

### 5.6.3. Experiment 3 results: Pressure loss rate

Figures 5.13 and 5.14 present the pressure loss rates for different models under dry and lubricated conditions, respectively. The box plots show the time taken for the pressure to decrease from  $600\text{mmHg}$  to  $100\text{mmHg}$  in increments of  $100\text{mmHg}$  for Model 1, Model 2, Model 3, and the Kiwi replica. Increments of  $100\text{mmHg}$  are selected for measurement due to their ease of readability on the pressure gauge (Figure 5.3C).

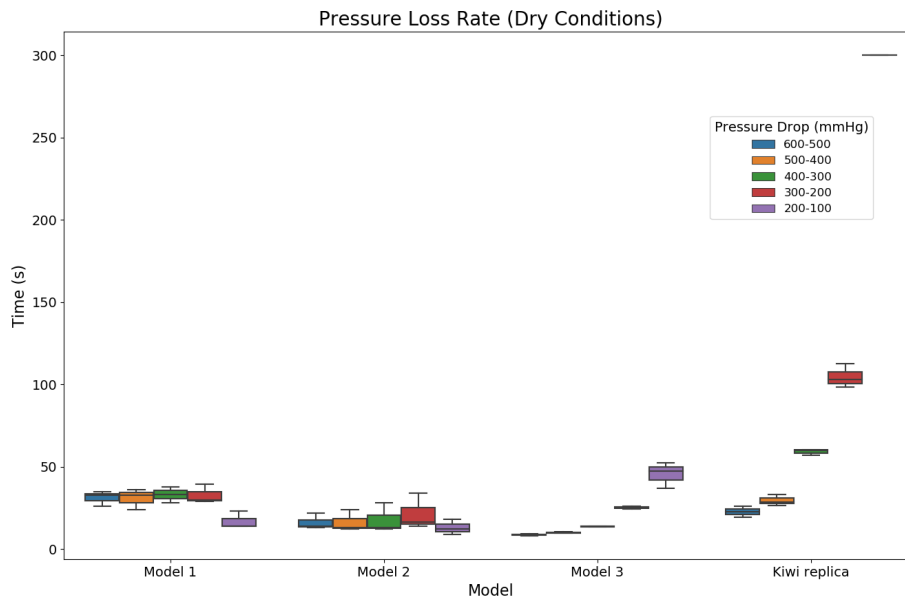


**Figure 5.13:** Box plot showing the pressure loss rate under dry conditions for three models and the Kiwi replica across various pressure drop ranges (600-500 mmHg, 500-400 mmHg, 400-300 mmHg, 300-200 mmHg, and 200-100 mmHg).

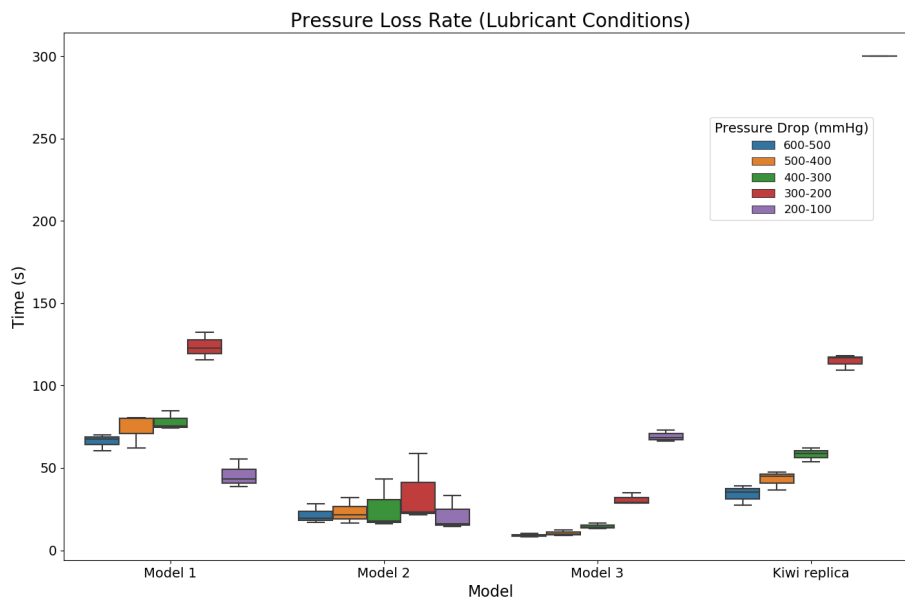


**Figure 5.14:** Box plot showing the pressure loss rate under lubricant conditions for three models and the Kiwi replica across various pressure drop ranges (600-500 mmHg, 500-400 mmHg, 400-300 mmHg, 300-200 mmHg, and 200-100 mmHg).

#### 5.6.4. Detachment observations

Videos taken during Experiment 1 reveal that the sealing lip begins to curl prior to detachment. This curling leads to a loss of negative pressure, resulting in rapid detachment. The curling is most likely attributed to

the overall deformation of the suction cup. Figure 5.15 illustrates the deformation of the suction cup during Experiment 1. It is evident that immediately before detachment, the suction cup adopts a more pointed shape. This change in shape reduces the vacuum area ( $A$ ) and contributes to the curling of the sealing lip. The curling of the sealing lip of the three models prior to detachment is depicted in Figure 5.16.



**Figure 5.15:** Deformation of the suction cup. (A) The suction cup before the application of traction force, and (B) the suction cup prior detachment. The images illustrate the deformation of the entire cup during experiment 1.



**Figure 5.16:** Observation of a curling lip immediately prior to detachment. The images from left to right correspond to Model 1, Model 2, and Model 3. The red arrows indicate the location of the sealing lip that curls which result in leakage of negative pressure

### 5.6.5. Evaluation of suction cup performance using the Force/Displacement ratio

Given that the maximum achievable traction force and the maximum displacement of the scalp for the proposed designs are both significantly lower than those for the Kiwi replica, directly comparing overall performance is challenging. To address this, the ratio of traction force to scalp displacement ( $N/mm$ ) is calculated. This ratio serves as a measure of the amount of traction force applied per millimeter of scalp deformation (chignon formation). A high traction force/displacement ratio indicates that the suction cup can transmit a significant traction force while causing minimal chignon formation, which is desirable. This ratio is calculated immediately prior detachment (maximal traction force and maximal displacement) and the results are depicted in Figure 5.17. The mean values are depicted in Table 5.3. The higher traction force/displacement ratios of the proposed designs demonstrate their improvement compared to the Kiwi replica. Compared to the Kiwi replica, Model 1 demonstrates the greatest improvement in this ratio, with an increase factor of 2.15 in a dry environment and 2.30 in a lubricant environment.



**Table 5.3:** Mean ratio of maximal traction force to maximal displacement for different models in dry and lubricant Conditions

Model	Mean Ratio (Dry) (N/mm)	Mean Ratio (Lube) (N/mm)
Kiwi replica	2.36	2.27
Model 1	5.06	5.22
Model 2	3.95	3.96
Model 3	3.51	3.64

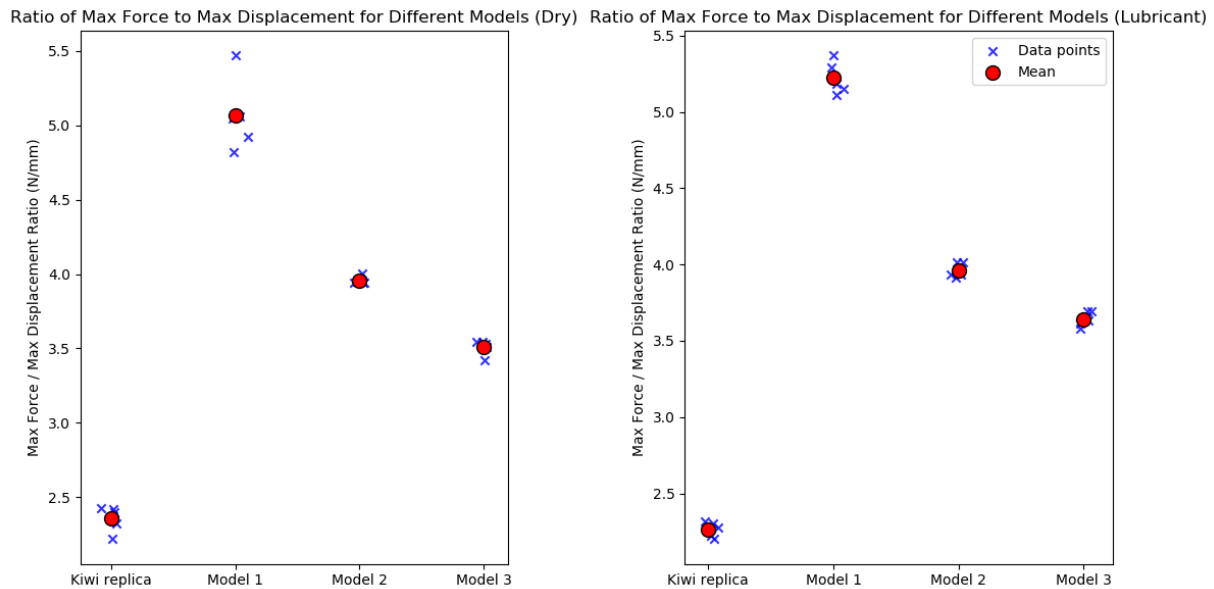


**Figure 5.17:** Comparison of the ratio of maximum force to maximum displacement for different models under dry (left) and lubricated (right) conditions. Each box represents the distribution of the ratio values for the Kiwi replica, Model 1, Model 2, and Model 3 across multiple tests. The plots illustrate the variation in performance among the models. Outliers are represented by individual points outside the whiskers.

### 5.6.6. Force-displacement ratio plotted over time

Although the maximal traction force was lower in the proposed designs, the improved force-displacement ratio (Section 5.6.5) indicates that the new designs may be more efficient in transferring force without causing excessive scalp deformation. However, this ratio does not accurately represent the actual ratio that would be observed if the same traction force as the Kiwi replica had been attained. This is due to the fact that the force-displacement relationship is not linearly proportional, meaning the increase in force does not result in a directly proportional increase in displacement. To gain a better understanding of how this ratio changes over time, it was calculated and plotted for all measurements in dry conditions and presented in Figure 5.18.

From this plot, several conclusions can be drawn:

- As the traction force increases, the difference in the ratio between the tested suction cups becomes smaller. This is because the contribution of the suction force to the total scalp deformation decreases, when increasing the traction force (Figure 6.1).
- The ratio for the Kiwi replica increases over time, indicating that the traction force increases with an higher rate compared to the displacement.
- At the beginning of the experiment (low traction forces/ displacement), the ratio of the proposed designs is significantly higher than that of the Kiwi replica.
- Between the three proposed models, a larger structural force ( $F_{struc}$ ) results in a higher Force/Displacement ratio.

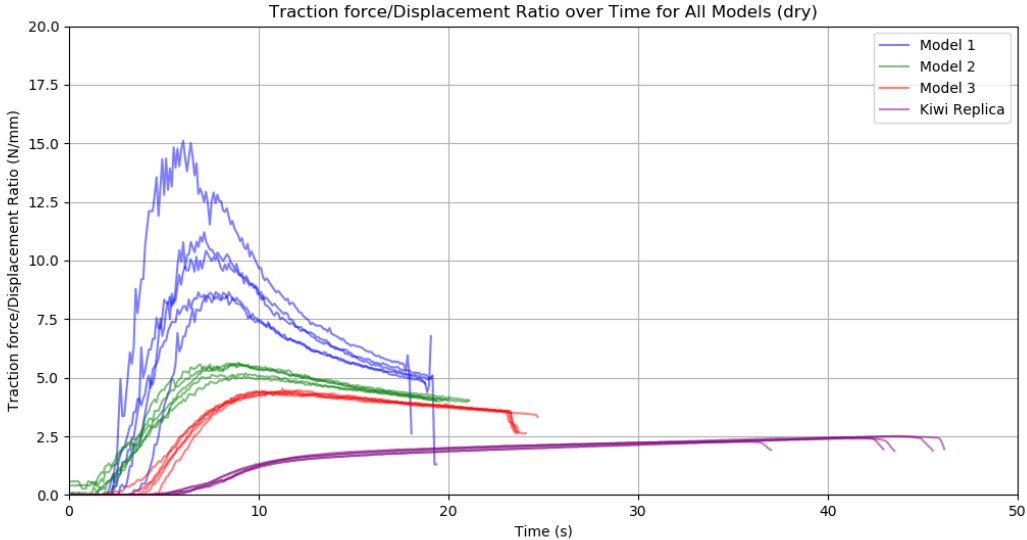


**Figure 5.18:** Overlaid force/displacement ratio over time for all tests conducted in dry conditions (Experiment 1). Each line represents an individual test for one of the four models. For clarity, the plot of an individual test is stopped once the suction cup detaches.

## Discussion

### 6.1. Main findings

#### 6.1.1. Requirement check

This study resulted in the development of a 3D-printed flexible VAD device. Table 6.1 displays the achievements of the proposed design with the design requirements outlined in Section 3.1.

**Table 6.1:** Achievement of the proof-of-principle prototype on the requirements and wishes. ✓ indicates the requirement is satisfied, - represents the performance should be investigated further, an X indicates the requirement is not satisfied.

Requirement	Description	Status
R1	It should be feasible to manufacture the design with a Fused Deposition Modeling (FDM) 3D printer.	✓
R2	The proposed design should be made from a single, flexible material.	✓
R3	The proposed design should reach a peak traction force of 135N without detachment.	X
R4	The pressure difference ( $\Delta P$ ) of 80 kPa should remain constant for 90 seconds.	X
R5	The chignon volume inside the scalp during suction should be reduced to 10% compared to the chignon volume induced by current suction cup designs.	-
R6	The outer dimensions of the suction cup are 20 mm in height from the scalp and 65 mm in diameter.	✓
R7	The suction cup should work in different environmental conditions.	-
R8	The suction cup should be made out of non-toxic materials.	✓
R9	The actuation of the suction cup should be pneumatic.	✓
W1	No sharp edges should be designed.	✓

#### 6.1.2. Maximal traction force

From Experiment 1, it was observed that the maximal achievable traction forces were lower than anticipated for all tested prototypes, including the Kiwi replica, none of which achieved the target traction force of 135 N. This is likely due to the silicone test surface used in the experiments. The interface between the suction cup and the silicone surface is more prone to leakage channels and slipping compared to the interface between the suction cup and human skin, as skin exhibits greater flexibility and conformity. Despite this limitation, the silicone test surface is still suitable for comparing the maximal traction forces of the Kiwi replica and the proposed designs, allowing for a consistent evaluation of their relative performance.

As shown in Table 5.1, the maximal achievable traction forces of the proposed designs were significantly lower than those of the Kiwi replica, achieving only between 45.4% and 56.1% of the Kiwi replica's traction

force in both dry and lubricated conditions. A possible explanation for this difference is the curling of the sealing lip, as discussed in Section 5.6.4. This curling is a consequence of the deformation of the suction cup body and result in leakage of negative pressure. Another explanation could be the slipping between the suction cup and the infant surrogate. Slipping of the suction cup decreases the vacuum area and increases the risk of leakage channels potentially leading to cup detachment (Section 2.4.4). This slipping is more likely to occur in a lubricated environment, as the lubricant reduces the friction between the sealing lip and the silicone surface. This could explain why the mean maximum traction forces in lubricated conditions are reduced by an average of 5% compared to dry conditions.

The structure forces and maximum traction forces for the proposed models are summarized in Table 6.2. It was expected that the model that exerts a larger structural force ( $F_{struc}$ ) result in a lower maximal achievable traction force (Equation 3.3). This expectation is supported by the results from Experiment 1, where Model 1 (the stiffest structure) reached the smallest maximal traction force. The maximal traction force is increasing as the structural force decreases in Models 2 and 3. The calculated difference in the structure force ( $F_{struc}$ ) is approximately 10 N (Table 6.2); however, the observed difference in maximal traction force among the three models is approximately 5 N. This difference is attributed to the fact that the lattices in Models 1 and 2 are not fully compressed (experiment 2), thereby not providing the calculated maximum structure force ( $F_{struc}$ ) depicted in Table 4.3.

**Table 6.2:** Summary of the calculated maximum structure forces ( $F_{struc}$ ) at the fully compressed state (compressed by 2 mm) and the measured mean maximum traction forces ( $F_{trac}$ ) under dry and lubricated conditions for the three proposed models. A decrease in structure force ( $F_{struc}$ ) leads to an increase in maximum achievable traction force ( $F_{trac}$ ) (Equation 3.3).

	Model 1	Model 2	Model 3
Calculated $F_{struc}$ (Fully-compressed) (N)	42.8	32.3	22.5
Mean maximum $F_{trac}$ (Dry) (N)	42.7	46.0	50.5
Mean maximum $F_{trac}$ (Lube) (N)	39.8	45.1	47.6

### 6.1.3. Scalp deformation

Both the traction force and the suction force contribute to the formation of a chignon. A schematic representation of the different causes of chignon formation is depicted in Figure 6.1. The chignon formation caused by the traction force (Figure 6.1B) is consistent across all suction cup designs since the scalp is always positioned between the suction cup and the infant's body to transmit the traction force. However, the chignon formation caused by the suction force (Figure 6.1A) varies between the proposed designs and was determined in Experiment 2, where scalp deformation before applying traction force was measured. A schematic representation of the maximum lattice deformation is depicted in Figure 6.2. The stiffest lattice is shown in Figure 6.2A, experiment 2 shows that it only deforms 0.88 mm which is a result of the largest structure force. The scalp in model 2 deforms 1.54 mm and the scalp of model 3 deforms 2.20 mm (Table 5.2). The 'fully compressed' state (blue line) is designed to be 2 mm above the scalp. This implies that the lattices in models 1 and 2 are not fully deformed, whereas the lattice in model 3 is fully deformed at the maximum pressure difference. The lattice structure in Model 2 was specifically designed such that its fully compressed state provided a total lattice force of 23.1 N (Table 4.3). When combined with the sealing force of 9.3 N, the total structural force remained below the 33 N threshold, which represents the available margin when compared to the Kiwi replica (Section 4.1.2). However, since the lattice was not fully compressed during suction, the force exerted on the scalp was lower than its maximum potential. Theoretically, the lattice in Model 2 could be made stiffer or positioned closer to the scalp, thereby increasing the lattice force. This adjustment would further reduce chignon formation by providing greater resistance to scalp deformation during vacuum application. The lattice in model 3 reaches the maximum theoretical structural force. However, this is considered undesirable, as it reduces the effective vacuum area ( $A_{eff}$ ), potentially limiting the suction performance (Section 4.1.2). However, model 3 does not show a reduction in maximal achievable traction force. A potential explanation is that the suction cup deforms following the application of the traction force, leading to a potential decompression of the lattice (Section 5.6.4).

Figure 5.12 illustrates that the proposed models resulted in significantly reduced scalp displacement

compared to the Kiwi replica. The scalp deformation in the Kiwi replica quickly reaches the maximum displacement of 14.19 mm even at low pressure differences, indicating that the scalp contacts the inner ceiling of the suction cup. In contrast, the proposed models demonstrate a more linear increase in scalp displacement as pressure differences increase, with the largest displacements occurring at the highest pressure differences. At a pressure difference of 600 mmHg, the scalp deformation in the proposed models are 6.2%, 10.8% and 15.5% of the scalp deformation in the Kiwi replica, depending on the lattice stiffness of the proposed models (Table 5.2). The reduced chignon formation observed with the proposed designs suggests a lower risk of neonatal scalp trauma.

When comparing scalp displacement between the phantom model and a real neonatal scalp, several important differences arise. In neonates, the scalp is slightly connected to the skull through layers of connective tissue, such as the periosteum and subcutaneous tissue, which play a key role in how the scalp responds to pressure ([48]). The phantom model, however, lacks these connective layers, leading to a more artificial response to suction forces. In neonates, scalp deformation occurs more gradually as negative pressure causes fluid to accumulate within the tissue, resulting in chignon formation. In the neonatal scalp, the pressure inside the scalp is a critical factor that influences the risk of blood vessel rupture and the development of subgaleal hemorrhage (SGH). In this study, the measurement of displacement serves as an indicator of the potential pressure inside the scalp. In contrast, the phantom model may show more immediate and uniform deformation, as it doesn't replicate the fluid-driven, gradual response seen in real neonatal tissue.

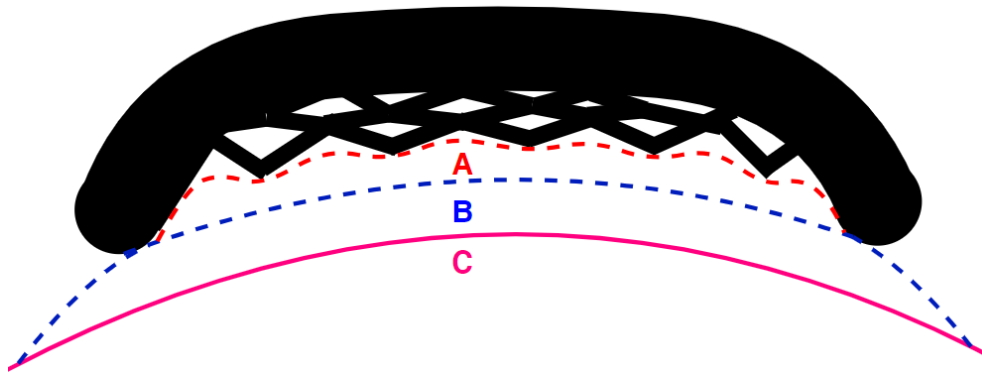


**Figure 6.1:** Demonstrating the variation in chignon formation caused by the suction force (A) and traction force (B) compared to the undeformed scalp (C).

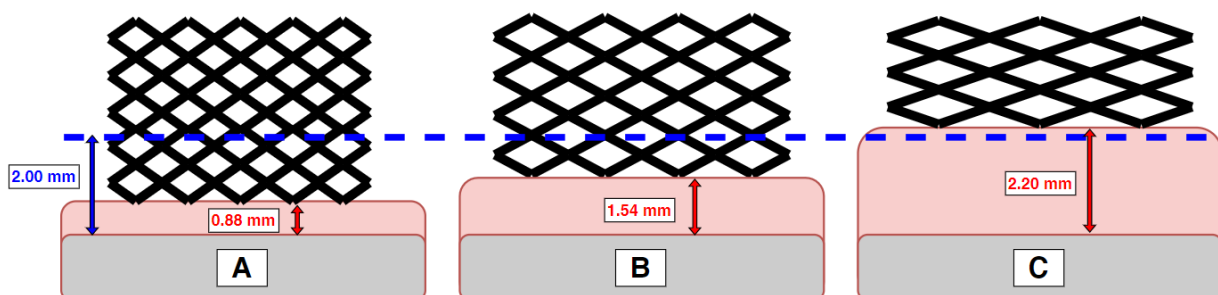


**Figure 6.2:** Schematic representation of the lattice structure deformation in the proposed models compared to their 'fully compressed' state (blue line) and the undeformed scalp (grey). The images depict lattice deformation in model 1 (A), model 2 (B), and model 3 (C).

#### 6.1.4. Pressure loss rate

To compare the sealing performance between the Kiwi replica and the proposed designs, the pressure loss rate was measured in Experiment 3. The pressure loss rate is highly dependent on the presence of leakage channels, which occur randomly during the 3D printing process. Consequently, even separate prints of the same design can exhibit significant differences in pressure loss rates. Additionally, it was observed

that slight changes in the cup's position could significantly affect the pressure loss rate, contributing to variability in the measurements for the same test-setup. Despite this variability, several conclusions can be drawn from the experiment.

Firstly, the use of a lubricant shows an overall decrease in the pressure loss rate because the lubricant enhances sealing by filling the leakage channels. However, Experiment 1 indicates that the lubricant condition does not increase the maximal achievable traction force. This is probably because, while the lubricant improves sealing, it also increases the likelihood of slippage. Furthermore, it is expected that the pressure loss rate would decrease at lower pressure differences. This behavior was observed in both the Kiwi replica and Model 3. However, the presence of structural forces that push the suction cup away can lead to quicker pressure loss at lower pressure differences. As a result, model 1 and 2 detach more rapidly under low-pressure conditions, most likely because of the larger structure forces compared to model 1.

## 6.2. Experiment limitations

The infant surrogate's scalp was mimicked using silicone, which only approximates the complex, multi-layered structure of actual tissue with varying thickness and binding characteristics to the skull. This simplification will not accurately reflect the true behavior of neonatal scalp tissue under suction and traction forces. The measured displacement is used to determine chignon formation and the force/displacement ratio. However as the silicone scalp does not behave like real scalp tissue. Real scalp tissue is expected to deform less due to the presence of connective tissues that keep it in place. The silicone scalp reacts almost immediately to pressure differences, whereas in reality, the scalp would likely deform more slowly as body fluids are drawn into a chignon. Consequently, while the results are useful for comparison of the proposed suction cup designs, the absolute values of scalp deformation should not be considered accurate and in reality the suction cup design will probably deform less and more slowly. Additionally, the silicone used is smoother and less conformable than real skin. This decreases the sealing performance and increases the risk of slippage. While the Kiwi OmniCup® is known to adhere to infants with hair, even the Kiwi replica could not adhere to the silicone scalp with hair in this setup. Consequently, no conclusions could be drawn regarding the performance of the proposed designs on a scalp with hair.

The load-cell and displacement sensors are considered accurate, however, the accuracy of the analog pressure gauge is suboptimal, which may affect the precision of the measurements. Only a limited number of measurements were taken. A larger sample size is required to provide more accurate results and draw definitive conclusions about the performance of the suction cups and the repeatability of the test setup.

The structure force is distributed to provide the largest force at the center and less at the rim. This force variation is based on the geometry of the infant scalp. However, it is not known if this force variation prevents that the lattice becomes 'fully compressed' in every section, as displacement measurements were only taken at the center. The behavior at other sections remains unknown.

## 6.3. Experiment recommendations

The measurement of force and displacement for the different lattice structures, varying in unit cell height and strut diameter, lacked precision. This was primarily due to the use of a measuring stick for displacement and a kitchen scale for force measurements. To more accurately assess the structural behavior of the lattice structures and determine whether they exhibit linear behavior, more precise measurement instruments should be used, and a larger dataset of measurements should be collected.

In Experiment 1, the protocol required increasing the vacuum with a manual pump when the pressure gauge dropped to 560 mmHg. It was observed that, prior to detachment, the sealing lip started to curl, necessitating a significant increase in pump frequency until it became impossible to pump fast enough. The number of pumps was not recorded during the experiments, but this could also serve as a measure to evaluate the sealing performance. To further enhance the accuracy and precision of the experiments, the manual vacuum pump could be replaced with an electric vacuum regulator, allowing for precise control and monitoring of the pressure difference rate.

Clinical testing of the proposed design by professional obstetricians is recommended to determine the ease of insertion and whether the design can reach the flexion point effectively. Obstetricians could provide additional feedback based on their experience with VAD devices. Additionally, all measurements

of a single model were conducted sequentially. It is recommended to alternate between models for each measurement to decrease the chance of bias.

Using a more realistic infant surrogate, along with a lubricant that closely simulates real-world conditions, would enable more accurate conclusions regarding scalp deformation and the performance of the proposed design in various environments. Additionally, employing an infant surrogate that measures the pressure inside the scalp rather than scalp displacement would provide more valuable insights into the risk of blood vessel rupture and the potential for subgaleal hemorrhage (SGH).

In Experiment 2, it is demonstrated that Model 3 reaches the 'fully compressed' state. It was assumed that the effective vacuum area ( $A_{eff}$ ) decreases when the lattice reaches this 'fully compressed' state (Section 4.1.2). However, due to the deformation of the suction cup after applying a traction force, it is uncertain if this 'fully compressed' state still occurs at maximal traction. Therefore, it cannot be concluded whether the reduced effective vacuum area leads to a decrease in the maximal achievable traction force. To determine whether the lattice structures reach the 'fully compressed' state and to calculate the force exerted by the lattice ( $F_{struc}$ ), it is beneficial to measure not only the displacement of the scalp but also the length of the lattice during the application of traction force. Moreover, since the lattice height is not uniformly distributed, measuring the lattice length and scalp deformation at multiple locations, rather than just the center, would provide more comprehensive insights into the extent of lattice deformation. This approach allows for a better assessment of whether the lattice structure reaches the fully deformed state.

## 6.4. Design recommendations

The deformation of the suction cup during traction leads to curling of the sealing lip, creating leakage channels and reducing the effective vacuum area ( $A_{eff}$ ) due to slippage. To mitigate this issue, increasing the thickness or stiffness of the suction cup body may improve its resistance to deformation. However, the suction cup must remain foldable to allow for easier insertion. Introducing radial ribs on the top surface of the suction cup could help to distribute traction forces more evenly across the rim while preserving sufficient flexibility to allow for folding during insertion. Furthermore, the bellow-shaped sealing lip currently curls as its circumference decreases under deformation. While the lip is flexible in the vertical direction, it lacks flexibility in other directions. Further investigation could focus on enhancing the lateral flexibility of the sealing lip to prevent curling, potentially through the use of more flexible materials.

In the current design, the desired traction force has not been achieved. As concluded from Experiment 1 (Section 5.6.1), a reduction in structure force results in an increase in traction forces. Achieving a traction force of 135 N is crucial for successful vacuum-assisted delivery (VAD). If this traction force is still not reached after resolving the curling issues and deformation of the suction cup, the stiffness of the lattice structure should be reduced, or the lattice should be repositioned further from the scalp.

The current design is made of the softest material available for FDM 3D printers (Filaflex 60A, Recreus, Spain), but variability in the FDM printing process can affect the sealing performance. Under-extrusion can occur randomly, leading to leakage channels that compromise the seal. Additionally, the minimal thickness of the sealing lip is constrained to ensure it remains airtight, which limits the flexibility of the sealing lip. A more flexible lip would better conform to surface irregularities and hair, and would also reduce the force needed to achieve a seal, potentially increasing the maximal achievable traction force. Beyond FDM printing, more precise methods like SLA (Stereolithography) could provide higher accuracy and allow for the incorporation of microstructures inspired by natural organisms to improve sealing performance (Appendix A.3). The current flexible BCC lattice is a basic structure that provides a sufficient counterforce while still being flexible. With other manufacturing methods and materials, other lattice structures could be explored.

The vacuum inlet is designed on top of the suction cup. To make the device suitable for use in various infant positions where the flexion point is not easily reachable, the vacuum inlet should be repositioned to the side of the cup. Integrating the traction cable inside the vacuum tube, similar to the Kiwi OmniCup®, could improve usability. The performance should then be tested under angled traction forces.

The sealing ring is currently set at 5 mm. Testing smaller sealing rings could determine if they also provide sufficient sealing. Reducing the sealing ring size without increasing the outer dimensions of the suction cup could enhance the effective vacuum area.

By optimizing the suction cup's material properties, structural design, and addressing the deformation issues such as lip curling, future iterations could more closely match the traction forces achieved by the Kiwi replica, while also reducing the risk of neonatal complications. Such advancements hold promise for the development of a more effective and safer device, with the potential to significantly improve clinical outcomes in neonatal care.



## Conclusion

This study introduced a novel suction cup design for vacuum-assisted delivery (VAD) aimed at reducing chignon formation while maintaining adequate traction force. The proposed designs are manufactured using an FDM 3D printer with a flexible material. Three designs with varying flexible lattice structure stiffness were designed to minimize chignon formation, and a bellow-shaped sealing lip was used to enhance the sealing performance. The stiffness of the lattices was varied across the three models: Model 1 (stiff), Model 2 (medium stiff), and Model 3 (less stiff), with a structure force difference of  $10N$  between each model. Scalp displacement and maximum traction force were evaluated through experimental testing. Validation of the models was performed on an infant head surrogate and compared to a replica of the commonly used Kiwi OmniCup®.

At maximum suction force, the scalp deformation (chignon) in the proposed models ranged from 6.2% to 15.5% of the deformation observed in the Kiwi replica, depending on the lattice stiffness of the proposed models, which significantly reduces the chance of neonatal injuries. However, achieving the desired traction force remains challenging. The traction force/displacement ratio was used as a metric to compare the performance of the different suction cup designs. Model 1 demonstrated the greatest improvement in this ratio, with an increase factor of 2.15 in a dry environment and 2.30 in a lubricated environment compared to the Kiwi replica, indicating better efficiency in transmitting force with minimal chignon formation. Among the proposed designs, a trade-off can be made between chignon formation and the maximum achievable traction force by adjusting the lattice stiffness. Nevertheless, for all proposed designs, the maximal traction forces achieved were lower (45.4 – 56.1%) than those of the Kiwi replica, highlighting the need for further optimization.

The proposed models are made of a single soft material and manufactured using an FDM 3D printer, which allows for the design of complex geometries. However, FDM 3D printing limitations have impacted the sealing performance. Additionally, while the soft, low-profile suction cup design is practical for nearly all infant positions, its flexibility poses challenges. Specifically, the curling of the sealing lip leads to leakage channels and detachment.

While challenges remain in optimizing the maximum traction force, this study offers a promising step toward a safer vacuum-assisted delivery method. By significantly reducing chignon formation, the proposed designs have the potential to lower neonatal injury risk. With further refinement, these advancements could pave the way for more effective and gentler interventions, improving outcomes for both infants and healthcare providers.

# References

- [1] Dushyant Goordyal et al. "An engineering perspective of vacuum assisted delivery devices in obstetrics: A review". In: *Proceedings of the Institution of Mechanical Engineers, Part H: Journal of Engineering in Medicine* 235.1 (2021), pp. 3–16.
- [2] Thomas F Baskett et al. *Munro Kerr's Operative Obstetrics E-Book*. Elsevier Health Sciences, 2014.
- [3] Alison J MacFarlane et al. "Wide differences in mode of delivery within Europe: risk-stratified analyses of aggregated routine data from the Euro-Peristat study". In: *BJOG: An International Journal of Obstetrics & Gynaecology* 123.4 (2016), pp. 559–568.
- [4] Unzila A Ali et al. "Vacuum-assisted vaginal delivery". In: *Reviews in obstetrics amp; gynecology* 2.1 (2009), pp. 5–17.
- [5] Deirdre J Murphy et al. "Early maternal and neonatal morbidity associated with operative delivery in second stage of labour: a cohort study". In: *The Lancet* 358.9289 (2001), pp. 1203–1207.
- [6] Tage Malmström. "The vacuum extractor an obstetrical instrument and the parturiometer a tokographic device". In: *Acta obstetricia et gynecologica Scandinavica* 36.sup3 (1957), pp. 5–87.
- [7] Sun Jin Lee et al. "The clinical characteristics and prognosis of subgaleal hemorrhage in newborn". In: *Korean journal of pediatrics* 61.12 (2018), p. 387.
- [8] Thomas F Baskett. "Operative vaginal delivery—An historical perspective". In: *Best Practice & Research Clinical Obstetrics & Gynaecology* 56 (2019), pp. 3–10.
- [9] TVASurg - The Toronto Video Atlas of Surgery. *Routine Forceps Delivery*. 2021. URL: <https://pie.med.utoronto.ca/TVASurg/project/routine-forceps-delivery/>.
- [10] Ana Beatriz Chorão Estêvão. "Vacuum-assisted vaginal delivery: a biomechanical study". PhD thesis. Universidade do Porto (Portugal), 2021.
- [11] Richard Johanson et al. "Soft versus rigid vacuum extractor cups for assisted vaginal delivery". In: *Cochrane Database of Systematic Reviews* 2010.1 (1996).
- [12] Y Vallet et al. "Analysis of suction-based gripping strategies in wildlife towards future evolutions of the obstetrical suction cup". In: *Bioinspiration & biomimetics* 17.6 (2022), p. 061003.
- [13] John W. Huffman Alfred C. Beck. "birth". In: *Encyclopædia Britannica* (2015).
- [14] Jihan Jeon et al. "Vacuum extraction vaginal delivery: current trend and safety". In: *Obstetrics & Gynecology Science* 60.6 (2017), p. 499.
- [15] Katarina Åberg. *Neonatal complications following birth by vacuum extraction*. Inst för kvinnors och barns hälsa/Dept of Women's and Children's Health, 2017.
- [16] Roberto Angioli et al. "Severe perineal lacerations during vaginal delivery: the University of Miami experience". In: *American journal of obstetrics and gynecology* 182.5 (2000), pp. 1083–1085.
- [17] Martina Kreft et al. "Birth tears after spontaneous and vacuum-assisted births with different vacuum cup systems—a retrospective cohort study". In: *Journal of perinatal medicine* 48.6 (2020), pp. 575–581.
- [18] Thomas Christensen et al. "Neonatal subgaleal hemorrhage in a multihospital healthcare system: twenty years of trends in incidence, associations, and outcomes". In: *retrospective analysis* (2022).
- [19] Dhiraj Uchil et al. "Neonatal subgaleal hemorrhage and its relationship to delivery by vacuum extraction". In: *Obstetrical & gynecological survey* 58.10 (2003), pp. 687–693.

- [20] Gabriel Levin et al. "Risk factors associated with subgaleal hemorrhage in neonates exposed to vacuum extraction". In: *Acta obstetrica et gynecologica Scandinavica* 98.11 (2019), pp. 1464–1472.
- [21] Stergios K Doumouchtsis et al. "Head trauma after instrumental births". In: *Clinics in perinatology* 35.1 (2008), pp. 69–83.
- [22] Jette Kuit. *Clinical and physical aspects of obstetric vacuum extraction*. 1997.
- [23] G JUSTUS HOFMEYER et al. "New design rigid and soft vacuum extractor cups: a preliminary comparison of traction forces". In: *BJOG: An International Journal of Obstetrics & Gynaecology* 97.8 (1990), pp. 681–685.
- [24] Unzila A Ali et al. "Vacuum-assisted vaginal delivery". In: *Reviews in Obstetrics and Gynecology* 2.1 (2009), p. 5.
- [25] KEVIN L MUISE et al. "The effect of artificial caput on performance of vacuum extractors". In: *Obstetrics & Gynecology* 81.2 (1993), pp. 170–173.
- [26] J. Schmalz GmbH. *Suction cup shapes*. URL: <https://www.schmalz.com/en/vacuum-knowledge/the-vacuum-system-and-its-components/vacuum-suction-cups/suction-cup-shapes/>.
- [27] Yong-Lae Park et al. "Design and fabrication of soft artificial skin using embedded microchannels and liquid conductors". In: *IEEE Sensors journal* 12.8 (2012), pp. 2711–2718.
- [28] Hee Joong Jung et al. "Ultrastructural characteristics of neonate scalp hair". In: *Indian Journal of Science and Technology* (2016).
- [29] Ganga L Verma et al. "Instruments for assisted vaginal birth". In: *Cochrane Database of Systematic Reviews* 9 (2021).
- [30] Tiffany Tonismae et al. *Vacuum Extraction*. StatPearls Publishing, 2017.
- [31] Alyssa M Hernandez et al. "Stickiness in shear: stiffness, shape, and sealing in bioinspired suction cups affect shear performance on diverse surfaces". In: *Bioinspiration & Biomimetics* 19.3 (2024), p. 036008.
- [32] Avinash Tiwari et al. "Physics of suction cups". In: *Soft matter* 15.46 (2019), pp. 9482–9499.
- [33] Aldo Vacca. "Vacuum-assisted delivery: an analysis of traction force and maternal and neonatal outcomes". In: *Australian and New Zealand journal of obstetrics and gynaecology* 46.2 (2006), pp. 124–127.
- [34] Kristina Pettersson. "Complicated Vacuum Extraction: Focus on Traction Force". PhD thesis. Karolinska Institutet (Sweden), 2018.
- [35] Mark I Evans et al. "Uterine contraction frequency in the last hour of labor: how many contractions are too many?" In: *The Journal of Maternal-Fetal & Neonatal Medicine* 35.25 (2022), pp. 8698–8705.
- [36] Jae Young Choi et al. "Extracranial vertebral artery rupture likely secondary to "cupping therapy" superimposed on spontaneous dissection". In: *Interventional Neuroradiology* 23.2 (2017), pp. 156–158.
- [37] L.M. Tham et al. "Cupping: From a biomechanical perspective". In: *Journal of Biomechanics* 39.12 (2006), pp. 2183–2193. DOI: <https://doi.org/10.1016/j.jbiomech.2005.06.027>. URL: <https://www.sciencedirect.com/science/article/pii/S0021929005003222>.
- [38] Stephen P Timoshenko et al. *Theory of elastic stability*. Courier Corporation, 2012.
- [39] Mahmoud Ahmed El-Sayed et al. "Design optimization of additively manufactured titanium lattice structures for biomedical implants". In: *The International Journal of Advanced Manufacturing Technology* 110 (2020), pp. 2257–2268.
- [40] Hafiz Muhammad Asad Ali et al. "Insight into the mechanical properties of 3D printed strut-based lattice structures". In: *Progress in Additive Manufacturing* 8.5 (2023), pp. 919–931.
- [41] Tobias Maconachie et al. "SLM lattice structures: Properties, performance, applications and challenges". In: *Materials & Design* 183 (2019), p. 108137.

- [42] Jinqi Shang et al. "An Analytical Method for Elastic Modulus of the Sandwich BCC Lattice Structure Based on Assumption of Linear Distribution". In: *Materials* 16.9 (2023), p. 3315.
- [43] Duane T Lowe. "Cupping therapy: An analysis of the effects of suction on skin and the possible influence on human health". In: *Complementary therapies in clinical practice* 29 (2017), pp. 162–168.
- [44] Syed Fouzan Iftekar et al. "Advancements and limitations in 3D printing materials and technologies: a critical review". In: *Polymers* 15.11 (2023), p. 2519.
- [45] Juan M Barrios et al. "Improvement of surface roughness and hydrophobicity in PETG parts manufactured via fused deposition modeling (FDM): An application in 3D printed self-cleaning parts". In: *Materials* 12.15 (2019), p. 2499.
- [46] Louise C Kenny et al. *Obstetrics by ten teachers*. CRC Press, 2024.
- [47] Eric Bauer Follow. *Human fetal skull - download free 3D model by Eric Bauer (@ebauer4)*. 2007. URL: <https://sketchfab.com/3d-models/human-fetal-skull-bc94ea0ac45b46e2b7c13d04ae1e67c4>.
- [48] Jahan Tajran et al. "Anatomy, head and neck, scalp". In: *StatPearls [Internet]*. StatPearls Publishing, 2023.
- [49] E Norwitz et al. "Obstetrics; normal and problem pregnancies". In: *Obstetrics: Normal and Problem Pregnancies. 4th ed. New York: Churchill Livingstone* (2002), pp. 353–394.
- [50] Warren C Plauche. "Fetal cranial injuries related to delivery with the Malmström vacuum extractor". In: *Obstetrics & Gynecology* 53.6 (1979), pp. 750–757.
- [51] Fidelma O'Mahony et al. "Choice of instruments for assisted vaginal delivery". In: *Cochrane Database of Systematic Reviews* 11 (2010).
- [52] Mark C Williams et al. "Obstetric correlates of neonatal retinal hemorrhage." In: *Obstetrics and gynecology* 81.5 (Pt 1) (1993), pp. 688–694.
- [53] Kitaw Demissie et al. "Operative vaginal delivery and neonatal and infant adverse outcomes: population based retrospective analysis". In: *Bmj* 329.7456 (2004), p. 24.
- [54] Gili Kenet et al. "Neonatal IVH—mechanisms and management". In: *Thrombosis research* 127 (2011), S120–S122.
- [55] Colin A Walsh et al. "Mode of delivery at term and adverse neonatal outcomes". In: *Obstetrics & Gynecology* 121.1 (2013), pp. 122–128.
- [56] Margareta Mollberg et al. "Obstetric brachial plexus palsy: a prospective study on risk factors related to manual assistance during the second stage of labor". In: *Acta obstetrica et gynecologica Scandinavica* 86.2 (2007), pp. 198–204.
- [57] Suneet P Chauhan et al. "Neonatal brachial plexus palsy: incidence, prevalence, and temporal trends". In: *Seminars in perinatology*. Vol. 38. 4. Elsevier. 2014, pp. 210–218.
- [58] Cassandra M Wilkinson et al. "A translational perspective on intracranial pressure responses following intracerebral hemorrhage in animal models". In: *Brain Hemorrhages* 2.1 (2021), pp. 34–48.
- [59] K Pettersson et al. "Traction force during vacuum extraction: a prospective observational study". In: *BJOG: An International Journal of Obstetrics & Gynaecology* 122.13 (2015), pp. 1809–1816.
- [60] Kristina A Pettersson et al. "Association of traction force and adverse neonatal outcome in vacuum-assisted vaginal delivery: a prospective cohort study". In: *Acta obstetrica et gynecologica Scandinavica* 99.12 (2020), pp. 1710–1716.
- [61] Tianqi Yue et al. "Shape-Conformable Suction Cups with Controllable Adaptive Suction on Complex Surfaces". In: *IEEE Robotics and Automation Letters* (2023).
- [62] Arman Goshtasbi et al. "A bioinspired stiffness tunable sucker for passive adaptation and firm attachment to angular substrates". In: *Frontiers in Robotics and AI* 10 (2023), p. 1080015.

- [63] T Tomokazu et al. "Vacuum gripper imitated octopus sucker-effect of liquid membrane for absorption". In: *2015 IEEE/RSJ International Conference on Intelligent Robots and Systems (IROS)*. IEEE. 2015, pp. 2929–2936.
- [64] Sina Sareh et al. "Anchoring like octopus: biologically inspired soft artificial sucker". In: *Journal of the royal society interface* 14.135 (2017), p. 20170395.
- [65] Siwei Su et al. "Vertical fibrous morphology and structure-function relationship in natural and biomimetic suction-based adhesion discs". In: *Matter* 2.5 (2020), pp. 1207–1221.
- [66] Kojiro Uetani et al. "Elastomeric thermal interface materials with high through-plane thermal conductivity from carbon fiber fillers vertically aligned by electrostatic flocking". In: *Advanced Materials* 26.33 (2014), pp. 5857–5862.
- [67] Siqi Wang et al. "A biomimetic remora disc with tunable, reversible adhesion for surface sliding and skimming". In: *Bioinspiration & Biomimetics* 17.3 (2022), p. 036001.
- [68] Petra Ditsche et al. "Learning from Northern clingfish (*Gobiesox maeandricus*): bioinspired suction cups attach to rough surfaces". In: *Philosophical Transactions of the Royal Society B* 374.1784 (2019), p. 20190204.
- [69] Dylan K Wainwright et al. "Stick tight: suction adhesion on irregular surfaces in the northern clingfish". In: *Biology letters* 9.3 (2013), p. 20130234.
- [70] Weimian Zhou et al. "Enhanced Adhesion of Synthetic Discs with Micro-Patterned Margins". In: *Biomimetics* 7.4 (2022), p. 202.
- [71] Jessica A Sandoval et al. "Reversible adhesion to rough surfaces both in and out of water, inspired by the clingfish suction disc". In: *Bioinspiration & biomimetics* 14.6 (2019), p. 066016.
- [72] Gui Won Hwang et al. "Soft Microdenticles on Artificial Octopus Sucker Enable Extraordinary Adaptability and Wet Adhesion on Diverse Nonflat Surfaces". In: *Advanced Science* 9.31 (2022), p. 2202978.
- [73] Hyeongho Min et al. "Enhanced biocompatibility and multidirectional wet adhesion of insect-like synergistic wrinkled pillars with microcavities". In: *Chemical Engineering Journal* 429 (2022), p. 132467.
- [74] Recreus. *TPU filament Filaflex 60A, flexible filament for 3D printing*. 2021. URL: <https://recreus.com/gb/filaments/1-filaflex-60a.html>.



# Appendix

## A.1. Prerequisites and requirements before VAD is executed

The prerequisites that should be fulfilled before performing VAD are listed in Table A.1.

**Table A.1:** Prerequisites for Operative Vaginal Delivery ([49])

Maternal Criteria	Fetal Criteria	Uteroplacental Criteria	Other Criteria
Adequate analgesia	Vertex presentation	Cervix fully dilated	An experienced operator who is fully acquainted with the use of the instrument
Patient in the lithotomy position	The fetal head must be engaged in the pelvis	Membranes ruptured	Ability to monitor fetal well-being continuously
Bladder empty	The position of the fetal head must be known with certainty	No placenta previa	The capability to perform an emergency cesarean delivery if required
Clinical pelvimetry must be adequate in dimension and size to facilitate an atraumatic delivery	The station of the fetal head must be $\geq 0/+5$		
Verbal or written consent obtained	The estimated fetal weight must be documented (ideally 2500–4500 g)		
	The attitude of the fetal head and the presence of caput succedaneum and/or molding should be noted		

## A.2. Other neonatal injuries

### Clinically non-significant injuries

Superficial scalp injuries are common, occurring in approximately 10% of vacuum-assisted deliveries ([50]). These injuries are more frequent with the use of metal or hard plastic cups compared to soft cups ([51]).

Retinal hemorrhage, bleeding in the membrane at the back of the eye, is a frequent finding in newborns. It occurs in 18% of spontaneous deliveries and 28% of vacuum-assisted deliveries ([52]). Retinal hemorrhage usually resolves within days to months and does not cause permanent damage.

Cephalohematoma is an extracranial bleed located between the skull and periosteum (Figure 2.5). The periosteum is connected to the suture lines of the bone plates in the skull, limiting the potential blood

volume that can accumulate in this area. Cephalohematomas occur in approximately 1.67% of unassisted deliveries and 11.7% of vacuum-assisted deliveries ([53]). Clinically, cephalohematomas do not cross the suture lines, distinguishing them from the more severe subgaleal hemorrhages. Cephalohematomas are more common with the use of metal cups compared to soft or plastic cups ([11]).

### **Clinically significant injuries - intracranial hemorrhage**

Intracranial hemorrhage (ICH) is defined as any bleeding within the cranial vault. Improved neuroimaging techniques, such as magnetic resonance imaging (MRI), have revealed that small intracranial hemorrhages are common findings, even in asymptomatic term infants, regardless of the mode of delivery ([15]). However, symptomatic ICH is very rare in term infants, occurring in 0.3-0.8% of cases ([54]). The association between VAD and ICH is debated. Most large studies have found an increased rate of ICH following all methods of assisted delivery except cesarean section ([55]).

### **Indirect injuries**

Brachial plexus palsy is a neurological injury to the network of nerves that can affect the shoulder, arm, and hand, depending on the location of the injury. The primary causes are strain or compression of the brachial plexus ([56]). A vacuum extraction duration exceeding 10 minutes and a high number of pulls increase the risk of brachial plexus injury ([15]). While most children recover completely, 10% suffer permanent injury ([57]).

Neonatal hyperbilirubinemia (jaundice) is a common condition during the first week of life, resulting in yellowing of the baby's skin. Elevated bilirubin levels are caused by the breakdown of accumulated blood in chignons, cephalohematomas, and SGH. High bilirubin levels are neurotoxic and can potentially cause brain damage. Therefore, neonatal jaundice beyond certain age-specific limits is treated with phototherapy or, in rare cases, with exchange transfusion. Fortunately, the long-term outcomes of treated neonatal non-hemolytic hyperbilirubinemia are positive, with no adverse impact on adult neurodevelopment or cognitive performance ([15]).

### **Risks associated with high traction forces**

Compression in the birth canal leads to deformation of the fetal head and can increase intracranial pressure. Excessive pressure may result in intracranial hemorrhage (ICH) ([58]). Figure A.1 illustrates the fetal head with skin, showing that the traction force is transferred to the fetus via the scalp, compressing the spherical skull by forming a "sliding bag" around it ([22]).

Using small pressure transducers placed between the pelvis and the fetal head, average pressure values due to maternal bearing down efforts were found to be  $0.17 \text{ kg/cm}^2$ . Significantly higher values were found during vacuum extraction, with average pressures of  $0.32 \text{ kg/cm}^2$ , almost twice as high ([22]).

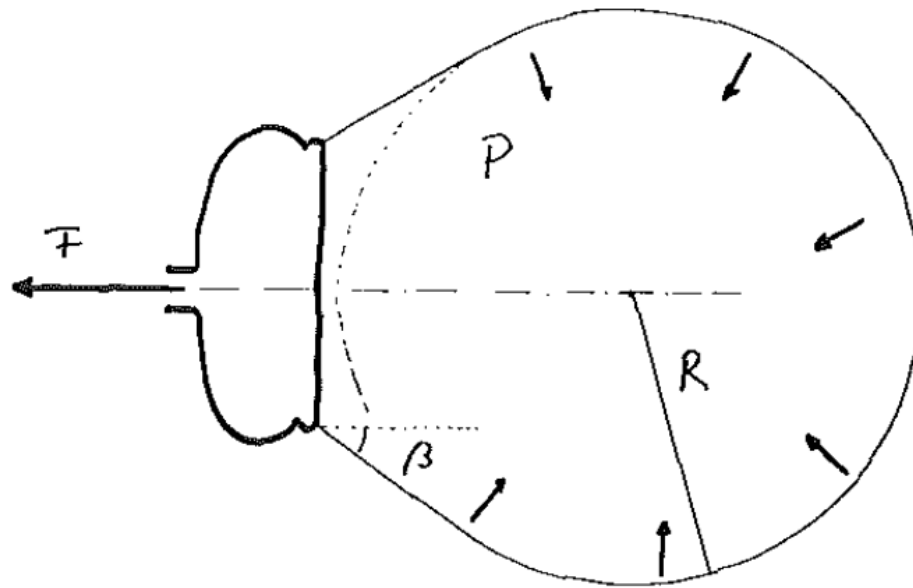


**Figure A.1:** The traction force ( $F$ ) increases the pressure ( $P$ ) on the fetal head ([22]).

The traction force and the duration for which it is applied are important risk factors for injuries ([59]). In certain studies, the duration of vacuum extraction varies between 1 and 26 minutes ([60]), with the procedure typically lasting around 10 minutes. During maternal contractions, which last around 0.5 to 1.5 minutes, the traction force applied by the obstetrician is highest ([1]).

### A.3. Sealing features found in wildlife

Besides the flexibility of the suction cup lip, features that enhance the sealing by forming around surface irregularities can be found in wildlife. In nature, the suction cups all have the same architecture: a rigid muscular part connected to the skeleton, and a soft tissue part isolating an inner cavity which ensures good sealing ([12]). In this section, a few examples of suction cups found in nature and their features enhancing the sealing performance will be described.

#### Conformability of suction cup to increase sealing

Several studies developed suction cups that can change shape to objects of a wide variety of sizes and shapes ([61], [62], [63]). Conformability of the suction cup means that the suction cup can change its shape to different surfaces. Due to this conformability a large contact area is achieved which results in a better sealing ([61]). In nature it is found that the muscles of the Octopuses infundibulum and the gastropod of the Abalone make their suction cup conformable by changing their stiffness. In that way they can conform their flexible suction cup lip around irregular surfaces to ensure good sealing. [62] [64].

Su et al. created a bioinspired suction cup in which the fibrous architecture inside the Remora Suckerfish disc lip is mimicked, as can be seen in Figure A.2 [65]. The fibrous architecture demonstrates a high tensile modulus and a low compressive modulus. When the disc has a lower vertical compressive modulus, it can follow the contours of a substrate to form a better seal which reduces the risk of leakages. Electrostatic flocking is used to vertically insert short artificial fibers onto a soft substrate to mimic the fibrous network [66]. They concluded that on both smooth and rough surfaces the maximum normal force of the bioinspired suction cup is,  $404N$  and  $402N$ , respectively. Moreover, with the same test setup, they concluded that suction cup designs without the fibrous network performed way worse on rough surfaces ( $234N$ ).



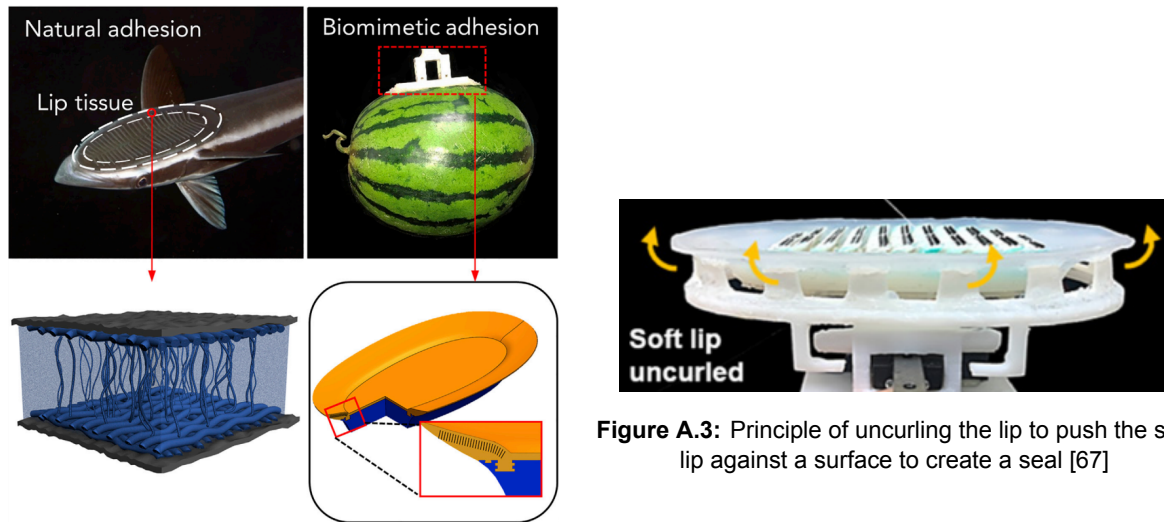


**Figure A.3:** Principle of uncurling the lip to push the soft lip against a surface to create a seal [67]

**Figure A.2:** Left: Fibrous network in the suction disc lip of the Remora Suckerfish. Right: Bio-inspired design where the fibrous network is mimicked with nylon fibers [65]

Wang et al. created a suction cup inspired by the Remora Suckerfish shown in Figure A.3. The inner cavity is surrounded by a soft lip that is used to seal. The Remora Suckerfish uses muscles to uncurl the soft lip against the surface which increases the sealing [67].

#### Microstructures to increase sealing

Aquatic organisms such as Northern Clingfish ([68],[69]) and Hillstream Loach [70] adhere by suction and maintain suction due to the creation of a seal on rough and slippery surfaces to prevent pressure loss. In A.4 an illustration of a bio-inspired suction cup with microstructures is depicted, which is inspired by the Northern Clingfish [71]. As can be seen, the setae structure ensures sealing with rough surfaces and therefore prevents leakages. The microstructures increase the adaptability of the suction cup lip to the target surface by filling up the tiny gaps on the rough surface. In this case, the adhesive force underwater is higher than the adhesive force on the same rough surface in the air due to capillary forces. This can be explained because the water flows in the tiny holes between the setae and increases sealing.

Ditsche et al. made a Northern Clingfish-inspired suction cup design with microstructures in the lip which ensured better sealing to rough and slippery surfaces. Due to the microstructures in the suction cup lip high tenacity of  $70kPa$  is reached by adhering to a wet, rough rock (Figure A.5).

Hwang et al. did research on microdenticles on the infundibulum of an octopus suction cup. Hwang et al. developed a bio-inspired suction cup with microdenticles. Like the setae, the microdenticles assist in sealing by filling up surface irregularities, which makes the suction cup more adaptable to surface irregularities [72].

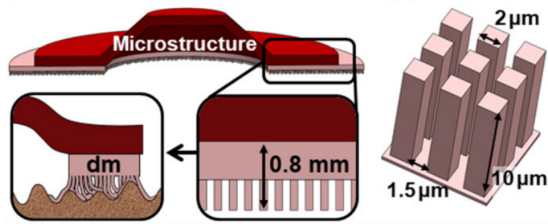


**Figure A.4:** Clingfish inspired microstructure to increase sealing of suction cup lip. [71]

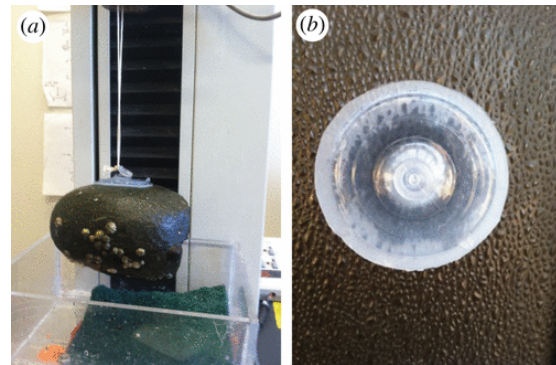


**Figure A.5:** Bio-inspired suction cup (a) holding a rock (about 5 kg) in the mechanical testing machine and (b) attaching to a very rough surface. The microstructures are located in the outer ring of the suction cup [68]

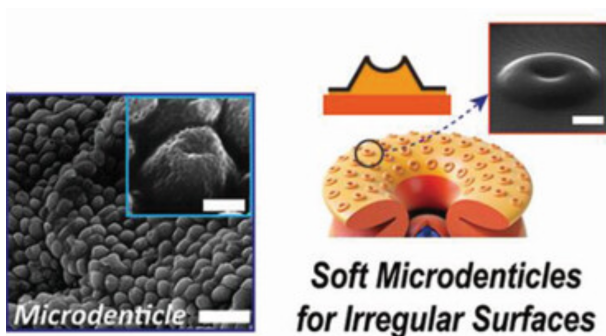


**Figure A.6:** Bio-inspired suction cup with microdenticles. Left: the image of microdenticles on an octopus suction cup. Right: mimicked suction cup with microdenticles. [72]

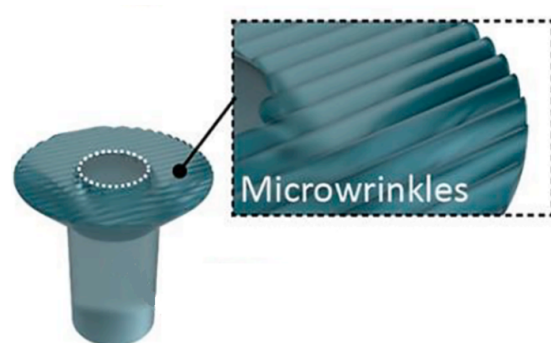


**Figure A.7:** Schematic illustration of the mushroom-shaped pillars with diving beetle-inspired microwrinkles. [73]

Min et al. developed a suction cup design consisting of microwrinkles inspired by the foreleg structure of the male diving beetles A.7. The microwrinkles are designed for better adhesion on wet, rough surfaces like skin. Because of the wet surface, the water flows through the wrinkles and capillary forces increase which results in high adhesion. Capillary forces are attractive forces between the liquid and the solid surfaces. Capillary forces cause the liquid to be drawn into the microwrinkles, creating a stronger and more effective seal between the suction cup and the surface. Moreover, the soft microwrinkles have a higher surface area, which increases the contact area ( $C$ ) on rough surfaces. Both the higher surface area and capillary forces result in better sealing [73].

The dimensions and shape of the microstructure discussed in this section influence the sealing capabilities. When the microstructures are too small compared to the surface irregularities, not all leakage 'channels' are sealed. On the other hand, when the microstructures are too large it can result in tiny gaps and decreased sealing capabilities. Therefore it depends on the surface roughness what microstructure dimensions and shape result in the best sealing.

All microstructures found are made from a certain type of silicone. Silicones are polymers with elastic properties (elastomers). The flexibility of the microstructures is important to ensure that they can conform to surface irregularities to ensure tight sealing. Moreover, elasticity is important to ensure that the microstructures change back to their original shape after detaching. This allows for more suction cycles to be achieved.

## A.4. Technical datasheet Filflex 60A

Material properties of Filflex 60A (Recreus) [74].

**Table A.2:** Physical and Mechanical Properties of Filaflex 60A

<b>Physical Property</b>		
<b>Property</b>	<b>Value</b>	<b>Unit</b>
Material density	1,070	g/cm <sup>3</sup>
	1070,000	kg/m <sup>3</sup>
Melt flow rate (230°C/2,16kg)	0,000	g/10min
<b>Mechanical Property</b>		
<b>Property</b>	<b>Value</b>	<b>Unit</b>
Hardness	63,00	shore A
Tensile strength	26	MPa
Elongation at break	950,00	%
Stress at 20% elongation	1,00	MPa
Stress at 100% elongation	2,50	MPa
Stress at 300% elongation	4,50	MPa
Tear strength	40,00	N/mm
Abrasion resistant	45,00	mm <sup>3</sup>
Compression set 23°C/72 hours	40,00	%
Compression set 70°C/24 hours	25,00	%

## A.5. Grid structure

### A.5.1. Comparison grid structures

Several grid structures, including square, circular, triangular and pillar configurations (Figures A.8, A.9, A.10 and A.11, respectively), were considered as grid structure within the suction cup design. The grid pattern influences the effective vacuum area, contact area, and the shape of the chignon formed. For consistency in comparison, the thickness of the struts in all grid patterns was maintained at 1.5 mm. Additionally, the maximum distance from any point on scalp to the nearest strut was set to 5 mm. The vacuum areas of these different grid patterns were compared to a standard 50 mm suction cup, and is shown in Table A.3.

The pillar and circle grid structures exhibit a significantly larger effective vacuum area compared to the square and triangle grid structures. However, a larger vacuum area presents two disadvantages. Firstly, a larger vacuum area results in a greater portion of the scalp being sucked into the suction cup. Despite this, the maximum distance to the nearest structural element is maintained at 5 mm for all grid patterns, limiting the extent of scalp deformation. Secondly, a larger vacuum area reduces the stability of the grid structure. For example, the pillars are more prone to buckling under high forces compared to other structures.

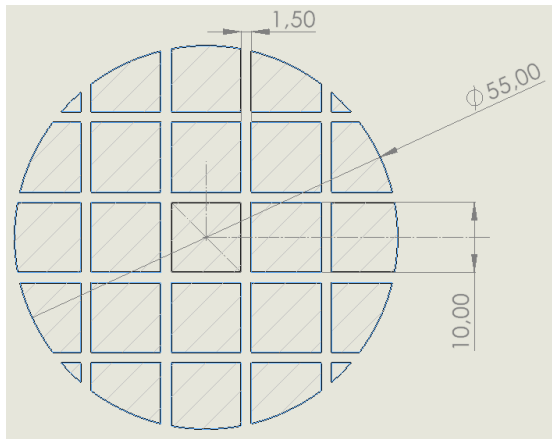


**Figure A.8:** A 2-dimensional square grid structure, showing the dimensions for a vacuum area of  $1832mm^2$  (Hatch)

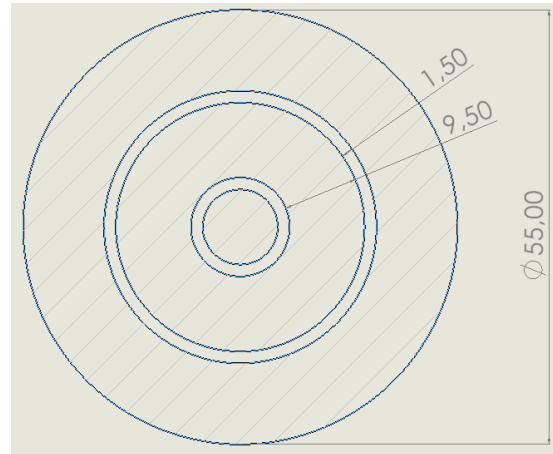


**Figure A.9:** A 2-dimensional circle grid structure, showing the dimensions for a vacuum area of  $2168mm^2$  (Hatch)

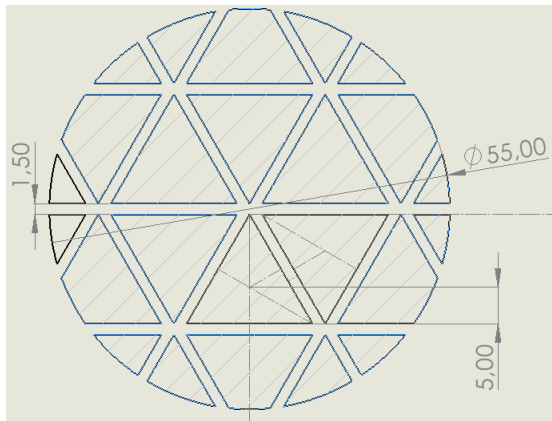


**Figure A.10:** A 2-dimensional triangle grid structure, showing the dimensions for a vacuum area of  $1771mm^2$  (Hatch)

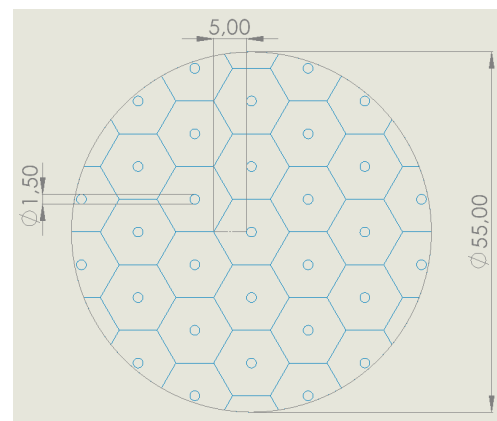


**Figure A.11:** A 2-dimensional pillar grid structure, showing the dimensions for a vacuum area of  $2302mm^2$  (Hatch)

**Table A.3:** The vacuum area for different grid structures. For comparison, the thickness of all structures is 1.5mm.

		Vacuum area	
50mm inner diameter suction cup	No grid	1963	$mm^2$
	No grid	2376	$mm^2$
55mm inner diameter suction cup	Pillar grid	2321	$mm^2$
	Circle grid	2168	$mm^2$
	Square grid	1832	$mm^2$
	Triangle grid	1771	$mm^2$

### A.5.2. Circular grid configuration

The configuration of a circular grid depends on the number and thickness of the rings, which can be adjusted. A key requirement is that the effective vacuum area must be at least equal to the vacuum area of a standard suction cup with an inner diameter of 50 mm, which is  $1963 mm^2$ . The effective vacuum area of a suction cup with an outer diameter of 65 mm depends on the space allocated for a sealing solution, the ring thickness, and the number of rings. The spacing between the rings is kept constant for different numbers of rings to ensure consistent chignon formation and pressure peaks inside the scalp.

The vacuum areas for different circular grid configurations with sealing rings of 5 mm and 6 mm are shown in Tables A.4 and A.5, respectively. If the effective vacuum area is larger than the vacuum area of the Kiwi Replica with an inner diameter of 50 mm, it is highlighted in green. The outer diameter is fixed at 65 mm, therefore a larger sealing ring results in a smaller effective vacuum area. Additionally, the thickness of the ring structure and the number of rings are varied.

To determine the most suitable parameter combination, it is argued that a sealing ring of 5 mm will be sufficient to ensure proper sealing. More sealing rings result in a smaller distance between the rings; therefore, a configuration with four rings and a thickness of 1 mm is proposed, which results in an effective vacuum area of 2069 mm<sup>2</sup>.

To prevent buckling during suction, the circular grid structure must be sufficiently strong. Buckling would result in a larger portion of the scalp being sucked inside the suction cup. A thicker structure provides more strength but decreases the vacuum area. It should be experimentally validated whether buckling occurs with a structure of 1 mm thickness, as the properties of the scalp are not precisely known.

5mm sealing ring	Thickness structure	Vacuum area				Unit
		1 ring	2 rings	3 rings	4 rings	
Vacuum area	1mm	2318	2238	2154	2069	mm <sup>2</sup>
	1.5mm	2289	2168	2043	1915	mm <sup>2</sup>
	2mm	2261	2099	1932	1761	mm <sup>2</sup>
Spacing between structures	1mm	17.33	10.00	6.86	5.11	mm
	1.5mm	16.83	9.50	6.36	4.61	mm
	2mm	16.33	9.00	5.86	4.11	mm

**Table A.4:** Comparing vacuum area and spacing between sealing rings for different ring thicknesses and amount of rings for a suction cup with outer diameter of 65mm. A sealing ring of 5mm is considered. Red cells show vacuum areas smaller than a standard suction cup of 50mm, green cells show vacuum areas larger than a standard suction cup of 50mm

6mm sealing ring	Thickness structure	Vacuum area				Unit
		1 ring	2 rings	3 rings	4 rings	
Vacuum area	1mm	2151	2073	1992	1910	mm <sup>2</sup>
	1.5mm	2123	2006	1885	1762	mm <sup>2</sup>
	2mm	2095	1940	1778	1614	mm <sup>2</sup>
Spacing between structures	1mm	16.67	9.60	6.57	4.89	mm
	1.5mm	16.17	9.10	6.07	4.39	mm
	2mm	15.67	8.60	5.57	3.89	mm

**Table A.5:** Comparing vacuum area and spacing between sealing rings for different ring thicknesses and amount of rings for a suction cup with outer diameter of 65mm. A sealing ring of 6mm is considered. Red cells show vacuum areas smaller than a standard suction cup of 50mm, green cells show vacuum areas larger than a standard suction cup of 50mm

## A.6. Stringing problem in 3D printing

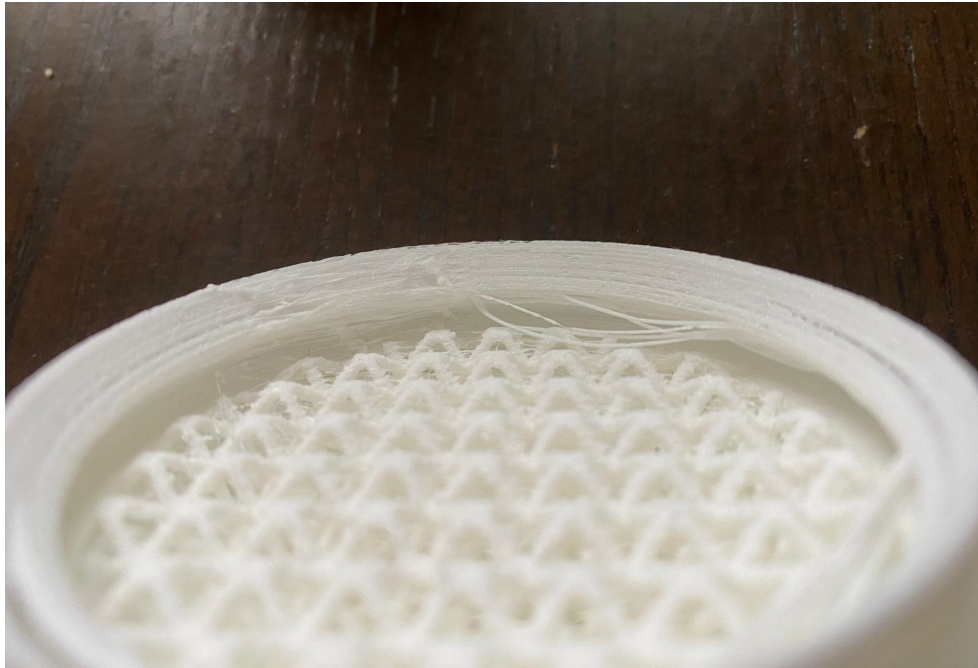


**Figure A.12:** A sealing lip of  $1\text{mm}$  is too thin, which results in stringing and air leakages.

## A.7. Sealing lip force

The measurement setup was designed to capture the force exerted by the sealing lip as it conforms to an infant surrogate. The infant surrogate was modeled to replicate the curvature and surface properties of an average infant's scalp (Appendix A.9). The suction cup with the flexible sealing lip was then applied to the surrogate. The force was recorded when the sealing lip conformed around the surrogate, forming a seal (Figure A.13).



**Figure A.13:** Measuring the force that is needed to form a seal with the infant surrogate surface.

## A.8. Lattice forces

To measure the forces in different lattice structures, each structure was compressed until no light was seen through its struts, a point referred to as the 'fully compressed' state. Compression beyond this point results in non-linear behaviour. This test was conducted by two individuals. One person measured and recorded the change in height while applying downward pressure on the structure. The other person recorded the corresponding force using a kitchen scale. Additionally, the force for each lattice structure was recorded at half of the maximum compression distance. From the graphs it can be concluded that the total lattice show approximately a linear behaviour and therefore follows hooks law. The results are plotted in Figure A.16 and A.17.



**Figure A.14:** Measuring the lattice force and deformation (Extended)



**Figure A.15:** Measuring the lattice force and deformation until no light can be visually be seen (Compressed)

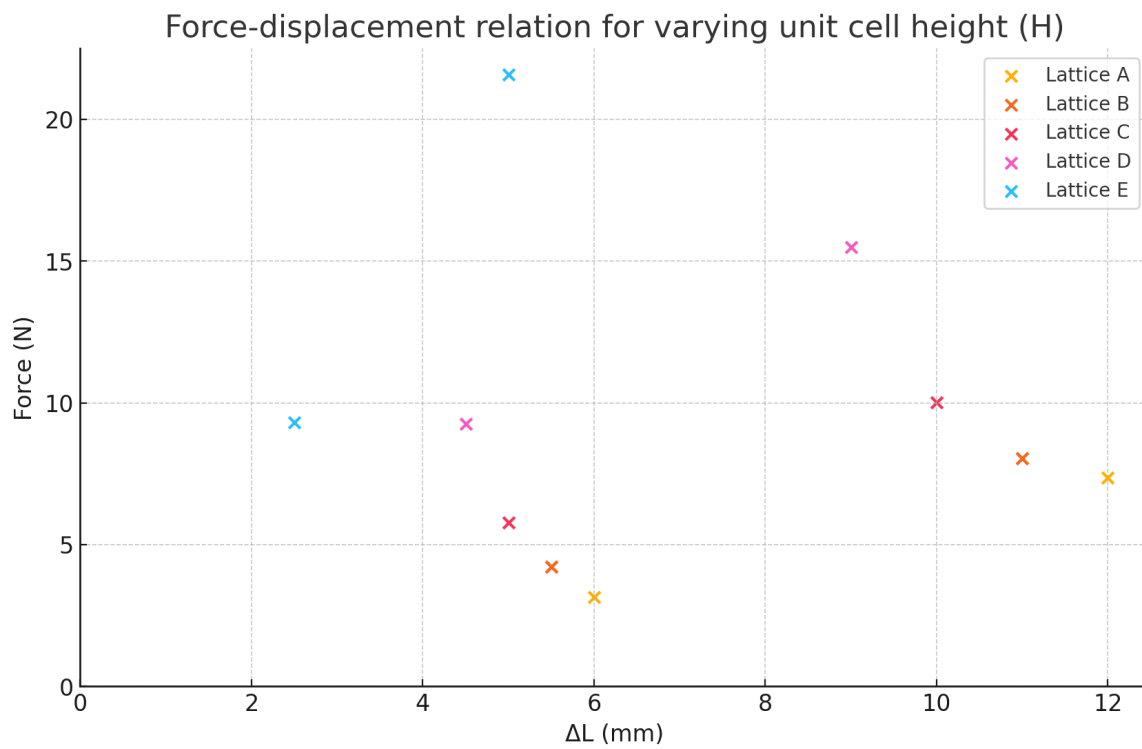


Figure A.16: The Force-displacement relationship for lattice A,B,C,D and E.

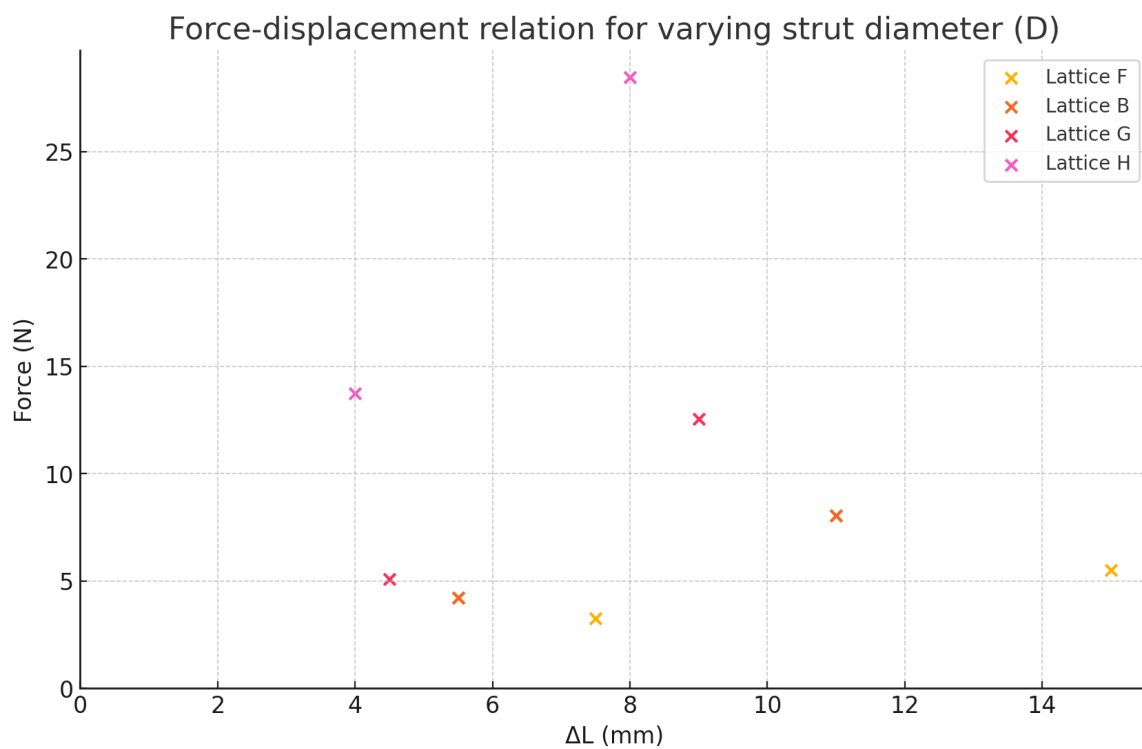


Figure A.17: The Force-displacement relationship for lattice F,B,G and H.

## A.9. Infant skull model

A 3D model of the infant skull is found on sketchfab.com [47]. It is guessed to be an infant skull of the age of the late second trimester (circa. 24-27 weeks in pregnancy).





**Figure A.18:** Model of an infant skull [47]

To make this model suitable for this research it is scaled to an average-size newborn infant with the following dimensions [46]:

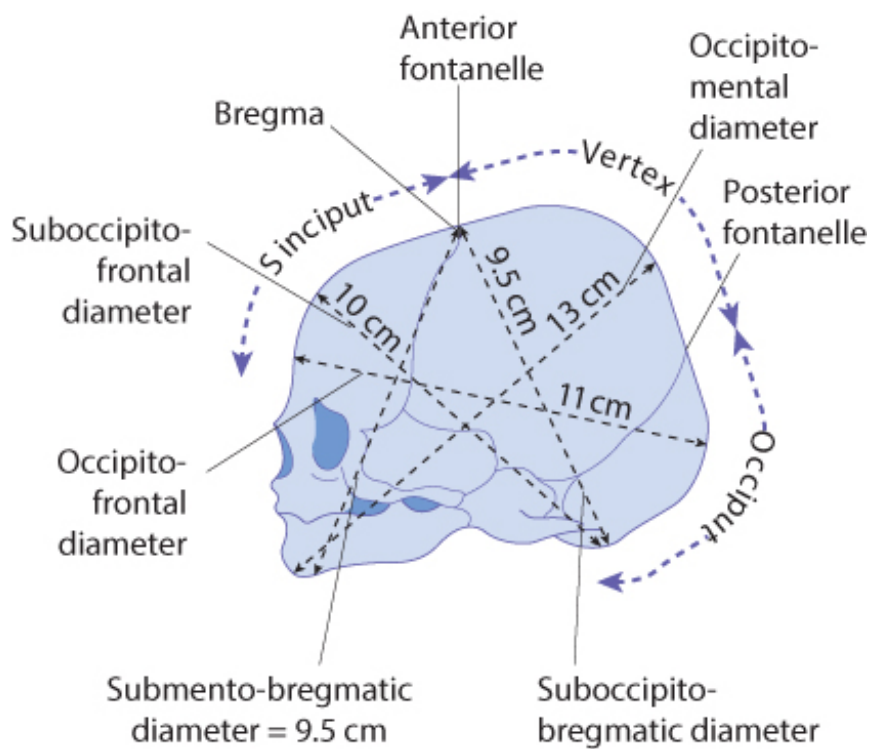


**Figure A.19:** Dimensions of newborn infant [46]

The scaled 3D model is scaled in SolidWorks. For correct placement, the suction cup should be placed on the flexion point, situated 3 cm anterior to the posterior fontanelle along the midline of the sagittal suture. The flexion point is depicted and a circle of 6cm is drawn to show the size of the suction cup relative to the infant.

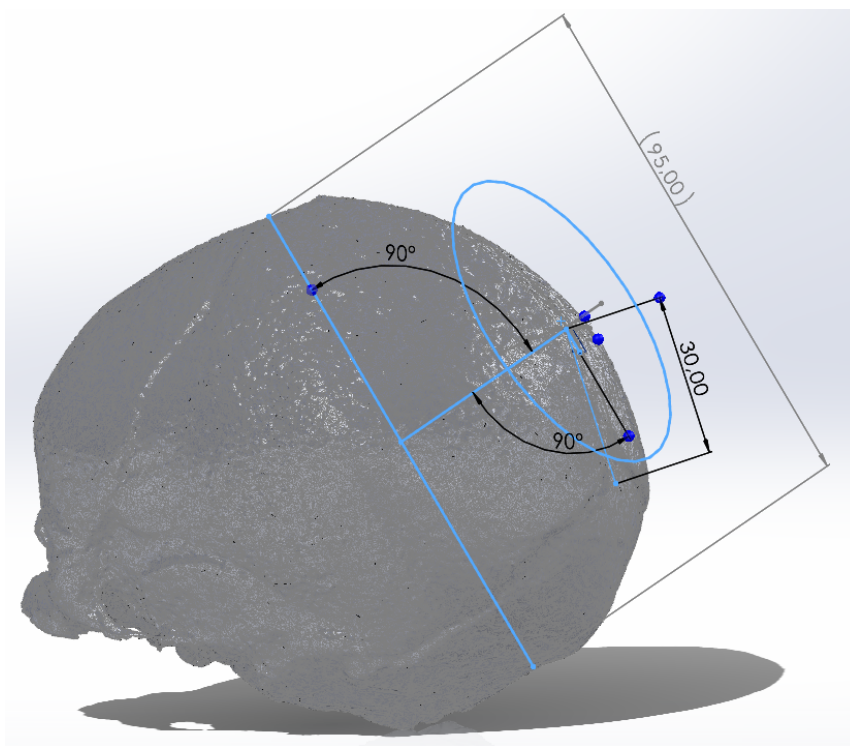


**Figure A.20:** Scaled 3D model of the infant skull, the correct location for placement of the suction cup is depicted with a circle (60 mm diameter)

The curvature of the skull at the flexion point is approximated with a sphere with a diameter of 110cm (Figure A.21)

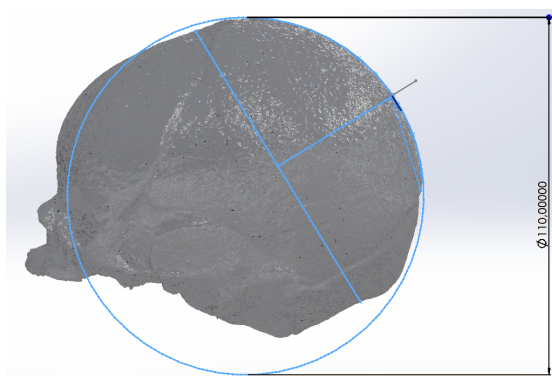


**Figure A.21:** The curvature of the infant skull at the flexion point is approximated with a circle with a diameter of 110cm. (View: Sagittal plane)

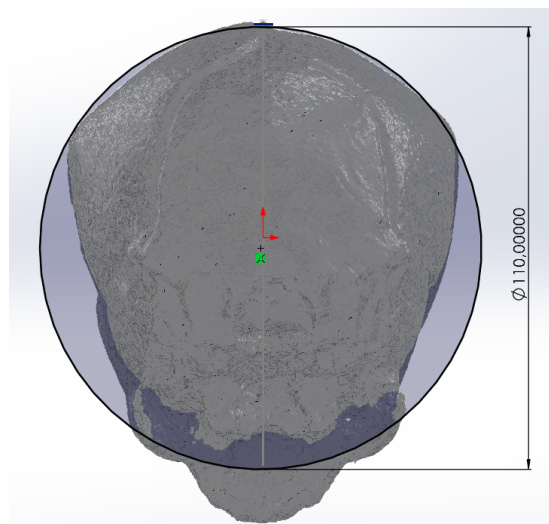


**Figure A.22:** Approximation of the curvature of the infant skull at the flexion point (View: Coronal plane, rotated that flexion point is located at the top)

### A.10. Vacuum inlet diameter

The diameter of the vacuum inlet was incrementally increased until no leakage occurred. The various 3D printed vacuum inlets are depicted in Figure A.23. A diameter of 6.73 mm was chosen as the tube still fitted securely and the pressure remained stable when a vacuum was applied.

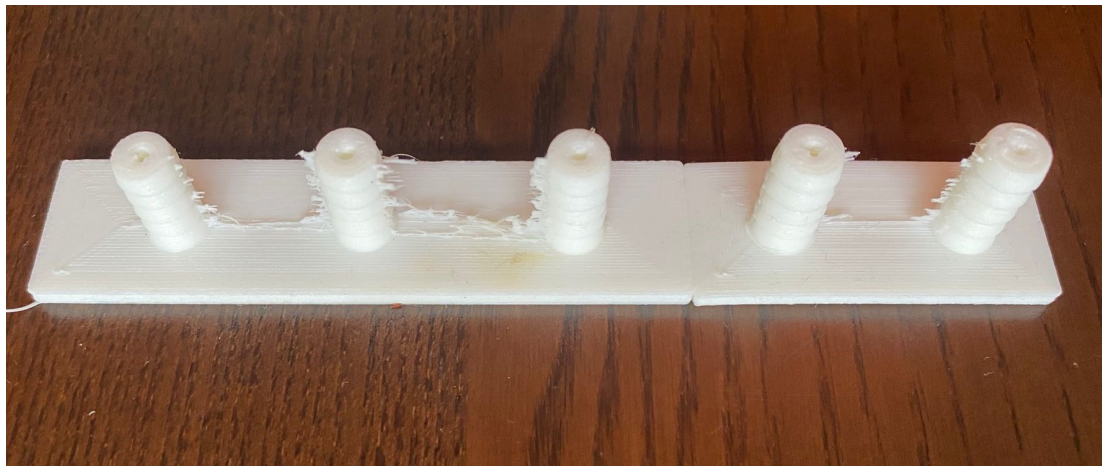


Figure A.23: Testing different vacuum inlet diameters

### A.11. Simulation cup-scalp interface

Tham et al. ([37]) developed a finite element model (FEM) that predicts normal stresses in human soft tissue. Large normal stresses in the soft tissue increase the risk of tissue damage and fluid accumulation, which is an indication of chignon formation. Similar to mushroom-shaped VAD devices, the suction cup was assumed to be rigid. The model representation is shown in Figure A.24. The stress distribution is plotted after applying a pressure differential of  $30\text{ kPa}$  in Figure A.25.

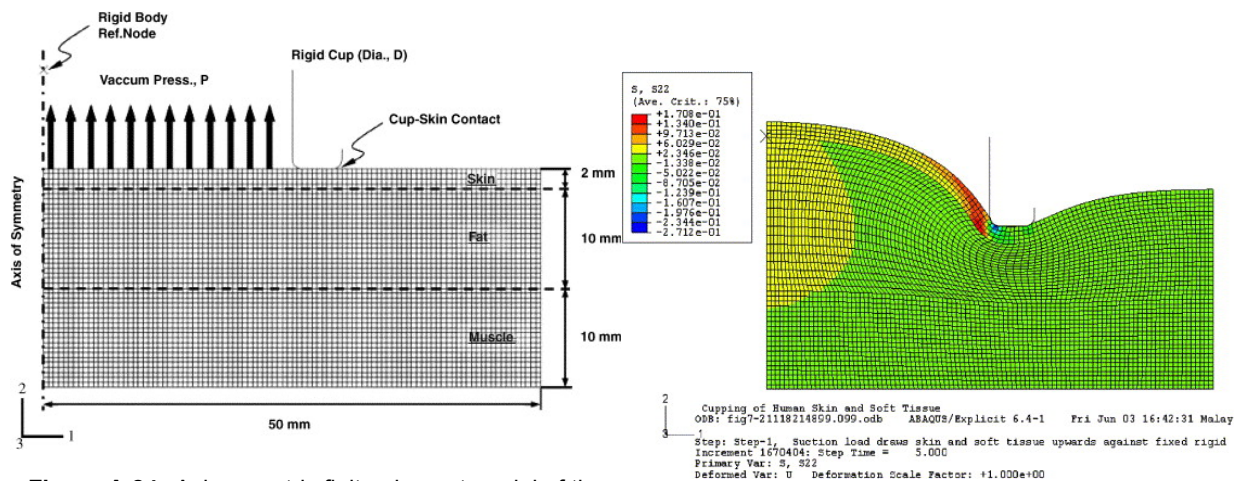
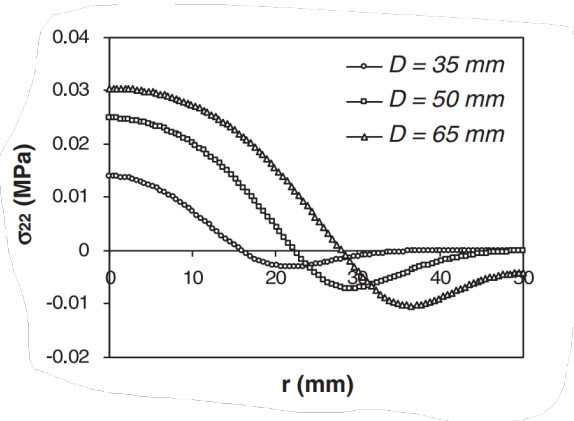


Figure A.24: Axisymmetric finite element model of the cupping of soft tissue. The soft tissue is composed of skin, fat, and muscle. All three soft tissue layers were assumed to be nonlinearly elastic and linearly viscoelastic. The suction force was applied to the surface of the skin in the area enclosed by the cup. Only a portion of the cup was modeled (rim and part of the side wall) and it was assumed to be rigid. ([37])

Figure A.25: Predicted distribution of the normal stress in the soft-tissue layers at the vertical direction,  $\sigma_{22}$  (MPa), in the soft-tissue layers at time ( $t=5\text{ s}$ ), (simulation parameters: cup diameter=50 mm, cup rim fillet radii=1 mm, vacuum pressure=30 kPa, ramping period=1.5 s, friction coefficient=0.5).([37])

The normal stress at the fat-muscle interface is illustrated in Figures A.26 and A.27. In Figure A.26, the stress for different suction cup diameters is plotted. A larger suction cup diameter results in greater normal

stress due to the increased total suction force (Equation 2.3). In Figure A.27, the friction between the suction cup rim and skin is varied. It can be concluded that higher friction results in lower normal stresses within the skin.



**Figure A.26:** Predicted normal stress,  $\sigma_{22}$ , for the different cup diameters,  $D$ , at the fat–muscle interface,  $t=5s$  (simulation parameters: cup rim fillet radii=1 mm, ramping period=1.5 s, vacuum pressure=30 kPa, friction coefficient=0.5).([37])

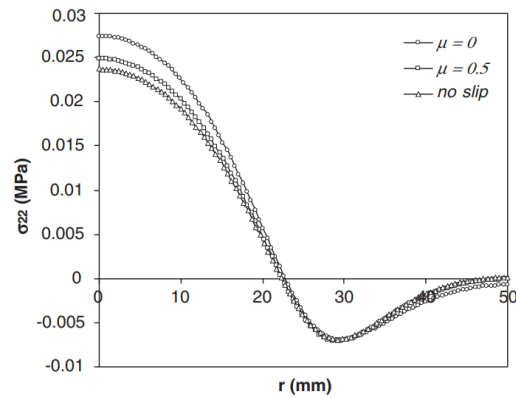


**Figure A.27:** Predicted normal stress,  $\sigma_{22}$ , for the different friction coefficients,  $\mu$ , at the interface between the fat and muscle layers at time,  $t = 5 s$  (simulation parameters: cup diameter = 50 mm, cup rim fillet radii = 1 mm, ramping period = 1.5 s, vacuum pressure = 30 kPa).([37])

### A.12. Dimensions final design

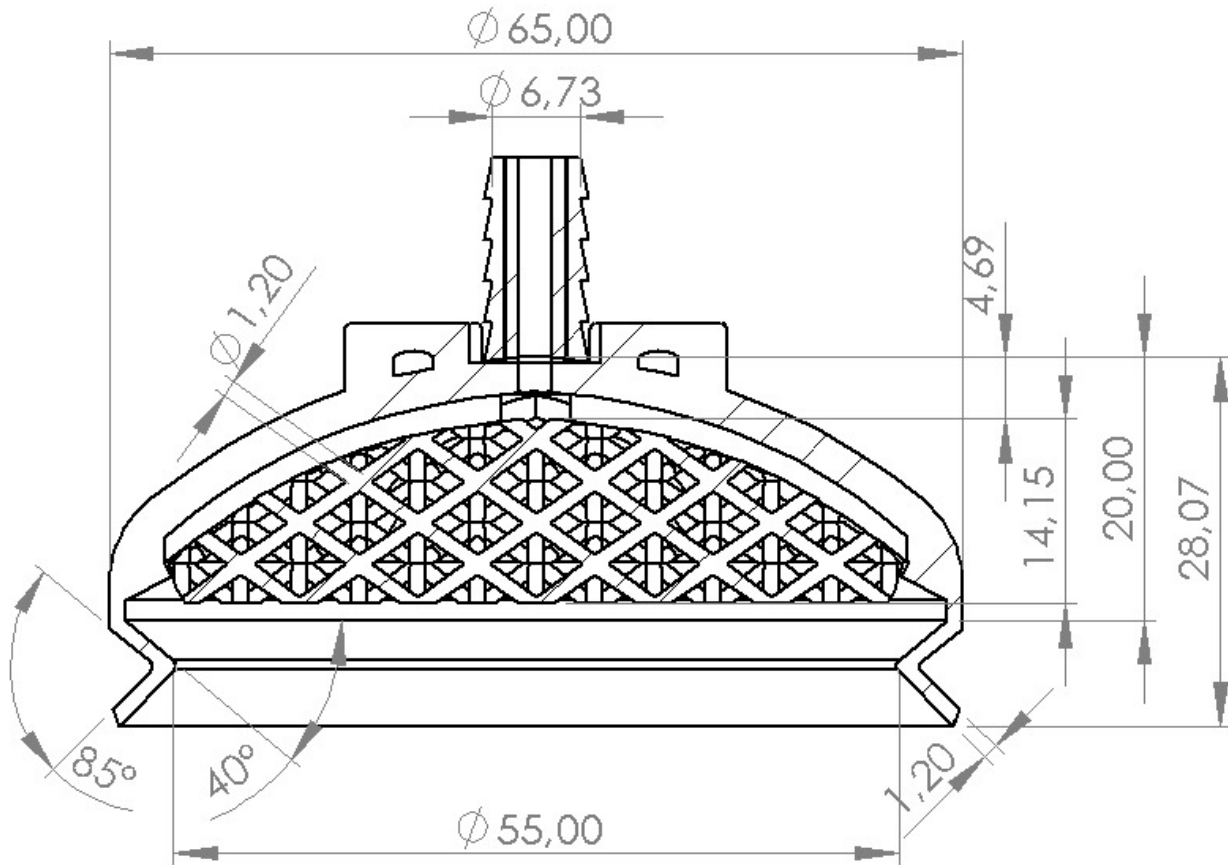


**Figure A.28:** A section view of the final design, showing all dimensions.

### A.13. Chignon formation compared to the Kiwi replica

Estimation of the chignon volume of the proposed suction cup designs without the application of a traction force. The chignon volume is calculated in SolidWorks.

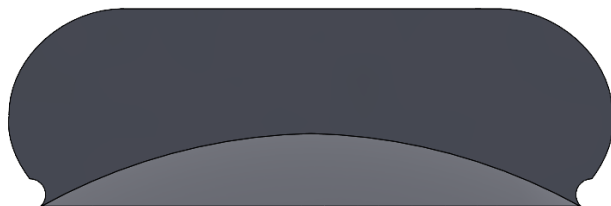


**Figure A.29:** Potential chignon formation inside the Kiwi replica.



**Figure A.30:** Potential chignon formation inside the proposed design (2mm, when the scalp deformation is equally distributed)

**Table A.6:** Comparison of the chignon volume and percentage for different the designs compared to the Kiwi replica. For the calculation of the chignon volume in the proposed designs, the potential scalp displacement is considered equally distributed.

	Max displacement	Chignon volume (mm <sup>3</sup> )	Percentage
<b>Kiwi replica</b>	Fully filled (11.7 mm)	34494	100%
<b>Proposed design (Desired)</b>	1.36 mm	3451	10.0%
<b>Proposed design (Max.)</b>	2 mm	5079	14.7%
<b>Final design (model 1)</b>	0.88 mm	2238	6.5%
<b>Final design (model 2)</b>	1.54 mm	3913	11.3%
<b>Final design (model 3)</b>	2.20 mm	5586	16.2%

### A.14. Conversion table from mmHg to kPa

**Table A.7:** Conversion from mmHg to kPa

Pressure (mmHg)	Pressure (kPa)
100	13.3
200	26.7
300	39.9
400	53.3
500	66.7
600	80.0
700	93.3
800	107